3 8006 10127 4051

41/372

CRANFIELD INSTITUTE OF TECHNOLOGY
School of Mechanical Engineering

Applied Mechanics Group

PH.D. THESIS

Academic Year 1987-1988

by D W Hammond

FATIGUE FRACTURE IN THE PRESENCE OF SHOT PEENING RESIDUAL STRESSES: INITIATION, PROPAGATION AND RELAXATION PHENOMENA

Supervisor: Dr S A Meguid

September 1988

ProQuest Number: 10832331

All rights reserved

INFORMATION TO ALL USERS
The quality of this reproduction is dependent upon the quality of the copy submitted.

In the unlikely event that the author did not send a complete manuscript
and there are missing pages, these will be noted. Also, if material had to be removed,
a note will indicate the deletion.

ProQuest 10832331

Published by ProQuest LLC (2019). Copyright of the Dissertation is held by Cranfield University.

All rights reserved.
This work is protected against unauthorized copying under Title 17, United States Code
Microform Edition © ProQuest LLC.

ProQuest LLC.
789 East Eisenhower Parkway
P.O. Box 1346
Ann Arbor, MI 48106 – 1346

To friends and family

ACKNOWLEDGEMENT

The author is truly grateful to a number of people without whose efforts this work could not have been performed.

Firstly, acknowledgements are due to the Science and Engineering Research Council for providing a substantial proportion of the funding for the work.

Support was also forthcoming from a number of industrial sponsors, notably Dowty Rotol Limited, Rolls-Royce plc for providing test materials, Vacu-Blast, Barton Abrasives and the Metal Improvement Company Inc. for providing peening equipment and consumables.

Secondly, thanks are due to Dr Gillian Smith of NEI-Parsons, Newcastle, for performing the x-ray residual stress measurements associated with this study, Mr T Barwick, who swiftly and skillfully machined the hundreds of fatigue specimens expended during the work, and Mrs S Jones, who with great patience typed this thesis.

Finally, a special note of thanks to Professor S A Meguid, supervisor, who, in addition to genuine friendship, provided the support and coaching which saw this work to its conclusion.

SUMMARY

This thesis describes both experimental and theoretical work performed in order to analyse fatigue fracture in the presence of shot-peening induced residual stresses.

In the study, four contrasting alloys were examined by fatigue testing and use was made of different test techniques to illustrate some of the phenomena associated with fatigue fracture in shot-peened components.

The results demonstrate that in order to characterise the process of fatigue in a component bearing residual stresses, it is necessary to consider three groups of variables. These are the applied and residual stress state, the geometry of the component and the flaws it contains and the nature of the alloy itself, including any propensity to work harden, recover or undergo phase changes due to peening or fatigue loading.

CONTENTS

Page No.

CHAPTER ONE

INTRODUCTION 1

SUMMARY 1

1.1 The Importance of the Shot-Peening Process to Fatigue Conscious Components 2

1.2 Definition of the Problem and Aims of the Study 3

1.3 Method of Approach 4

1.3.1 Theoretical Investigations
1.3.2 Experimental Investigations

1.4 Layout of Thesis 9

REFERENCES 11

CHAPTER TWO

LITERATURE SEARCH 12

SUMMARY 13

2.1 Origin of Residual Stresses 13

2.2 Fatigue Fracture 15

2.2.1 Historical Perspective

2.2.2 Initiation Dominated Fatigue

Page No.

2.2.3 Propagation Dominated Fatigue

2.3 Influence of Residual Stresses 24

2.4 Relaxation of Residual Stresses 26

2.4.1 Residual Stress Relaxation by Plastic Deformation

2.4.2 Thermal Residual Stress Relaxation

LIST OF FIGURES 30

REFERENCES 30

CHAPTER THREE

EXPERIMENTAL TECHNIQUES 35

SUMMARY 36

3.1 Fatigue Testing Techniques 36

3.1.1 Rotating Bend Fatigue Testing

3.1.2 Servo-hydraulic Uniaxial Fatigue Testing

3.2 Crack Size Measuring Techniques 47

3.2.1 Industrial Non-Destructive Examination

3.2.2 Laboratory Techniques

3.3 A Novel Stroboscope Using Light Emitting Diode Lamps for the Inspection of Fatigue Cracks 58

3.4 Shot Peening 75

3.5 Residual Stress Measurement 81

3.5.1 X-ray Diffraction

3.5.2 Hole Drilling

3.5.3 Dissection Method

LIST OF FIGURES 85

REFERENCES 87

Page No.

CHAPTER FOUR 90

THREE-DIMENSIONAL FINITE ELEMENT ANALYSIS OF CIRCUMFERENTIALLY-CRACKED BODIES

SUMMARY 91

4.1 Background 91

4.2 Interactive Modelling 91

4.2.1 Model Creation and Mesh Definition

4.2.2 Model Checking

4.2.3 Simulation of Cracked Bodies using the Finite Element Method

4.3 Finite Element Approach 95

4.4 Determination of Stress Intensity and Stress Concentration Factors 96

4.5 Finite Element Results 99

LIST OF FIGURES 103

REFERENCES 104

CHAPTER FIVE 105

FATIGUE CRACK PROPAGATION IN THE PRESENCE OF SHOT-PEENING RESIDUAL STRESSES

SUMMARY 105

5.1 INTRODUCTION 105

5.2 Experimental Analysis 107

5.2.1 Selection of Test Materials and Specimen Preparation

5.2.2 Equipment and Procedure

5.2.3 Measurement Techniques Used

5.2.4 Experiment Programme

5.3 Analysis of Results and Discussions 115

5.3.1 Preliminary Test Results

5.3.2 Main Test Results

Page No.

5.4 CONCLUSIONS 125

LIST OF FIGURES 127

LIST OF TABLES 129

REFERENCES 130

CHAPTER SIX 133

FATIGUE CRACK INITIATION AND PROPAGATION

SUMMARY 134

6.1 Introduction 134

6.2 Experimental 135

6.2.1 Materials Tested

6.2.2 Specimen Preparation

6.2.3 Fatigue Testing and Crack Detection

6.3 Results and Discussion 144

6.4 CONCLUSIONS 163

LIST OF FIGURES 164

LIST OF TABLES 166

REFERENCES 167

CHAPTER SEVEN

CONCLUSIONS 168

CHAPTER ONE

INTRODUCTION

SUMMARY

1.1 The Importance of the Shot-Peening Process to Fatigue Conscious Components

1.2 Definition of the Problem and Aims of the Study

1.3 Method of Approach

1.3.1 Theoretical Investigations
1.3.2 Experimental Investigations

1.4 Layout of Thesis

SUMMARY

This chapter defines the areas of interest to this study, justifies why these areas are of importance and defines the aims of the work. The basic method of approach is described in order to help the reader follow the work more effectively, and finally the layout of the thesis is described.

1.1 THE IMPORTANCE OF THE SHOT-PEENING TO FATIGUE CONSCIOUS COMPONENTS

Fatigue fracture remains one of the most common modes of structural failure in metallic structures both large and small. Automotive parts, tools, bridges, oil rigs, sports equipment, together with thousands of the products which frequently have lives limited by their ability to withstand the repeated application of loads which in themselves are much lower than those necessary to deform permanently or break the new structure.

The mechanism which most clearly aids an understanding of how fatigue failure can occur is the development and growth of cracks. Even at nominally low applied loads, macroscopic and microscopic discontinuities in any real structure will produce limited zones of non-recoverable deformation which lead to the development of cracks. In many instances cracks will begin at the surface and grow into the structure. There are three reasons for this pattern; firstly, the surface of a material contains flaws associated with how that surface was created. If these flaws are larger than the inherent flaw size of the material, they will represent the 'weakest link'. Secondly, few materials are not reactive to some extent. The irregular build up of corrosion products, or the absorbtion of elements such as hydrogen into the free surfaces of components, will affect the properties and micro profile of the surface material. Finally, any bending and/or torsion stresses acting on the component, be they associated with the principal load path, or misalignment distortions, will increase the level of the surface stress to beyond that in the bulk of the component.

With the strength of most fatigue conscious components basically being limited by the fatigue strength of the surface, it is clear that surface engineering processes which improve the integrity of the surface are of considerable importance. Shot-peening is one of the most effective and easily applied surface treatments currently available for improving the fatigue performance of metallic components [1.1]. The details of the process and exactly how it works are dealt with in Chapter Two, but peening affects the second and third of the aforementioned factors, that is, the peened surface layer has a modified structure, which is manifest in its hardness as well as numerous other properties, but almost without doubt, more important is the residual stress imparted by the process. Since fatigue crack growth is highly sensitive to the nature, of cyclic loading, compressive or tensile, the existence of a compressive residual stress in the peened surface profoundly affects the development of fatigue cracks.

Confirmation of the importance of the peening process can be gleaned from the extent of its usage in industry. A large variety and number of parts ranging from springs costing a fraction of a penny to large forgings worth £10^5+ are systematically peened. Generally, such parts are required to have high strength to weight ratios, i.e., critically stressed components are peened as a matter of course, in diference to the view that the peened component will outlive the un-peened one, the only question remaining being is, by how long?

1.2 DEFINITION OF THE PROBLEM AND AIMS OF THE STUDY

As has been outlined in section 1.1, peening is used widely in numerous diverse situations. In that section, the nature of fatigue fracture and the effect of the peening process are briefly discussed. To recapitulate, peening pre-stresses the surface of the component so that it will experience a less tensile load history than it otherwise might. Fatigue on the other hand implies highly localised zones of plastic deformation which give rise eventually to crack development. The residual stresses produced by peening are not then necessarily permanent, but will be modified by local permanent strains. This is not to say that peening will be ineffective. It may be highly effective in slowing the process down, but if it were assumed for a

moment that the desirable peening induced residual stresses were to decay, the component would have expended some of its fatigue life and crack development would begin as in an un-peened component. Suppose at this stage the component were to be peened again, or re-peened, the residual stresses would be restored and the life of the component may well have also, in part, been restored, perhaps.

The aim of this project then is to explore this possibility of utilising periodic re-peening on components in order to make them last even longer than peened components. To be more specific the aims of the project may be drafted in the form of four questions which need to be answered. These are as follows:-

(i) Can peening be used to delay the formation or 'initiation' of a fatigue crack?

(ii) Can one slow down the rate of growth of a crack by peening it?

(iii) How rapidly do the beneficial residual stresses associated with shot-peening relax, if at all?

(iv) Can re-peening be used to counter the relaxation of residual stresses, or will other factors begin to influence the fracture process?

Satisfactory answers to these questions would enable engineering decisions to be made on such questions as the re-use of components containing cracks of known size by peening them, or the re-design of critical components where advantage may be taken of periodic re-peening.

1.3 METHOD OF APPROACH

In order to answer the questions mentioned in section 1.2, a combined experimental and theoretical approach has been adopted.

1.3.1 Theoretical Investigations

The purpose of this part of the work is to provide the analytical basis for both the analysis of experimental results and the formulation of predictive relationships for fatigue fracture in the presence of residual stresses.

Both three-dimensional finite element analysis and analytical solutions are compared and used for the determination of crack tip stress intensity factors. Classical linear elastic fracture mechanics, and crack closure models are used in order to analyse the propagation of fatigue cracks within a residual stress field.

Crack Initiation and Surface Residual Stresses

Application of fracture mechnics to fatigue fracture has been limited only to the propagation of a pre-existing crack, and efforts made in analysing the crack initiation stage has been relatively meagre [1.2]. Crack initiation is usually defined as the mechanism by which a crack forms to some finite length, but it could also be defined as that portion of the fatigue process not involved in crack propagation [1.3]. A crack of a finite length may be present, but if the fatigue stress intensity amplitude ΔK is less than the threshold stress intensity amplitude ΔK_{th} (below which no crack propagation occurs), then the system may be considered to be in the crack initiation stage.

Consider a fatigue crack propagation process that obeys Paris's relationship, $da/dN = C(\Delta K)^n$, (N represents number of cycles, ΔK stress intensity amplitude C and n are frequently called material constants). Furthermore, limit the consideration to rotating bending fatigue tests, for which ΔK may be replaced by the maximum stress intensity K_{max}. Then, the influence of the shot-peening compressive residual stresses is to decrease K_{max} by certain amount K_I^r may be predicted by utilising either the weight function approach or the stress intensity formula for a point acting on a crack face. It is known that a threshold value of stress intensity amplitude ΔK_{th} or K_{th} exists, below which a crack will not propagate. Knowledge of ΔK or

K_{max}, K_I^r and K_{th} will enable us to determine whether a crack is in the initiation or the propagation stage from a theoretical point of view.

Fatigue Crack Growth in a Residual Stress Field

Two approaches will be considered: (i) superposition of the respective stress intensity factors for the residual stress field and for the applied stresses, and (ii) a crack closure model. Limitations of the different approaches and their relative advantages and drawbacks for use in design analysis will be considered.

(i) Superposition Approach for Existing Residual Stress

To quantify the influence on crack growth of residual stresses originating from shot peening, the following items are needed: (a) an accurate estimate of the original residual stress field (both in magnitude and distribution in depth); (b) a method for expressing the influence of residual stress on growth rate, preferably in a linear elastic fracture mechanics format so that existing da/dN-ΔK data may be utilised; and (c) knowledge of how the residual stress fields may be altered by loadings before a crack starts and as it grows.

The approach employed most frequently to account for the effect of residual stress on crack growth involves superposition of therespective stress intensity factors for the initial residual stresses K_I^r and for the applied stress K_I [1.4].

An "effective" stress intensity is then taken as $K_{eff} = K_I^r + K_I$. The superposition principal is illustrated schematically in Figure 1.1 for an edge crack growing through a compressive residual stress field which decreases linearly from a maximum value of the surface to zero at some depth a_o. For constant-amplitude, zero-to-maximum tension (R=0) loading, growth rate can be correlated in terms of the range of ΔK_{eff}, by using basic da/dN - ΔK data.

(ii) Crack Generated Residual Stress and the Closure Approach

The significance of crack generated residual stress was pointed out by Elber [1.5], who observed that the residual tensile displacement left in the wake of a crack would cause it to close before tensile load was removed (under $R \geq o$ loading) and thus generate compressive residual stresses in its wake. The crack would not open until a certain level of tensile loading was applied to overcome the crack opening stress resulting from the compressive residual stress. In this case, it is necessary to conduct elasto-plastic finite element analyses to keep track of crack-opening stress under variable amplitude loading.

To summarise, the superposition approach can be used primarily to predict growth rate under constant amplitude loading of cracks in a stable residual stress field. The closure model can be used to predict load sequence and mean stress effects in a specimen with crack-generated residual stress field. Due to its direct relevance to the present study, emphasis will be placed upon (i), and some attention will be devoted to (ii).

Influence of the Position of Residual Stress Peak on Fatigue Crack Propagation

It is of interest to the present study to find out which part of the peening induced residual stress field (for example, the part far away from the crack tip or that very near the crack tip) gives rise to a greater change in stress intensity. Efforts will be made to determine the relative contribution of the position and peak upon the net or effective stress intensity.

1.3.2 Experimental Investigation

The scarcity of experimental data in this area dictates that this work must involve extensive experimental work.

Fatigue testing using both rotating bend and uniaxial loading configurations have been extensively performed on un-notched and notched test specimens in four dissimilar widely used alloys. The

results from these tests have been supplemented by fractography, residual stress measurements and metallurgical examination in order to try to reveal the nature of the response of these materials to the peening and re-peening treatments.

In choosing experimental variables such as heat treatment condition, shot-peening process variables, machining parameters, surface finish and the severity of notches used, an attempt has been made to similate conditions which would typically be encountered in a fatigue conscious component in an aerospace application.

Fatigue Testing

Rotating bend fatigue testing using both a large specially built four point bend rig for testing relatively large specimens and two smaller "Krouse" type machines for testing small specimens were used to investigate the effect of peening and re-peening on the life of specimens made of the four materials used in the study. The use of both large and small specimens permitted the examination of stress gradient and size effects, whilst the larger specimens facilitated the evaluation of crack growth rate data.

Uniaxial fatigue testing was performed using a 100kN series-D Mayes Servo Hydraulic test rig fitted with a 45 lit/min hydraulic power supply, allowing test frequencies typically 50Hz. This type of testing was performed in order to examine more closely the propagation of short cracks in shot-peened components. It also permitted the investigation of the effect of the load ratio. The test machine was also fitted with a clam shell type furnace which could be used to test specimens at elevated temperatures.

Anciliary Testing

Attention was paid to the appearance of fracture surfaces in both peened and un-peened fatigue specimens. Optical and scanning electron microscopy was used to identify the location and nature of crack initiation sites, and to trace the shape of the crack throughout its development. This could then be compared to crack length observations made during the fatigue testing progress to give comprehensive crack

growth rate data. Crack detection and measurement during testing was performed using a number of techniques which are discussed in Chapter Three.

Residual stress measurements were performed both on fatigue specimens and small flat rectangular specimens in order to ascertain the degree of residual stress relaxation occurring and the effectiveness of re-peening in restoring residual stresses.

Additionally, routine mechanical testing and metallurgical examination, including x-ray diffraction were used to complete the experimental program.

1.4 LAYOUT OF THESIS

This thesis is divided into five main parts and contains seven chapters in total.

The first part, which is contained in Chapter One provides a brief introduction to, and description of this study, as well as justification of the need for work in this area.

Part Two provides a critical review of the current literature and outlines its paucity in certain areas. Both theoretical and experimental work is reviewed. This constitutes Chapter Two.

Part Three, which is contained in Chapter Three is devoted totally to the experimental techniques adopted during the investigations. The use of both a specially designed and built rotating bend rig and an electro-servo-hydraulic uniaxial fatigue rig are described and discussed. Details of numerous techniques used in the detection and monitoring of cracks are given and critically assessed in terms of this investigation.

Part Four is devoted to the application of three-dimensional finite element analysis in the determination of stress intensity factors for circumferentially cracked notched and un-notched components. These results are used to enable the detection of fatigue crack growth vs ΔK data. This comprises Chapter Four.

Of vital importance to these studies are the interactions between the three main aspects with which the thesis is concerned. These are Fatigue Crack Initiaion, Fatigue Crack Propagation, and Residual Stress Relaxation or IPR for short. Accordingly, Part Five of this thesis, which contain Chapters Five to Seven discusses these aspects in detail. Chapter Five details work which illustrates the inter-dependence of these factors and presents an integrated view of Fatigue Fracture in the Presence of Residual Stresses, whereas Chapter Six concentrates on the initiation and propagation of fatigue cracks. Finally, Chapter Seven considers the implications of the results for the effectiveness of re-peening partially fatigued components and provides general conclusions.

The materials selected for use in the experimental parts of this investigation are in widespread usage in the aerospace industry, and were supplied by Dowty Rotol Ltd., and Rolls-Royce, plc. The work was sponsored by the Science and Engineering Research Council under contract number GR/D/25958. Additional support was provided by Dowty Rotol Ltd., Rolls-Royce, plc., Vacu-Blast B.T.R. Ltd., Barton Abrasives Ltd., The Metal Improvement Company I.N.C., and a number of other organisations associated with the British Impact Treatment Association.

REFERENCES

[1.1] Meguid, S.A., Chee, E.B., The effect of peening and re-peening upon partially fatigued components, Journal of Mechanical Working Technology, 8, 1983, pp 129-146.

[1.2] Misumi, M., Ohkuba, M., Deceleration of small crack growth by shot-peening. Int. J. of Materials and Product Technology, Vol. 2, No. 1, 1987, pp 36-47.

[1.3] Morrow, J., Cyclic plastic strain energy and fatigue of metals, Internal Friction, Damping and Cyclic Plasticity, ASTM STP378, American Society for Testing and Materials, 1965, pp 45-87.

[1.4] Parker, A.P., The mechanics of fracture and fatigue, E. & F.N. Spoon, London, 1981.

[1.5] Elber, W., Damage tolerance in aircraft structures, ASTM 486, American Society for Testing and Materials, 1971, pp 230-242.

CHAPTER TWO

LITERATURE SURVEY

SUMMARY

2.1 Origin of Residual Stresses

2.2 Fatigue Fracture

- 2.2.1 Historical Perspective
- 2.2.2 Initiation Dominated Fatigue
- 2.2.3 Propagation Dominated Fatigue

2.3 Influence of Residual Stresses

2.4 Relaxation of Residual Stresses

- 2.4.1 Residual Stress Relaxation by Plastic Deformation
- 2.4.2 Thermal Residual Stress Relaxation

SUMMARY

This chapter provides a critical review of the current literature relating to the effect of residual stresses upon the fatigue fracture of metallic alloys. In an attempt to evaluate the concepts and ideas presented in the technical literature, an assessment of some of these concepts is presented. The work is divided into three sections: the first deals with the concept of residual stresses with special emphasis devoted to those introduced by shot peening; the second, with fatigue crack initiation and growth in the presence of residual stresses; and finally, the influence of cyclic loading and other factors on the magnitude and distribution of residual stresses.

2.1 ORIGIN OF RESIDUAL STRESSES

The absence of an applied load rarely means that a component is not in a state of finite stress. Inhomogenities in the structure, localised zones of deformation associated with forming processes and thermal history are all associated with residual stresses which can be of considerable magnitude. Clearly, residual stresses must balance in order for the component to be in equilibrium. Any removal of material, however, will influence the residual stress state and the component may even change shape in order to regain equilibrium. This is commonly observed when machining rolled or extruded products and presents particular problems in the machining of large close tolerance components.

Under failure mechanisms such as "high cycle" fatigue, stress corrosion cracking and brittle fracture which are essentially elastic, residual stresses will become superimposed upon applied loads hence influencing greatly the integrity of the component. Whilst a residual stress field must be comprised of both tensile and compressive regions, whichever sense of stress that is present in the most critical areas will determine the observed influence of the residual stresses. Since, on the macroscopic scale, the surface is usually the most critical area of the component, residual stress fields involving compression at the surface can offer considerable enhancement in the fatigue and stress corrosion performance of a component.

On the microscopic scale, second phase particles are usually associated with significant residual stresses, due to differences in thermal expansion

or simple latice mis-match. Whilst residual stresses on this scale are essentially self-equilibrating on the scale of linearised fatigue crack growth, phase changes involving a change in volume can play an important role in residual stress development and metalurgical stability.

The shot-peening process, like nearly all cold working processes, produces a highly non-uniform deformation. In this case, the surface is bomabarded with small rounded particles which produce small zones of plasticity upon impact. Since the exposed material is forced into the surface, against the elastic constraint surrounding the impact zone, the rebound of the particle and associated unloading of the component leaves the plastic zone in a state of residual compression. The process has been analysed in a number of ways, but the complexity of constitutive relationships on this small scale at high strain rates makes precise analysis very difficult. Nevertheless, work by Kyriacou [2.1] and Wohlfahrt [2.2] amongst others essentially show the same trends and magnitudes of residual stresses as have been found experimentally.

The peening process itself has a number of variants and the consideration of how peening should be applied to any particular component involves a number of crucial factors. These include surface contamination, surface roughening, overworking, distortion, errosion and the consistency of the treatment as this profoundly affects the cost of applying the process.

Whilst shot-peening is an example of a process specifically used for the introduction of residual stresses, most other machining, forming and fabrication processes involve the generation of residual stresses. Occasionally, as with rolling or grinding, the process variables may be chosen to produce desirable residual stress distributions. However, where this is not feasible, components may contain significant deleterious residual stresses which must either be allowed for at the design stage or modified by subsequent treatment. The influence of residual stresses in weldments has been studied by Glinka [2.3]. Since welding residual stress fields tend to be on a larger scale than those due to peening, they represent an analogue which is more easily studied experimentally. The residual stresses associated with welds are due principally to the inside of the weld solidification and cooling first, due to greater conductive heat flow. The shape of the joint is then essentially fixed and the

contraction of surface layers as they cool, generates the residual tensile stress in the surface which is in part responsible for the generally poor fatigue performance of welds.

2.2 FATIGUE FRACTURE

2.2.1 Historical Perspective

Early observations of the failure of cyclically loaded components at stresses lower than those required to precipitate static failure prompted systematic studies of the "fatigue strength" of components. Wöhler studied the failure of railway axles in the 1850's and presented his data in the form of a load versus cycles to failure graph, a form which is recognised to this day and still used for design. An S.N. or Wöhler diagram of this type is depicted in Fig. 2.1.

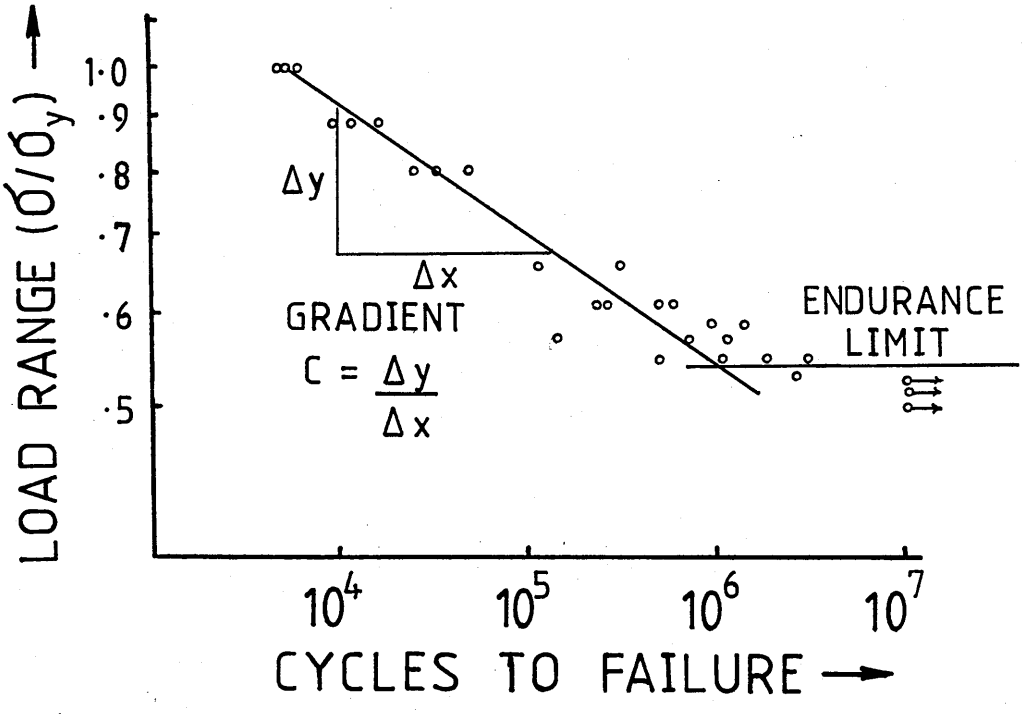

FIGURE 2.1 S.N. or Wöhler diagram

The fatigue life of a component is affected by a large number of factors. S.N. curves only convey information relating to the total life as a function of the applied stress range. The second factor to attract the attention of early workers was the influence of the mean load. Gerber and Goodman using early data, established relationships between mean stress and fatigue life which, are still in use for tensile mean stresses.

As more data became available it was apparent that other factors played important roles in determining the fatigue life and fatigue strength of components. Different materials appeared to react differently to stress raising geometrical features. A third factor was then proposed to aid in the evaluation of the effect of notches on the fatigue life and fatigue strength. This, the notch sensitivity factor 'q', in a purely empirical way, took in a large number of factors associated with stress gradient effects, material homogeneity, cyclic strain hardening/softening characteristics, characteristic defect size, etc., and in many cases did not yield accurate or conservative predictions.

The approach thus far discussed makes no distinction between fatigue crack initiation and propagation, and without individual component testing, requires the substantial idealisation of both geometry and load history to permit predictions to be made. S.N. curves do, however, illustrate a number of points in relation to fatigue life. In particular, the form of an S.N. curve can yield information on the nature of the fatigue, i.e., if it is initiation dominated or propagation dominated. The precise nature of initiation and propagation dominated fatigue is discussed in the following sections.

2.2.2 Initiation Dominated Fatigue

The intiation of a fatigue crack has no strict definition. Many investigators define a size of crack, e.g., a non-destructive test limit [2.4, 2.5] or a size where the crack behaves predictably [2.6] and cracks smaller than this are said to be in the initiation phase, whilst cracks of greater size are said to be in the propagation phase. Alternatively, since initiation processes are very sensitive to yield strength, components having initiation dominated fatigue life may be increased in fatigue life and strength by using a finer grain size and harder material condition. In components experiencing propagation dominated fatigue, an increase in hardness will have the opposite effect on fatigue life as the material will be less defect tolerant [2.7].

Initiation dominated fatigue is associated with components not already containing crack-like defects or acute stress raisers such as notches or brittle inclusions. In effect, once a crack is formed in these components, the gross stress concentration generated by the crack ensures that crack propagation is a relatively rapid process and so only accounts for a small proportion of the total fatigue life.

In the absence of a crack-like defect the behaviour of a component will be analagous to that of a plain fatigue specimen. The presence of a notch can be considered as depicted in Fig. 2.2 as used by Morrow [2.8]. In visualising the problem thus, use can be made of experimental results relating to the failure of plain specimens in strain controlled cycling. Essentially at the root of any geometical discontinuity a notional fatigue specimen is being subjected to strain cycles determined by the elastic deformation of the bulk of the component.

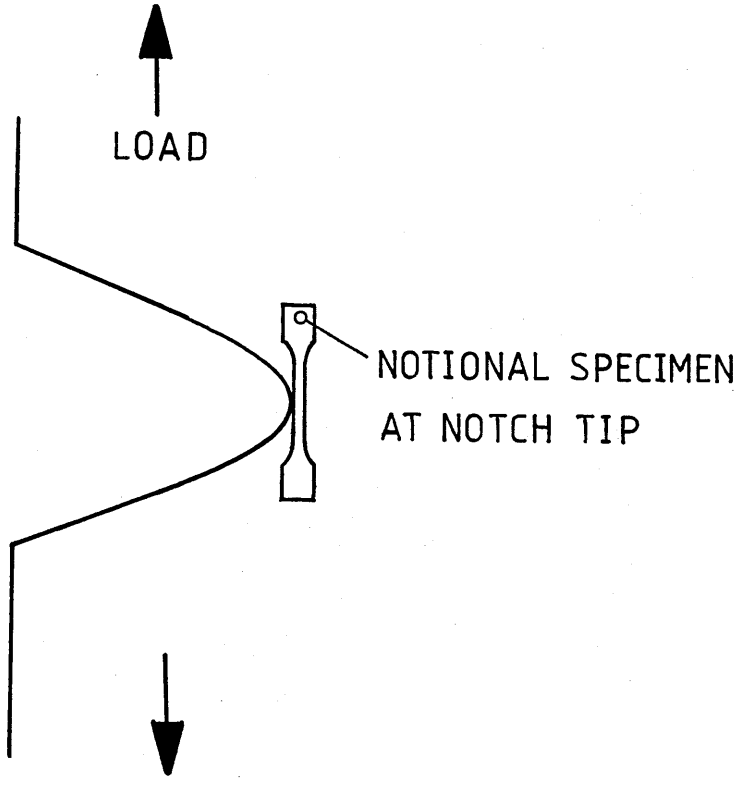

FIGURE 2.2 Initiation model in a notched specimen

Figure 2.3 gives the relationship between plastic strain range and cycles to failure for plain specimens. Naturally, part of the life of these specimens will be due to fatigue crack propagation, but as discussed earlier we are concerned with the behaviour of a small ligament in a component which when broken, by whatever means, will constitute a crack nucleus.

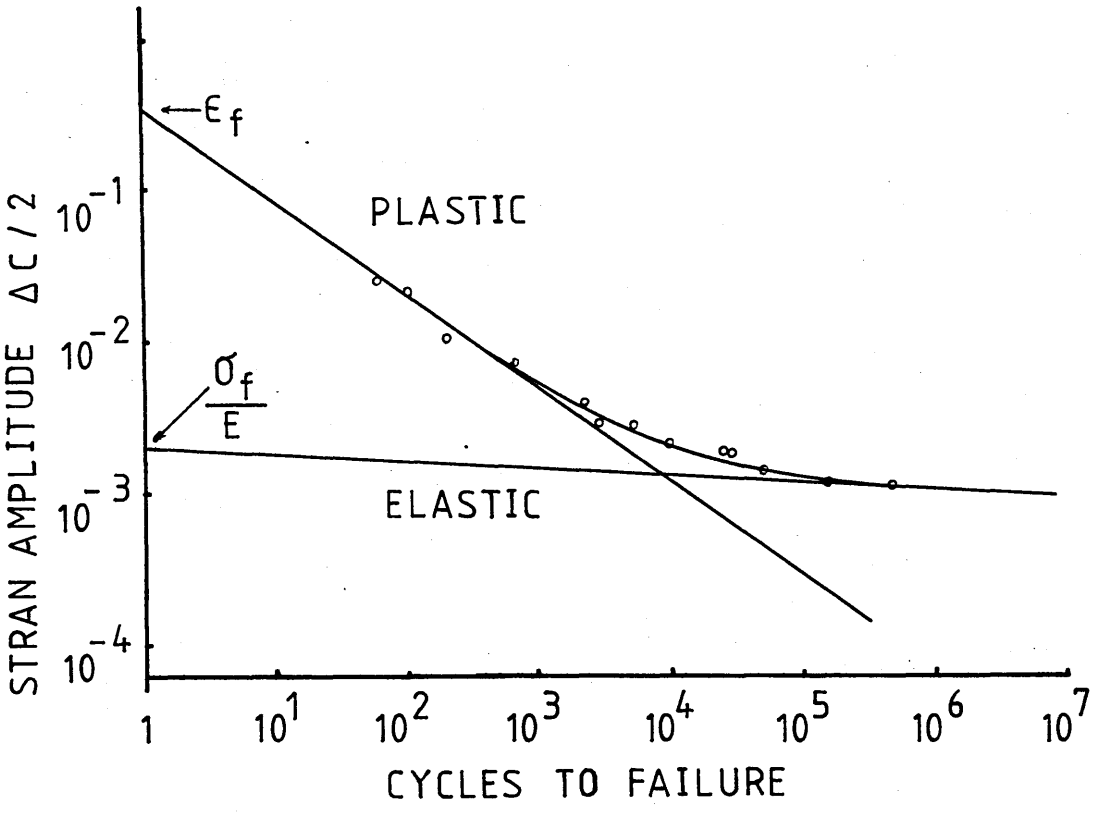

FIGURE 2.3 Relationship between plastic strain range and total life of a plain specimen

In essence initiation processes are those which concern local properties rather than those of the bulk. Therefore, it must be considered that initiation processes will demonstrate the response of the weakest domain in the critical area, not the average as with a plain test piece. This aside, the gradient C of a plastic strain range versus cycles to failure is reflected in the gradient of S.N. curves for components with initiation dominated fatigue life [2.7].

A further illustration of the difference between initiation and propagation dominated behaviour has been advanced by Kitagawa and Takahashi [2.9]. The full significance of this will emerge in the next section, but at this stage, it is evident in Fig. 2.4 that the threshold for crack growth is dependant on crack length down to a particular value, whereas behaviour below this level of defect size is independent of crack size, and coincides with the plain fatigue limit of the material.

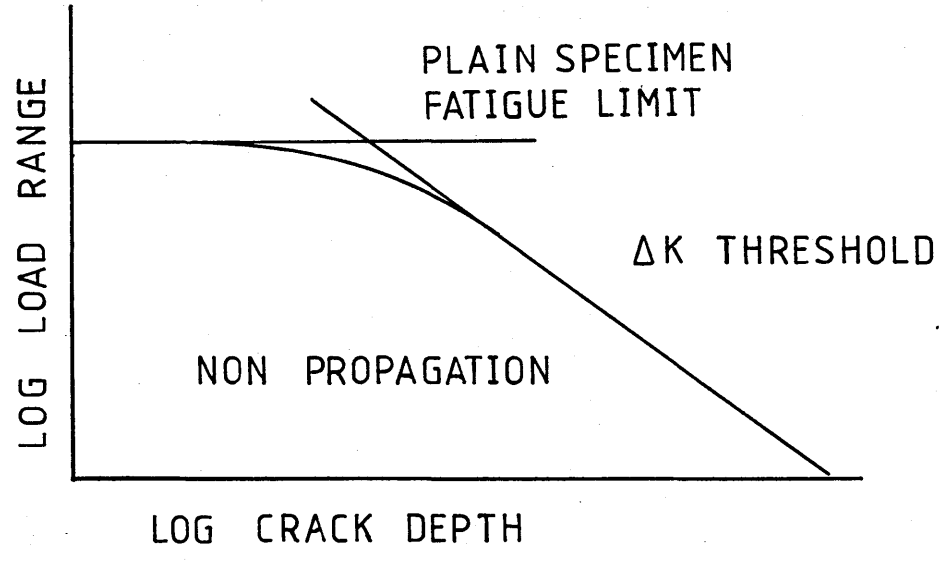

FIGURE 2.4 Kitagawa Takahashi diagram

The nature of the crack initiation processes has attracted attention for a long time and slip mechanisms proposed which account for the development of recognisable microstructural features associated with crack initiation, e.g., persistent slip bands, voids, extrusions and intrusions [2.10]. The significant feature of these processes is that they involve slip, and hence may be greatly affected by mechnical working processes which refine substructure and increase dislocation density.

Crack initiation frequently occurs at free surfaces as surface intersecting grains are less constrained by their surroundings and hence exhibit a lower flow stress. The existance of any bending or stress concentration effects also ensures that stress levels are generally higher at surfaces than in the bulk material. External surfaces may also be associated with compositional inhomogeneities such as decarburisation or oxidation. These factors tend to promote surface initiation, though initiation at sub-surface features is also not uncommon [2.11, 2.12] and is particularly associated with situations where surface crack initiation is suppressed by local hardening or residual stresses. This being the case, crack nucleation at sub-surface inclusions, voids or triple points can be observed.

2.2.3 Propagation Dominated Fatigue

Propagation dominted fatigue has attracted much attention in the literature. This is in part due to the number of situations where components contain crack-like defects which in effect condense the initiation stage to a small number of cycles. Another reason for the richness of the literature in this area is that some success has been encountered in predicting the growth rate of cracks in many situations though many anomalies still remain.

Forsyth [2.13] proposed that the progress of fatigue fracture could be sub-divided into four distinct regimes. These are shown in Fig. 2.5. Initiation as we have discussed previously is concerned with yielding on the microscopic scale, and is very much influenced by structural features within the material. Stage I crack propagation occurs when the fatigue crack follows planes of maximum resolved shear stress. This occurs at 45° to the direction of the maximum principle stress. These cracks are hence loaded in mixed mode. Stage II propagation involves crack extension in the plane of the maximum principle stress, i.e., mode I loading. The transition from Stage I to Stage II propagation frequently occurs at short crack lengths, with the result that only a small proportion of the area of the fatigue fracture surface represents Stage I propagation. Work by Cox and Field [2.14] highlighted the effect of the stress state on the mode of crack propagation. Whilst microstructural features influenced the change over point, Stage I propagation was found to be unstable at values of the ratio of the maximum principle stress to maximum shear stress of 1.5:1 and above. After this value had been exceeded, cracks tend to revert to Mode II behaviour.

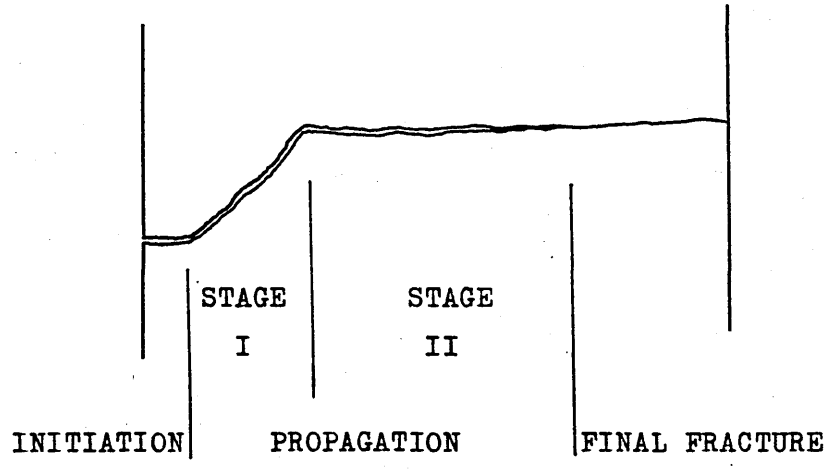

FIGURE 2.5 Four regimes of failure after Forsyth

Before considering the impact of the Linear Elastic Fracture Mechanics Methodology, it is vital to consider the relative sizes of cracks, microstructural features and specimen geometry. Figure 2.6 shows some of the features which affect fatigue crack propagation. The essential point is that crack propagation is influenced by many types of interactions. The growth of a crack which is large in comparison to these features can be approximated to a continum problem. Cracks of dimensions comparable to these features will, however, not behave in this way. This is occasionally referred to as the "Short Crack Problem" though as can be seen it is inevitable given the nature of fatigue.

The use of K, the stress intensity factor, to characterise the stress state ahead of a crack tip is well discussed in the literature and has been described in [2.15]. Representing crack growth rate in Mode I in terms of ΔK_I the tensile part of the applied stress intensity range, Fig. 2.7 shows a sigmoidal relationship. The central part of this curve can be approximated to a straight line and fitted to a simple crack growth law such as that of Paris:

$$\frac{da}{dN} = C\ \Delta K^m \qquad (2.1)$$

where a = crack length, N = number of cycles, and C and m are experimentally determined constants.

In situations where the pre existing defect size in the material is large enough to place the behaviour of the component into the central portion of the fatigue crack growth curve, the Paris Law, or one of its derivatives can successfully be used to predict the growth of the crack. This is typical of many large forgings containing laps and defects of the 500μm to 2mm size, or welded structures, where defects may be a substantial proportion of the component's thickness.

Final fracture will occur when the fatigue crack has attained a size where the component fails by leakage, brittle fracture, ductile overload, excessive deformation, etc. This may well lie within the linear section of the growth rate versus ΔK curve enabling an accurate prediction of life to be made by integrating such a law as that of Paris. Considering this case, i.e., propagation dominated fatigue where the crack obeys a Paris-type Law, the S.N. curve will be characterised by two lines. The slope of the low-cycle end of the curve will have a gradient of -m where m is the exponent

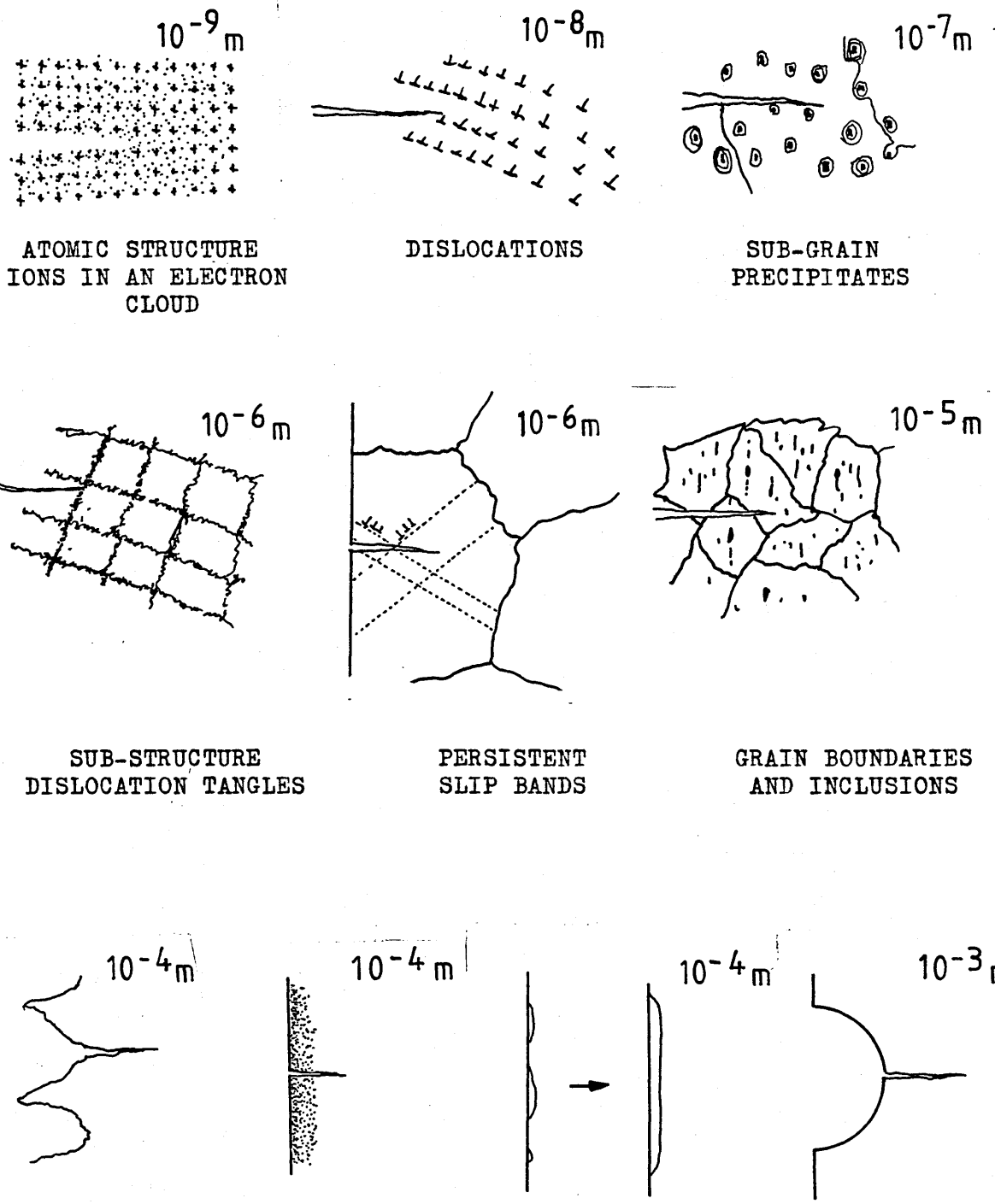

FIGURE 2.6 Relative scale of cracks and microstructural features

in the growth rate law and the threshold will be determined by a ΔK threshold which will be a function of the initial defect size, i.e.,

$$\Delta\sigma_{th} = \frac{\Delta K_{th}}{\sqrt{\pi a}} \qquad (2.2)$$

where $\Delta\sigma_{th}$ = the fatigue limit and ΔK_{th} = threshold stress intensity range below which a crack will not propagate.

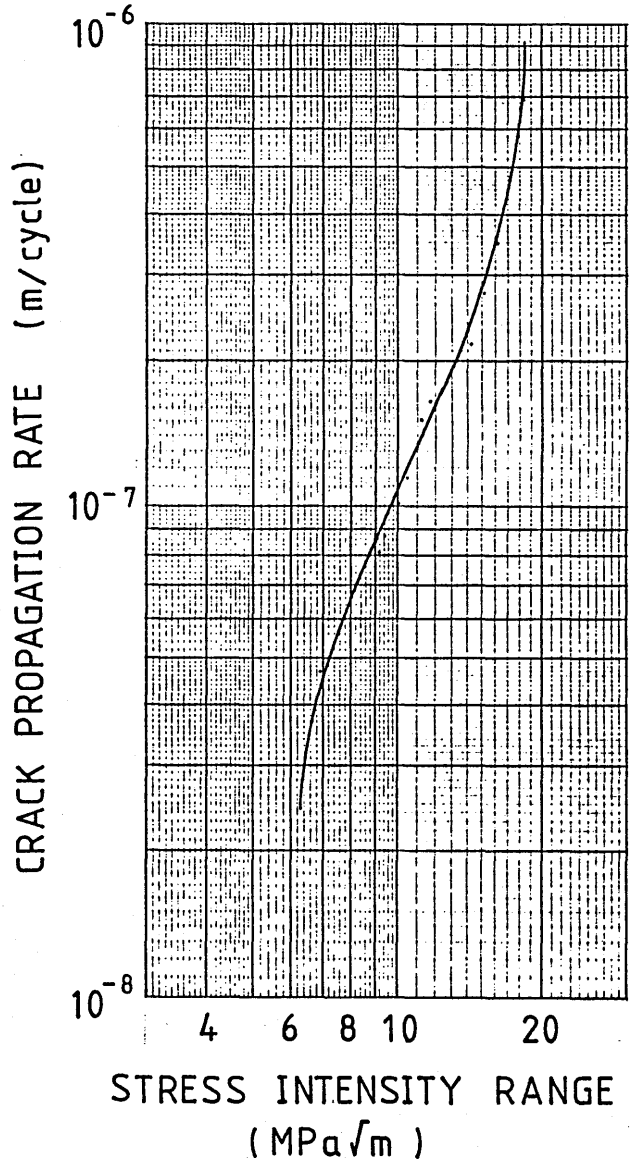

FIGURE 2.7 Crack growth rate as a function of K_I

2.3 INFLUENCE OF RESIDUAL STRESSES

Fatigue crack propagation is a process involving the successive blunting and re-sharpening of a crack within a zone of plasticity. At its simplest, when a crack opening load is applied, the plastic zone yields intension. When the load is removed, the crack closes and the elastic recovery of the bulk of the specimen generates a residual compressive stress in the plastic zone. Application of a compressive load will not always reverse this situation as the closed crack faces will carry much of the load. This is referred to as "crack closure", which creates another discrepanccy between short cracks with little closure effect, and longer cracks. Plastic zone size, r_p, is given approximately by the following equation:

$$r_p = \frac{1}{c\pi}\left(\frac{\Delta K}{\sigma_y}\right)^2 \qquad (2.3)$$

where c equals two for plane stress and six for plane strain.

Whilst steady crack propagation is in progress rp changes only slowly, hence the residual stress field generated in the vicinity of the crack is relatively constant, and its effect can be taken into the variables used in the linear approach.

The existence of a residual stress in addition to that associated with a steadily propagating crack must be accounted for in some way. Where the principle of superposition is applicable, i.e., elastic behaviour on the macroscopic scale, the residual stress may be characterised as a stress intensity and added to the applied load, as given below:

$$K_{Effective} = K_{Applied} + K_{Residual} \qquad (2.4)$$

In [2.16] Underwood and throop give the following solution for K_I residual for a linear varying residual stress of σ_o at the surface and σ_a at the crack tip:

$$\frac{K_I}{\sqrt{\pi a}} = 1.2\ \sigma_o - 0.68\ (\sigma_o - \sigma_a) \qquad (2.5)$$

Meguid and Coufopanos [2.17] give a solution derived from finite element results for a cracked plate partially yielded in tension using the

following expression for K_I as a function of a point load on the crack face. This is depicted schematically in Fig. 2.8.

$$K_I^r = \int_0^a \frac{2\sigma_v^\rho(x)}{\sqrt{\pi a}} F\left(\frac{x}{a}, \frac{a}{w}\right) \qquad (2.6)$$

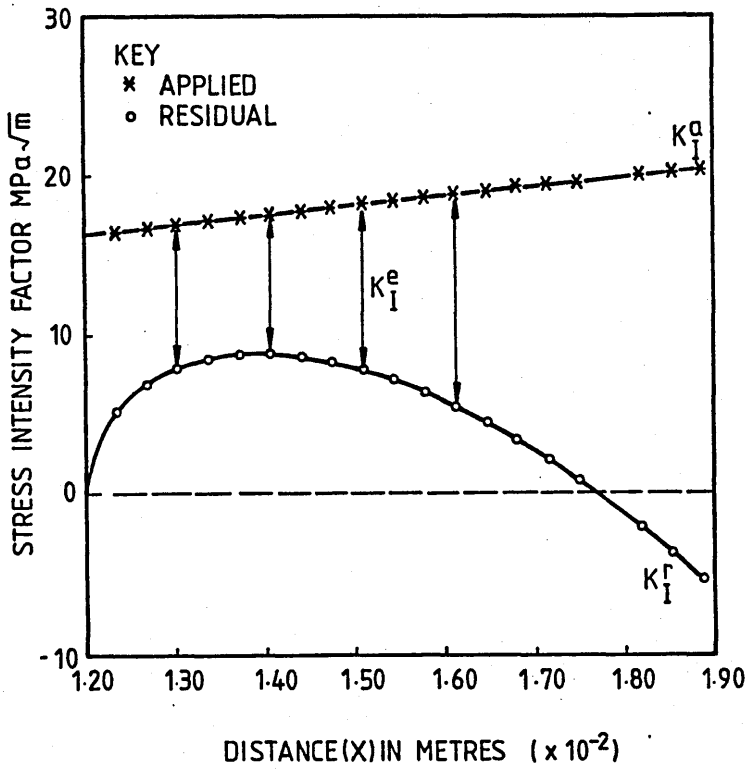

FIGURE 2.8 Schematic representation of the super position principal as applied to a partially yielded cracked plate

Alternatively, a weight function approach can be utilised as suggested by Bückner [2.18].

These characterizations of residual stress take no account of non linearity in the vicinity of the crack tip, but in effect supplement or cancel out part of the applied load consistently so that provided macroscopic yielding does not occur, the principal can be used accurately. In terms of fatigue, residual stresses change the mean stress level and are hence analagous to crack closure. Keyvanfar [2.19] used a closure model to predict the influence of residual stresses on fatigue crack propagation. Alternatively, by idealising a complex residual stress field, Glinka was able to model crack propagation in a welded specimen [2.3] and though the results were not entirely accurate, Parker [2.20] points out a means of reducing the error whilst still using the linearised approach.

2.4 RELAXATION OF RESIDUAL STRESSES

Having established that residual stresses play a vital part in the process of the initiation and propagation of fatigue cracks, it is clear that generation and decay of residual stresses will influence the integrity of fatigue conscious components. Three basic mechanisms exist by which residual stresses can be depleated. These are: firstly, plastic deformation; secondly, thermally activated relaxation, and finally metal removal or the generation of new surface, for example, crack extension.

2.4.1 Residual Stress by Plastic Deformation

James [2.21] proposed the delineation of these relaxation phenomen into three regimes: loads inducing general plasticity, loads below the endurance limit, and an intemediary regime. The first regime concerns macroscopic yielding where the rapid redistribution of residual stresses may be accompanied by material recovery or work hardening processes [2.22, 2.23 2.24]. Loads below or near the endurance limit have also been reported to effect residual stress relaxation [2.25, 2.26]. This is generally attributed to small scale plasticity effects such as dislocation pile up and stress concentration effects at grain and phase boundaries. The third regime accounts for situations lying between these extremes. Situations within this regime are characteristic of many critical fatigue conscious components. The distinction is useful in that, whilst fundamentally only a matter of scale separates the extremes, it is convenient to isolate essentially elastic conditions from elasto-plastic conditions.

It is, of course, not possible to satisfactorily separate load induced relaxation and relaxation produced by exposure to elevated temperatures as loads represent the driving force for relaxation and thermally activated processes represent the mechanism by which relaxation can occur. They will hence act synergistically.

Having referred to the relaxation of residual stresses due to loading, it is worth highlighting one of the observations of Zurek et.al [2.27].

Initially, stress free 7075 specimens were found on cycling, R=0 σ_{max} = 450MPa ~ σ_y to rapidly generate a compressive residual surface stress of around 200MPa as shown in Fig. 2.9. Surface grains, being less constrained, exhibit a lower flow stress and so deform at stress levels

where the bulk of the component behaves more or less elastically. The resulting inhomogeneous deformation generates residual stresses and James's observation that the residual stress development was most marked in coarser grained material supports this. The presence of any features such as inclusions, cracks or voids will also generate inhomoheneous deformation and hence residual stresses.

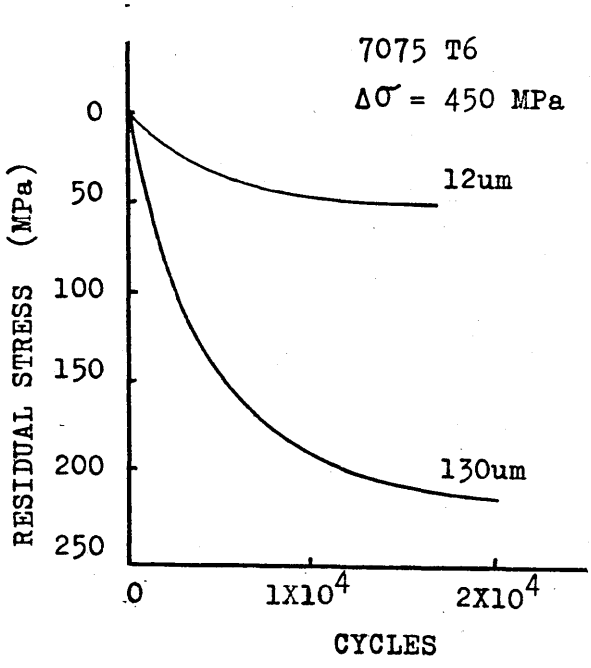

FIGURE 2.9 Residual stress due to cycling in 7075 after Zurek et. al.

In a consideration of the fatigue life of blast cleaned cast components, Neff [2.28] by defining the change in residual stress as a discontinuous function of the applied stress range, was able to equate the endurance limit of the material with the stress range at which negligible relaxation occurred, Fig. 2.10.

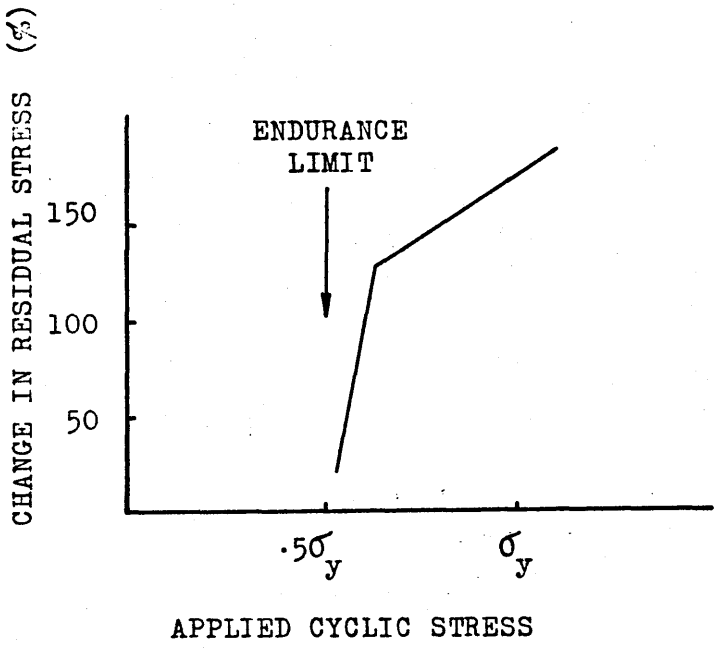

FIGURE 2.10 Coincidence of endurance limit and point of negligable residual stress, after Neff.

Finally, controlled plastic deformation can be used to reduce undesirable residual stresses in certain product forms and components. Referring to the international aluminium designation system, the condition T—51 refers to the controlled stretching of bar products in order to attenuate residual stresses associated with forging and extrusion. A variety of static and vibratory loading techniques may be used on components and structures, but in many instances the processes go beyond the elimination of undesirable residual stresses, producing compressive residual stresses in the vicinity of strain concentrators.

2.4.2 Thermal Residual Stress Relaxation

Essentially any atomic re-arrangements will affect the state of stress or strain of the lattice. Yielding is a process of gross re-arrangement, but differs only in scale from minor disloation re-arrangements. Such atomic movements are governed by energetic consideration [2.29].

The Arhenius equation given below is based on the principle that the rate of a thermally activated process is dependent linearly on the number of atoms having more than a threshold activation energy ΔE. Where R is the universal gas constant, T is the temperature in degrees absolute and D_o is the rate constant.

$$D = D_o \, e \left(\frac{-\Delta E}{RT} \right) \qquad (2.7)$$

Whilst this accurately predicts the dependency of creep and yielding on temperature over small ranges of temperature, it cannot be used more generally as both D_o, the rate constant and ΔE, the activation energy are dependant on the precise mechanics of the process, and changes in mechanism with temperature and condition will necessitate the use of a different values.

In terms of residual stress relaxation, the most rapid diminuition will be associated with taking the material to a temperature at which its flow stress becomes less than the magnitude of the residual stress. In this situation the temperature determines the degree of relaxation and the time at temperature has less relative significance. Temperatures in this range will also be associated with other microstructural changes [2.30].

Relaxation is possible at lower temperatures as classical creep within the component will allow residual stress fields to relax. Phase changes involving the growth or shrinkage of particles of differing density to the matrix will also influence and be influenced by the residual stress state tending to reduce the residual stresses [2.31].

At lower temperatures the microstructural features of most structural alloys greatly limits the extent to which any minor atomic rearrangements such as dislocation glide produces residual stress relaxation [2.21]. In these situations both temperature, time at temperature and metallurgical condition are all critical.

LIST OF FIGURES

2.1 S.N. or Wöhler diagram

2.2 Initiation model in a notched specimen

2.3 Relationship between plastic strain range and total life of plain specimens. Gradient = c.

2.4 Kitagawa-Takahashi diagram

2.5 Four regimes of failure after Forsyth [2.13]

2.6 Relative scale of cracks and microstructural features

2.7 Crack growth rate in model as a function of ΔKI

2.8 Schematic representation of the superposition principle as applied to a partially yielded cracked plate [2.17]

2.9 Residual stress due to cycling in 7075 after Zurek et.al [2.17]

2.10 Coincidence of endurance limit and point of negligible residual stress relaxation after Neff [2.28].

REFERENCES

[2.1] Kyriacou, S., The mechanics of the shot-peening process, M.Sc. Dissertation, Cranfield, Instiute of Technology, 1987.

[2.2] Wohlfahrt, H., Shot peening and residual stresses, Proc. 28th Sagamore Army Materials Conference, 13-17 July, 1981, Ed. E. Kula and V Weiss, Plenum Press New York, 1982, pp 71-92.

[2.3] Glinka, G., Effect of residual stresses on fatigue crack growth in steel weldments under constant and variable loads, in Fracture Mechanics, ASTM STP 677, Ed. C.W. Smith, American Society for Materials and Testing, 1979, pp 198-214.

[2.4] Nelson, D.V., and Socie, D.F., Crack initiation and propagation approaches to fatigue analysis, in Design of Fatigue and Fracture Resistant Structures, ASTM STP 761, Ed. P.R. Abelkis and C.M. Hudson, American Society for Testing and Materials, 1982, pp 110-132.

[2.5] Rudd, J.L., Brussat, T.R., Chiu, S.T., and Creager, M., Experimental evaluation of initial flaw criticality and analysis methods for damage and tolerant airforce aircraft, in Design of Fatigue and Fracture Resistant Structures, ASTM STP 761, Ed. P.R., Abelkis and C.M. Hudson, American Society for Testing and Materials, 1982, pp 152-171.

[2.6] Bucci, R.J., Development of basis materials data for evaluating crack growth life, in Part Through Crack Fatigue Life Prediction, ASTM STP 687, Ed. J.B. Chang, American Society for Testing and Materials, 1979, pp 47-73.

[2.7] Pook, L.P., The role of crack growth in metal fatigue, The Metals Society, London, 1983.

[2.8] Morrow, J., Cyclic plastic strain energy and fatigue of metals, Internal Friction, Damping and Cyclic Plasticity, ASTM STP 378, American Society for Testing and Materials, 1965, pp 45-87.

[2.9] Kitagawa, H., and Takahashi, S., Applicability of fracture mechanics to very small cracks, Proc. Second International Conference on Mechanical Behaviour of Materials, Boston, 1976, pp 627-631.

[2.10] Frost, N.E., Marsh, K.J., and Pook, L.P., Metal fatigue, Clarendon Press, Oxford 1974.

[2.11] Starker, P., Wohlfahrt, H., and Macherauch, E., Sub-surface crack initiation during fatigue as a result of residual stresses, Fatigue of Engineering Materials and Structures, Vol. 1, 1979, pp 319-327.

[2.12] Syren, B., Wohlfahrt, H., and Macherauch, E., The influence of residual stresses and surface topography on bending fatigue strength of machined Ck45 in different heat treatment conditions, Proc. 2nd International Conference on Mechanical Behaviour of Materials, Boston, 1976, pp 212-235.

[2.13] Forsyth, P.J.E., in The physical basis of metal fatigue, Blackie, 1969.

[2.14] Cox, H.L., and Field, J.E., The initiation and propagation of fatigue cracks in mild steel pieces of square section, Aeronaut. Q., Vol. 4, 1952, pp 1-18.

[2.15] Paris, P.C., The fracture mechanics approach to fatigue - An inter-disciplinary approach, Proc. 10th Sagamore Army Materials Research Conference, Syracuse University Press, New York, 1964.

[2.16] Underwood, J.H., and Throop, J.E., Surface crack K-estimates and fatigue life calculations in cannon tubes, in Part Through Crack Life Prediction, ASTM STP 687, Ed. J.B.C. Chang, American Society for Testing and Materials, 1979, pp 195-210.

[2.17] Meguid, S.A., and Coufopanos, J.A., Elasto-plastic finite-element study of the effect of residual stresses upon double edge-cracked plate, Engineering Fracture Mechanics, Vol. 22, No. 4, 1986, pp p735-744.

[2.18] Bückner, H.F., Zeitschrift für Angewandte Mathematik and Mechanik, Vol. 50, 1970, pp 529-549.

[2.19] Kegvanfar, F., Effects of residual stresses on fatigue crack propagation, Doctoral Thesis, Stanford University, 1985.

[2.20] Parker, A.P., Written Discussion in Residual Stress Effects in Fatigue, ASTM STP 776, American Society for Testing and Materials, 1982, pp 188-195.

[2.21] James, M.R., The relaxation of residual stresses during fatigue in Residual Stress and Stress Relaxation, Ed. E. Kula, and V. Weiss, Plenum Publishing Corp., 1982, pp 297-313.

[2.22] Boggs, B.D., and Byrne, J.G., Fatigue stability of residual stress in shot peened alloys, Metallurgical Transactions, 4A, 1973, pp 2153-2157.

[2.23] McClinton, M., and Cohen, J.B., Changes in residual stress during the tension fatigue of normalised and peened SAE 1040 steel, Materials Science and Engineering, Vol. 56, pp 259-263.

[2.24] Voskamp, A.P., Österlund, R., Becker, P.C., and Vingsbo, O., Gradual changes in residual stress and microstructure during contact fatigue in ball bearings, Metals Technology, Vol. 7, 1980, pp 14-21.

[2.25] Gould, R.W., and Pitella, C.F., An x-ray investigation of fatigue behaviour of cold worked aluminium, in Advances in X-ray Analysis, Vol. 16, 1973, pp 534-566.

[2.26] Pattinson, E.J., and Dugdale, D.S., Fading of residual stresses due to repeated loading, Metallurgia, Vol. 66, No. 397, 1962, pp 228-230.

[2.27] Zurek, A.K., James, M.R., and Morris, W.L., The effect of grain size on fatigue growth of short cracks, Metallurgical Transactions A, Vol. 14, A. Aug. 1983, pp 1697-1705.

[2.28] Neff, P.J., A qualatative evaluation of surface residual stress and its relation to fatigue performance. Proc. Residual Stress for Designers and Metallurgists, Ed. Carry J-Vande Walle, American Society of Metals, 1981, pp 119-136.

[2.29] Adeyemi, M.B., Stark, R.A., and Modlen, G.F., Isothermal stress relief of cold-extruded mild steel rods. Proc. Heat Treatment 79, Birminghm, U.K., Metals Society, London, 1980, pp 122-125.

[2.30] Metals Handbook, Volume 4, Heat Treating, Ninth Edition, American Society for Testing and Materials, 1981.

[2.31] Potter, J.M., and Millard, R.A., The effect of temperature and load cycling on the relaxation of residual stresses in Advances in X-ray Analysis. Vol. 20, Ed. H.G. McMurdie, Plenum Press, 197, pp 309-319.

CHAPTER THREE

EXPERIMENTAL TECHNIQUES

SUMMARY

3.1 Fatigue Testing Techniques

3.1.1 Rotating Bend Fatigue Testing
3.1.2 Servo-hydraulic Uniaxial Fatigue Testing

3.2 Crack Size Measuring Techniques

3.2.1 Industrial Non-Destructive Examination
3.2.2 Laboratory Techniques

3.3 A Novel Stroboscope Using Light Emitting Diode Lamps for the Inspection of Fatigue Cracks

3.4 Shot Peening

3.5 Residual Stress Measurement

3.5.1 X-ray Diffraction
3.5.2 Hole Drilling
3.5.3 Dissection Method

SUMMARY

This chapter describes the experimental techniques used in the current work. The possibilities and limitations of these methods together with other approaches which are relevant but which were not selected for use are discussed within the context of the study of fatigue and fracture in metallic components.

Attention is paid to the industrial aspects of component integrity in so far as a common rational may be used to compare laboratory fatigue results with realistic engineering situations.

3.1 FATIGUE TESTING TECHNIQUES

The essence of engineering sciences is to collect and represent information and test data in such a way that it can be used to accurately predict the probable outcome of a particular situation.

The prediction of the fatigue life of a component relies upon fatigue testing at some stage. Whilst calculation procedures using crack length or some other measure of cumulative damage, can be used to predict the life of a new structure, the basis for the approach relies upon observations of the rate of damage accumulation in that material under loading conditions which can be related in some way to those of the new structure. Naturally, many factors influence fatigue life, and in particular, experimentalists are concerned with some of the following groups of variables:

Load – presence of stress gradients, degree of triaxiality, load waveform, magnitude, degree of load reversal, sequence effects.

Temperature – effect of uniform temperature, effect of thermal gradients, microstructural changes.

Time – test frequency, time at temperature, strain rate sensitivity.

Environment - effect of humidity or the presence of corrosive agents, neutron radiation.

Material - bulk properties and the influence of inhomogeneities.

The ideal or aim of the study of fatigue fracture is to develop a rational which enables consideration of all these factors so that, with reference to a limited amount of fatigue test data, an accurate estimate of the probable life of a new component or structure can be made. The current state of the art lies a little short of this, though some methodologies have gained widespread acceptance for particular types of problems [3.1,3.2].

In this investigation the factors which have been studied in detail are those relating to load and material. Attention is also paid to time and temperature in so far as that they affect residual stresses and material condition.

Fatigue testing may be performed in a variety of ways according to the aforementioned factors. The testing involved in this work utilised two different types of fatigue testing.

3.1.1 Rotating Bend Fatigue Testing

Rotating bend fatigue rigs have been in use since the work of Wöhler [3.3] as they provide a simple and effective means of examining effect of the cyclic applied stress range on a material. In its simplest form, the specimen is clamped into the test machine in such a way that it forms a section of a shaft which is subjected to a static bending moment. When the shaft is rotated any one point on the surface of the specimen will alternately be in a position where the bending moment induces tensile or compressive fibre stresses. Thus, one rotation of the shafft coincides with one fatigue cycle of sinusoidally varying load with a load ratio of R = -1, i.e., the load is fully reversed with $\sigma_{min} = \sigma_{max}$. Whilst it is in principle possible to apply an additional axial load to the specimen to give independent control of σ_{max} and σ_{min} this is not generally done as there exists much data in the literature on the influence of the load ratio [3.4].

The two basic configurations of rotating bend fatigue machine are depicted in Figure 3.1. The three point bend configuration as shown in Figure 3.1 (a). As a consequence of the finite length of the lever arm there will exist a bending moment gradient across the specimen. In practice, the use of a lever which is large in comparison to the central portion of the specimen minimises the effect of this non-uniformity. In the arrangement shown, the specimen is fixed to the motor by a collet arrangement. The other end of the specimen is fixed similarly to a shaft which is being subjected to a vertical force at its far end, thus creating the bending moment.

The four point bend configuration, however, does produce a uniform bending moment over the length of the specimen. This is accomplished by applying a moment at each end of the shaft so that, between the inner bearings the moment is uniform. In the arrangement shown in Figure 3.1(b), the inner bearings are supported, whilst the outer bearings are subjected to a downward force. In order to rotate the shafts and specimen, flexible couplings are employed to attach the motor which is fixed, to the end of the drive shaft, which in this configuration will be displaced downwards by the load.

Conventional rotating bend fatigue testing is best suited to studying the integrity of specimens under the influence of constant amplitude testing, though simple load sequence effects can be studied by varying the test load during the test. It is also extremely well suited to the study of surface treatments as the influence of the bending in stressing the surface more highly than the sub-surface accentuates the influence of the surface treatment under used.

For the current investigation, use was made of a large specially built four point rotating bend rig, depicted in Fig. 3.2. This permitted the testing of larger specimens which may be shot peened without the risk of significant distortion. The specimen is clamped so that it forms the central portion of the main shaft. This shaft is supported by two pairs of self-aligning bearings. The outer bearings apply the load created by the weights to the shaft whilst the inner pair of bearings restrain the shaft vertically, and thus apply opposite

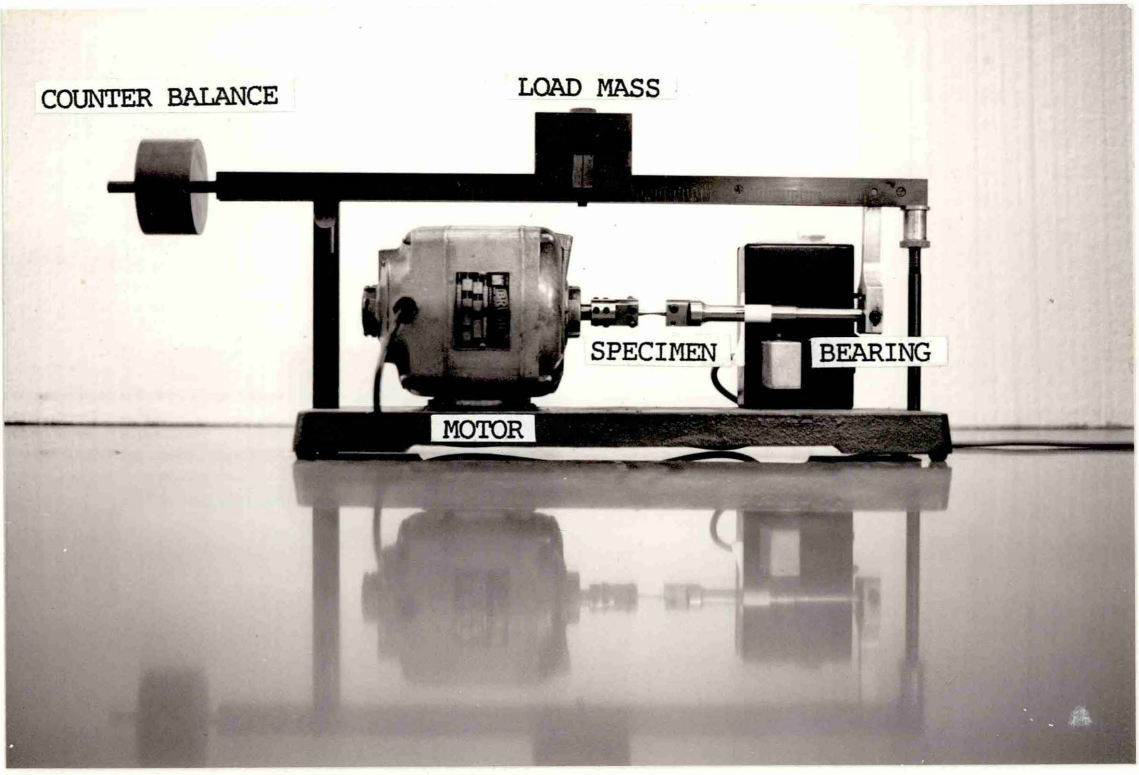

(a) Three point bend

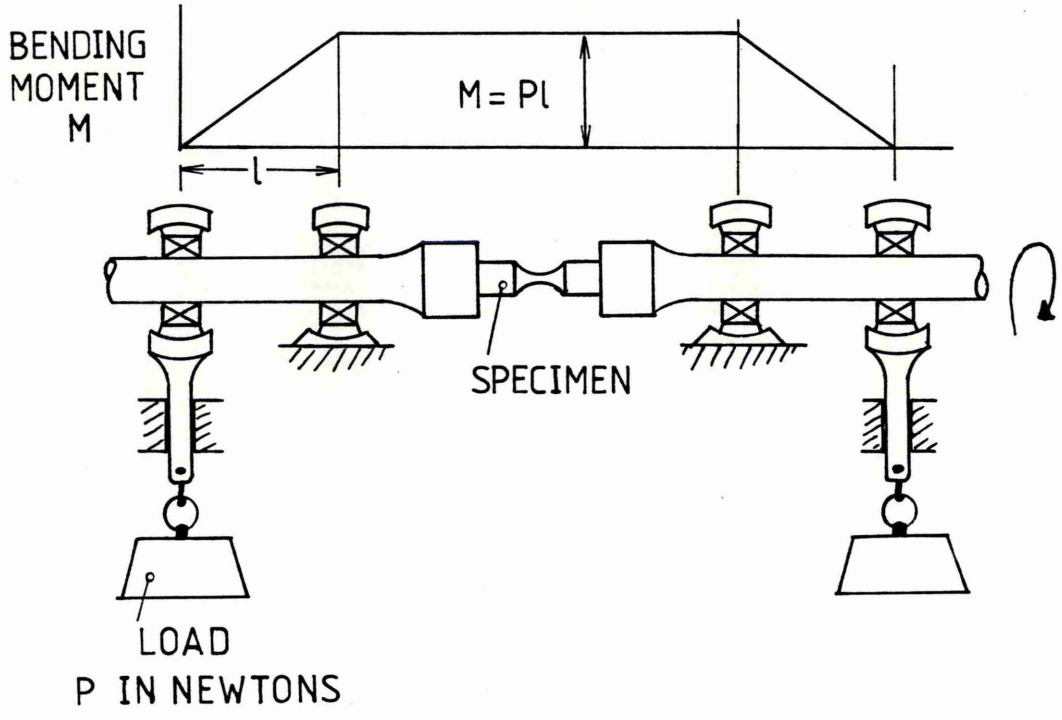

(b) Four point bend

FIGURE 3.1 Rotating bend configurations

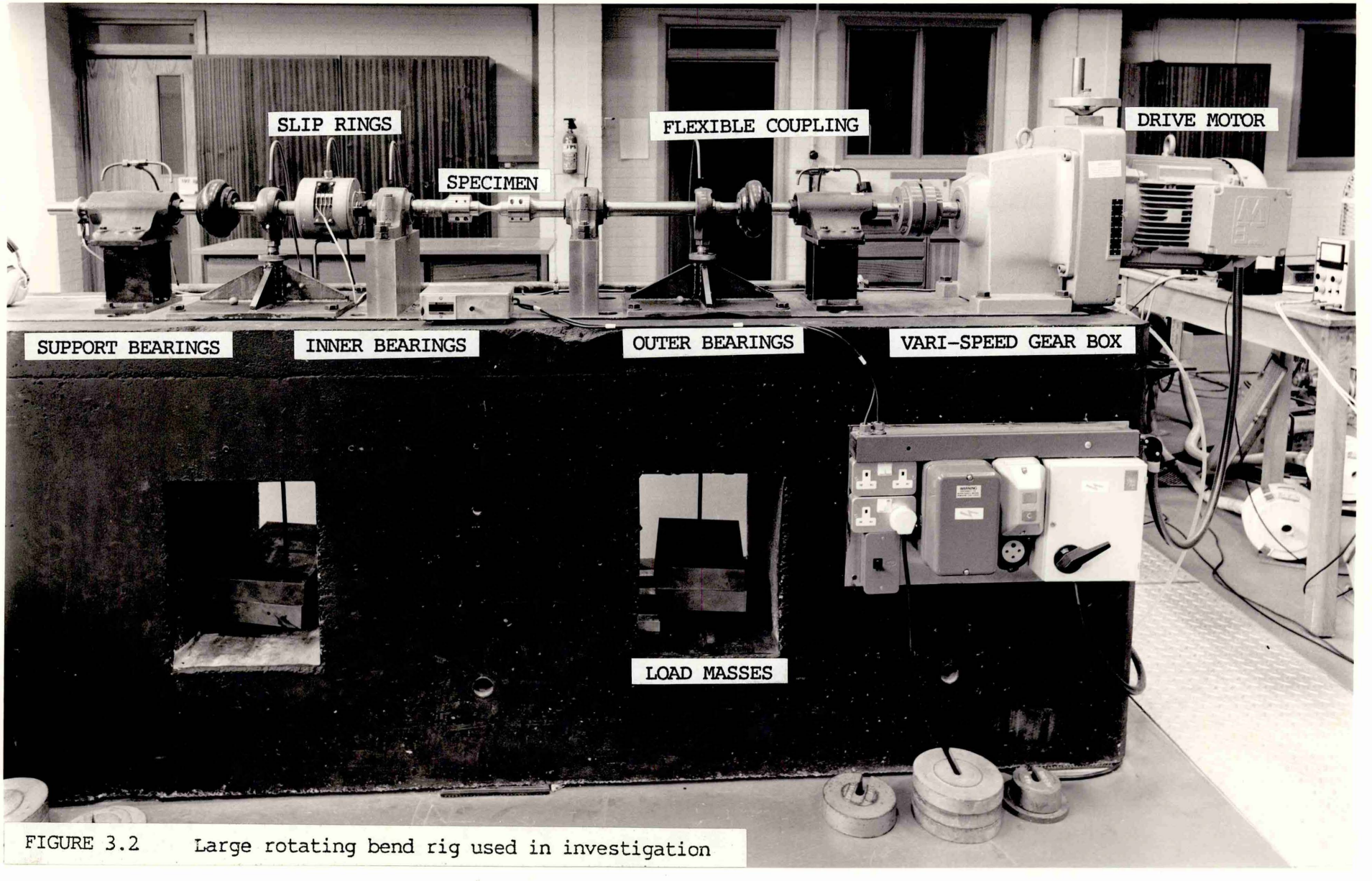

FIGURE 3.2 Large rotating bend rig used in investigation

(upward) forces to the shaft, creating a pure couple. This creates a uniform being moment between the inner bearings.

The compliant couplings allow the shaft's end to be displaced by the load force whilst enabling the shaft to be connected to the motor and variable ratio gearbox. An electronic cycle counter driven by an opto-electric switch coupled to a disc with a hole drilled in it attached to the shaft, and was used to indicate the number of cycles achieved. A trip, triggered a change in the axial alignment of the two parts of the shaft was used to stop the rig's motor when specimen failure occurred. Additionally, slip rings were fitted to facilitate calibration.

To ensure good alignment, the rig was aligned by Cranfield technical staff at the outset of the work. Periodic re-greasing of the bearings was also found necessary to maintain consistent performance. This was facilitated by the fitting of grease nipples to the bearings.

In order to maintain good alignment in inserting a fresh specimen the loads were removed from the machine beforehand. The tightening of the bolts which secured the specimen in the shaft was standardised so that any forces due to clamping were at least consistent.

Before the loads were placed on the machine, the shafts connecting the load bearings to the load were imobilised using knurled knobs at the head of the shaft assembly. The loads could then be applied after the motor had been started and the machine had passed through its critical speed.

Calibration of the fatigue rig was accomplished by strain gauging one fatigue specimen in each material tested, and subjecting it to fatigue in the same manner as the other specimens. Using the slip rings, the strain wave form was monitored. Figure 3.3 shows the gauged calibration specimen. A single active gauge with a temperature compensating gauge was used as it enabled the measurement of any direct stress in addition to bending moment.

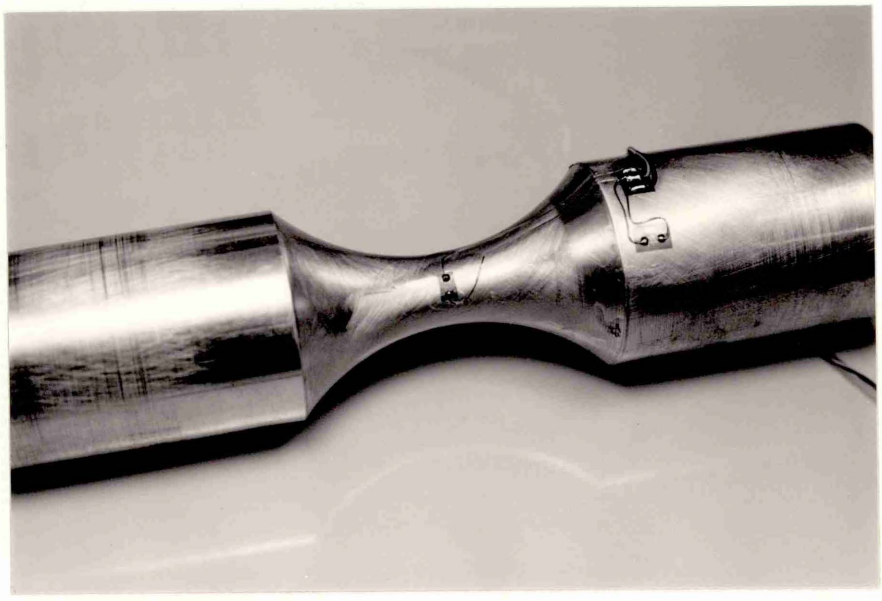

FIGURE 3.3 Calibration specimen

3.1.2 Servo-Hydraulic Uni-Axial Fatigue Testing

Figure 3.4 shows a schematic of the basic components of a typical electro-hydraulic servo-controlled uniaxial fatigue testing machine. In this type of machine, a double acting servo-hydraulic actuator, driven by a pump is mounted in a loading frame with two or more columns depending upon machine capacity, required stiffness and geometrical constraints. The actuator may be mounted in the base of the machine or in its crosshead.

In these machines, much effort has been devoted to produce leakage-free low-friction pistons. The main source of friction is generally due to the upper and lower piston rod bearings. To overcome this, hydrostatic bearings are frequently employed. Furthermore, whilst it is important for a frame to be of a stiff construction, it is also essential to maintain coaxiality of loading axis over the full working range of the machine and ensure good dynamic performance. Typically, the maximum error due to lack of coaxiality should not exceed $\pm$ 0.2mm for a typical 100kN machine.

Hydraulic pressure in the range of 200-300 Bars and power packs having a wide range of deliveries (15-150 L/min) are typical of current testing equipment. Servo-hydraulic testing equipment is very inefficient in the use of power, and a typical 40 L/min pack may

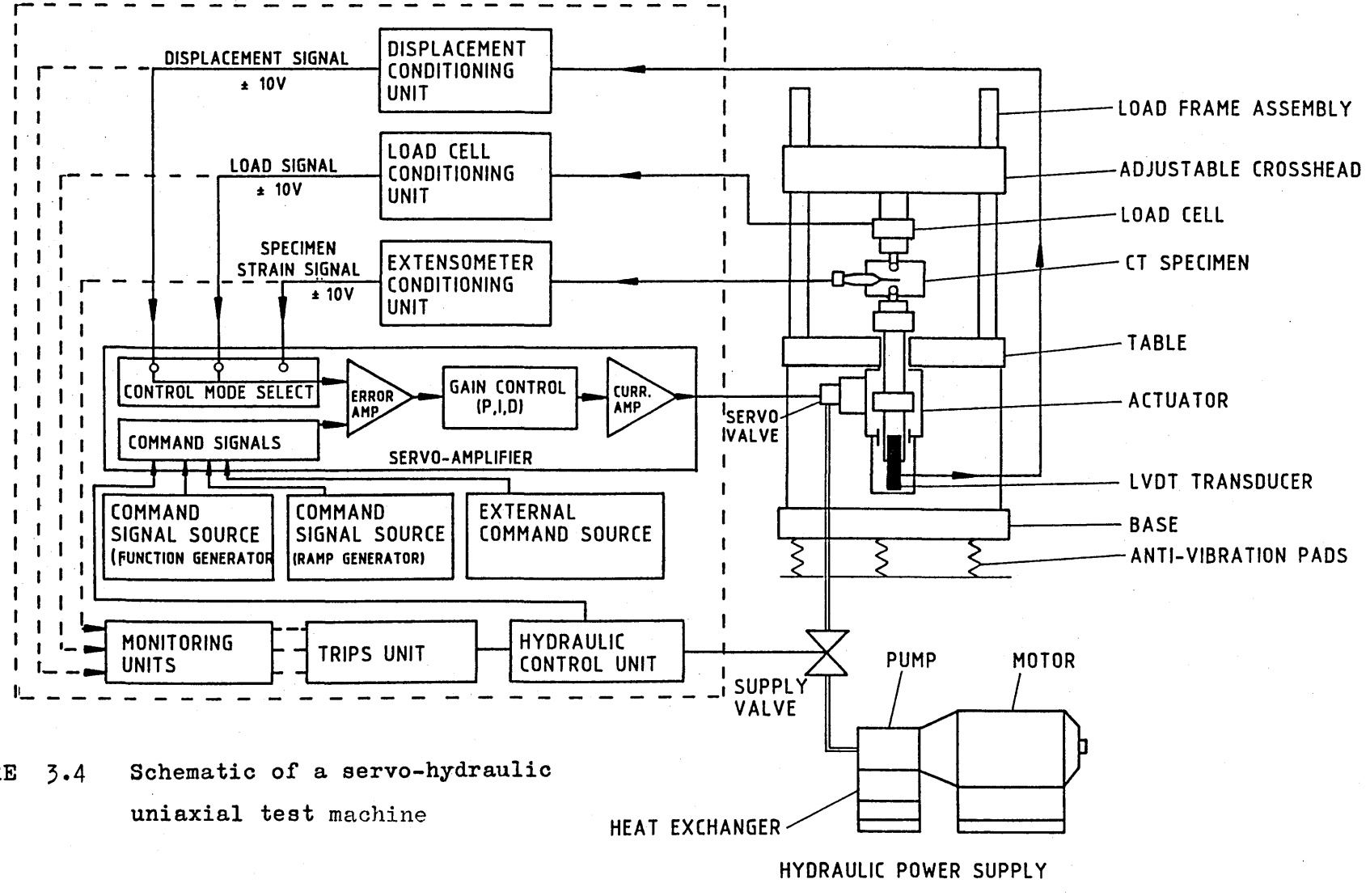

FIGURE 3.4 Schematic of a servo-hydraulic uniaxial test machine

employ a 20 kW motor with most of the power being dissipated by the cooling system. In view of the effect of temperature upon the viscosity of the hydraulic fluid, its temperature is generally maintained below 50°C using heat exchangers with or without forced cooling systems.

In these machines, load is measured using a load cell mounted usually on a rigid crosshead and displacement is measured using an LVDT transducer. In order to measure the displacement or strain in a specimen accurately, position transducers, such as clip gauges, may be directly mounted on the specimen. It is common practice to process these signals using a standard voltage range of ± 10 volts, where a negative sign implies a compressive reading.

Servo-hydraulic machines enable the definition of a required test via the use of an electrical command signal. The control is achieved by closed-loop or negative-feedback techniques using an electronic assembly known as servo-amplifier. The first stage of the servo-amplifier is to algebraically subtract the actual desired value of the specimen load or displacement signal from the command signal to produce an error signal, as depicted in Figure 3.4. This is then passed through further amplification generally with variable characteristics, and finally emerges as a current drive signal. This current is applied to the control coil of the servo-valve or valves which control the differential flow of the hydraulic oil through two ports. In response to this current, the valve preferentially admits oil to the two chambers of the actuator in such a way as to reduce the magnitude of the error signal by causing the actuator to move.

Like any other feed-back system problems of loop stability exist and for this purpose gain controls are used to optimise the response of the machine whilst maintaining loop stability. In general, lower specimen compliance and higher test frequencies are generally associated with more critical stability considerations.

In servo-controlled systems, the servo-amplifier represents the heart of the machine. It would generally comprise of several modules and would perform several functions. The first is to select the feedback or control mode, e.g., load, displacement, strain. The second is to select the required comman signal source either a function generator,

a ramp, an external signal, or a combination of these. The third is to scale to the required comman level and to add in any static command signal required. The feedback and command signals are then compared and the resulting error signal is used to drive the servo-valve typically via a proportional integral and derivative type drive amplifier.

The control system is supplemented by measuring devices, usually digital voltmeters (DVM) to monitor the system and electronic trip devices for protecting the machine and specimen from various malfunctions. Servo-hydraulic machines are widely available with dynamic force ratings from 10 kN to 40 MN and a band width extending up to 120 Hz.

The Servo-Hydraulic test system used in this investigation, which is depicted in Figure 3.5, consisted of a uniaxial test frame with a 100 kN capacity and hydraulic crosshead lifts and clamps, a table mounted actuator with a total travel of 100 mm, a hydraulic power supply delivering up to 45 litres per minute of oil at a pressure of 2 Bars, and a consol of control and readout instrumentation.

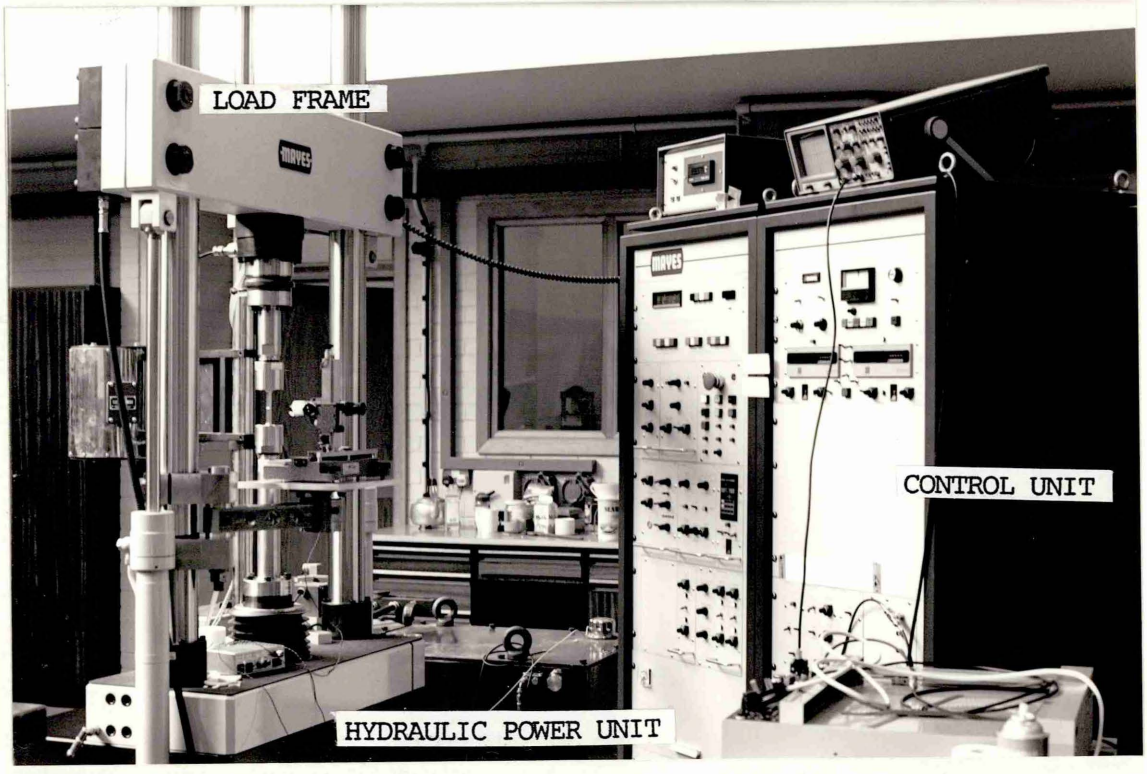

FIGURE 3.5 Servo-hydraulic test machine used in investigation

The combination of the actuator, servo-valve and the hydraulic power supply used meant that with actuator displacements of the order of .5 mm test frequencies of 50 Hz or so could be used giving load ranges of $\geq$20 kN depending on the stiffness of the specimen and any structural resonances set up. When performing quasi-static testing, the dual servo-valve set up could be re-configured conveniently by blanking off the larger valve using a screw driven blanking plate, giving the system a much higher resolution, though at a much lower performance level.

The load frame was fitted with a $\pm$ 100 kN capacity load cell which in conjunction with its supply and read out instrumentation gave a resolution of 1 N, and repeatability of 5 N on its most sensitive range, which was $\pm$ 10 kN. The actuator was fitted with a linear voltage differential transformer type position transducer with a range of 100 mm and a resolution better than 5 microns when used in conjunction with its drive and read out instrumentation.

The instrumentation and control gear allowed the machine to be used to perform a wide variety of quasi-static and dynamic tests. A combination of a 16 bit resolution cyclic ramp and hold generator and an analogue function generator could be used to apply complex load displacement, or strain, histories to a component. The system could also be driven from an external command signal, and external feedback signals could be used for control. The resolution and range of the system could be changed by up to a factor of ten to optimise the response of the system and its read out instrumentation for the testing being undertaken.

A dual beam digital storage oscilloscope with screen dump to plotter facilities was used to set up the servo amplifier, which was of the Proportionnal Integral, and Differential type. The oscilloscope was also used to visualise signals in cyclic tests to compliment the minimum and maximum reading four-and-a-half significant figure digital voltmeter incorporated in the system.

Finally, the system included a flexible system of overtravel, undertravel, and cycle counting trips which could be used to interrupt or terminate a test according to variations in any of the feedback signals independently of the control mode.

3.2 CRACK SIZE MEASURING TECHNIQUES

When considering surface treatments like shot-peening, it is of key significance to establish the severity of defects in the component prior to peening. This is particularly important if peening or re-peening is to be applied to a partially fatigued component as it has been shown [3.5] that the effectiveness of peening is very sensitive to the existing flaw size.

There exists many techniques for the location and measuring of crack-like defects. A number of these techniques have been developed by equipment manufacturers to a high level of sophistication and performance to satisfy the need to identify manufacturing flaws and fatigue cracks in highly specified components. Other techniques however, are not so highly developed and are better suited to laboratory applications.

This section on crack size measuring techniques outlines some of the more widely used industrial and laboratory techniques in so far as they affect the application of peening or re-peening.

3.2.1 Industrial Non-Destructive Examination

Ultrasonic Techniques [3.6]

Ultrasonic techniques use beams of elastic waves (vibration) of short wavelength (1-10 mm) and high frequency (0.1 - 20 MHz), transmitted from a piezoelectric transducer through the specimen. If a defect is present in the specimen, it will form a barrier to the ultrasonic waves and reflect some or all of them back to the source. The reflected waves are then converted into electric energy and to the amplitude of the waves together with the time of travel through the specimen. Some of the waves, however, are reflected from the opposite side of the specimen may be recorded. This backward reflection provides means of establishing the thickness of the specimen or calibrating the technique.

Figure 3.6(a) shows an oscilloscope display of the probe output s a function of time and is generally known as the A-scan. In this case,

the height of the reflected pulse is related to the flaw or defect size as seen from the transmitter probe. The relationship of flaw size, flaw distance and flaw reflectivity makes sizing of flaws using A-scan methods difficult.

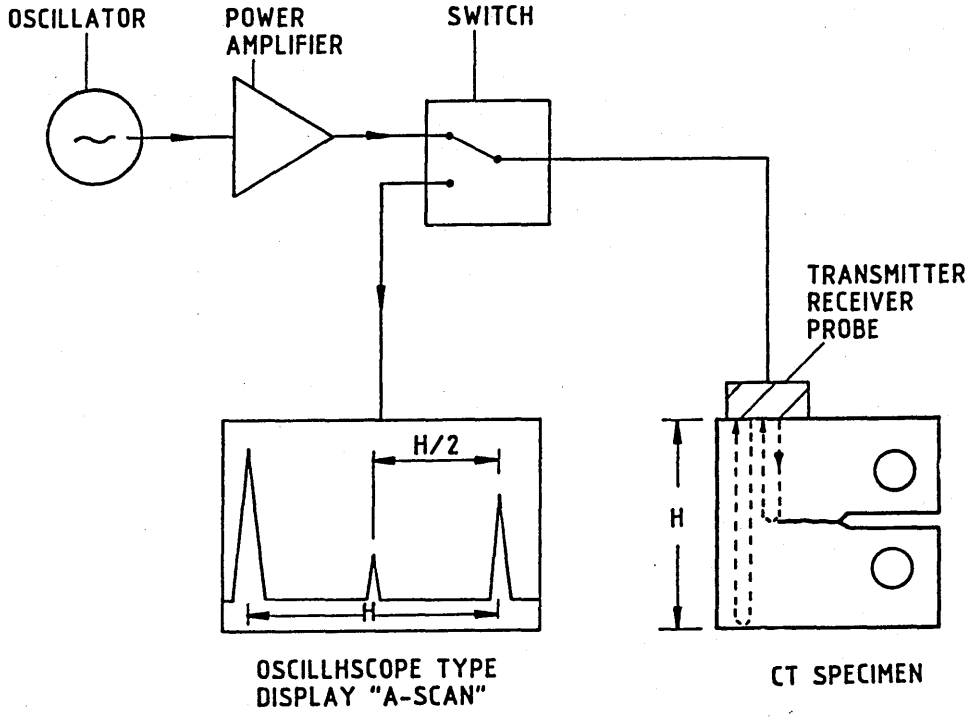

(a) Simple setup giving 'A' scan readout

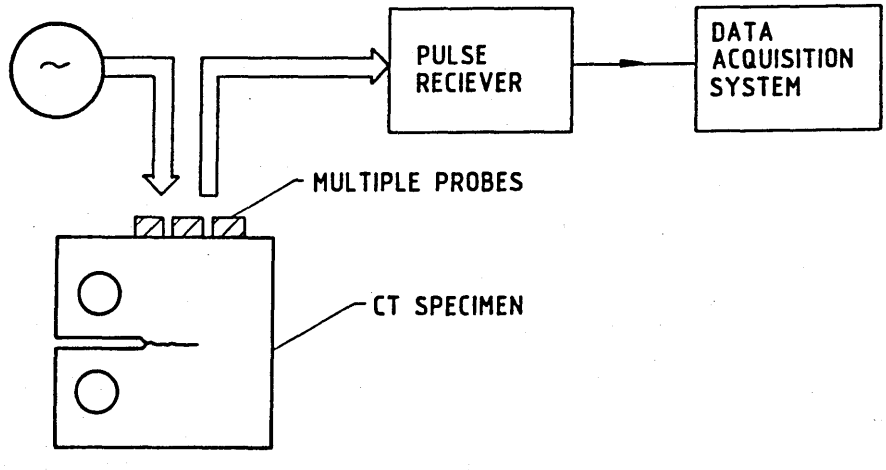

(b) Setup utilising multiple probes to size a crack in a C.T. specimen

FIGURE 3.6 Ultrasonic flaw detection

Figure 3.6(b) shows a schematic representation of a set up which could be used for measuring crack growth in a CT specimen. In this setup the oscillator supplies pulses of energy, through the probe, to the specimen. The reflected waves are then gathered in a pulse receiver and ther required data recording units. In this case, the technique relies upon a multiple probe arrangement to resolve the location of the crack-tip since only its vertical position can be established by the aid of A-scan techniques, unless the probe is traversed over the specimen.

Ultrasonic techniques can yield a crack-length measurement sensitivity in the order of $\pm$ 0.2 mm and provide a continuous record of crack length vs time which, in turn, can readily be converted into fatigue crack growth data, da/dN. This however, represents a large crack in terms of shot-peening, and this level of resolution is not always achievable in real components.

It is worth noting for instance, that ultrasonic waves can travel long distances in fine-grained structures without severe attenuation. However, in coarse-grained structures, attenuation problems limit the use of the technique. The technique will also defect other elastic discontinuities apart from cracks such as inclusions and even grain boundaries.

The development of ultrasonic techniques has resulted in the use of projection image scanning facilities (P-scan) in nuclear power plants, pressure vessels, refineries, off-shore installations, ship building, etc. These facilities are generally used for weld inspection and for corrosion mapping by means of three projection images corresponding to top, side and end views of the component. In the new generation of P-scan equipment, full advantage has been taken of recent improvements in microelectronics and computer technology, giving powerful data acquisition and data processing. In addition to P-scan, thickness scanning technique (T-scan), which is based upon the same principles as P-scan, is currently being used by a number of companies to examine corrosion severity in critical components.

It is this flexibility in mapping flaws in large and complex structures which accounts for the popularity of the ultrasonic techniques rather than their sensitivity to small defects. The use of the technique is then restricted to comparatively defect tolerant

components. It does not represent a means of identifying th sort of crack sizes which distinguish between components whose strength is limited by microstructure or surface flaws.

Acoustic Emission [3.7]

Acoustic-emissions can be defined as being low level stress waves emitted by a material when it is deformed, either by an external load or internal processes such as phase transformations. These emissions range in frequency from the audible to several Mega Hertz. Different processes, such as fatigue crack initiation and propagation, generate levels of acoustic-emission which can be detected by suitable sensors which are in direct contact with the surface of the specimen. These sensors generate electrical signals, which after conditioning, become suitable for monitoring.

An array of detectors may be used over the surface of a large component, and the time it takes for a signal to reach each sensor enables the source of emission to be located. Alternatively, if the rate of acoustic-emission is monitored, changes in this rate can be used to determine crack propagation and/or the formation of new flaws.

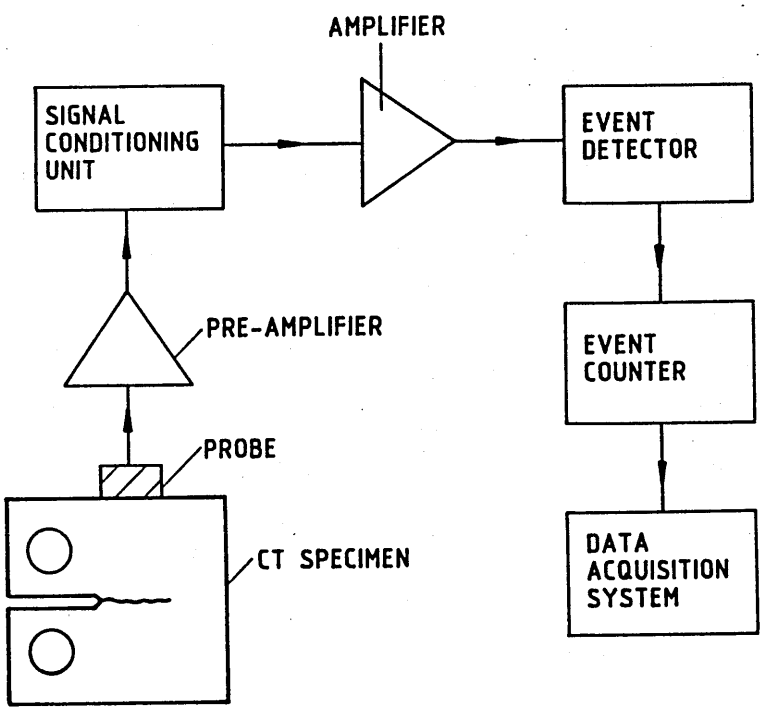

FIGURE 3.7 Schematic acoustic emission setup

Fig. 3.7 shows a schematic of an arrangement which could be used for monitoring crack propagation in a CT specimen. In this case, the probe is in direct contact with the surface of the specimen. In view of the low level of energy generated, some pre-amplification and conditioning of the corresponding signal is necessary in order to drive the cable to the rest of the equipment. The secondary amplifier and event detector are used to drive the event counter, which in turn feeds the data acquisition system. In data handling, a number of options can be used. These include counts distribution, pulse width distribution, amplitude distribution, energy distribution, linear location, and multiple probe time of flight analysis.

One limitation of this technique is the fact that background noise arising from, e.g., loading arrangement, hydraulic noise and other vibration sources, can mask the signal. Accordingly, measures must be taken to separate the desired signal from the background noise. Also, since materials will provide different intensities of emissions, some engineering materials may not be well-suited for the technique.

In the laboratory the technique is interesting in that extremely small defects can generate detectable acoustic emisisons. The problem of equating acoustic activity to crack size or crack growth rate, however, seems to have no simple solution. Industrially, the technique is now widely used as acoustic emissions can travel long distances in large structures and using suitable data reduction techniques, flaws may be mapped in a large structure using a static array of transducers. These flaws may then be individually investigated using ultrasonics or radiography.

Eddy Current Techniques

The basic principle of eddy current testing is that if a component is subjected to a fluctuating magnetic field, eddy currents will be induced in the component. The absorbtion of energy by the component from the field can be accurately measured so that physical discontinuities affecting the resistance and reactance of the component can be detected. Fig. 3.8 depicts a simple set up which could be used to finger print materials including the defects they contain. The setup consists of a coil wound around a ferrite pole

piece which is supplied with an alternating current. The cathode ray tube display is then used to show the potential across the coil, the current passing through the coil and the relative phase angle between them. More soiphisticated proprietory equipment can feature multi-frequency testing, the storage of results, and more complex probes with separate excitor and sensor coils.

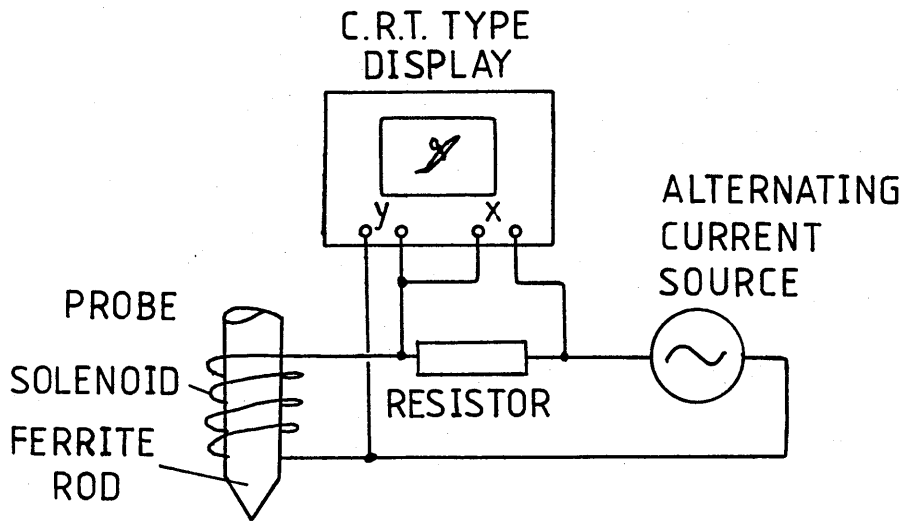

FIGURE 3.8 Basic Eddy current setup

Such equipment is still more qualitative than quantative with respect to crack size measurements, though advanced multi-frequency testing and data handling techniques are attracting research interest [3.8].

Other Techniques

A number of techniques rely on the crack as a space or void within the component in order to locate it. Radiographic techniques show cracks as changes in density in shadow. Low volume and shallow cracks can hence be difficult to locate and the direction of x-ray illumination is hence critical. Die penetrant techniques rely on the fact that surface breaking defects may be filled up with some intense die. This may then be drawn back onto the surface by applying a finely divided wettable powder to the surface, making the crack more visible. It is common to use fluorescent dies which give very high visibility when viewed under ultra violet illumination. Clearly to successfully use visual examination, with or without a die penetrant, the crack must

intertsect the surface of the component. Peened surfaces or coarse machined finishes can also obscure cracks. An additional hazard with die pentrants is that they can affect crack behaviour by either excluding the atmosphere from the crack tip or acting corrosively in their own right. Magnetic particle inspection, which is also comparatively insensitive to sub-surface defects, does not work particularly well on peened surfaces. The technique relies on passing a current or in some way magnetising the component. Magnetic particles, usually suspended in an inert liquid are then distributed over the surface. The particles tend to collect around features where the magnetic field is irregular, for instance, in the vicinity of a crack. Any surface features which impead the flow of the particles will reduce the sensitivity of the technique.

3.2.2 Laboratory Techniques

Electrical Potential Drop Techniques

Potential drop techniques are becoming established industrially, but usage is not as prevelant as the techniques mentioned in Section 3.2.1.

There exist two basic variants of the potential drop method, according to whether a.c. or d.c. current is used to create the electric field which the technique is reliant upon.

Fig. 3.9 depicts schematically the components of a d.c. potential drop setup. A constant current source is used to pass a steady current through the component. A movable probe may then be used to measure local values of the field in the component. This is done simply by measuring the voltage or 'potential' drop meausred across the two pole pieces of the probe. The presence of a crack will increase the effective resistance of that area of the component. This gives a greater potential drop across the crack. The technique can be used for continuous monitoring by following the potential drop as a function of time, or the measurement may be compared to a non-cracked reference or datum [3.9].

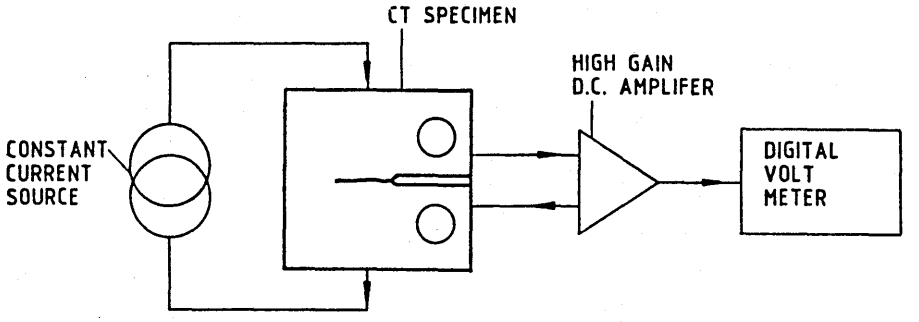

FIGURE 3.9 D.C. potential drop setup

Fig. 3.10 gives the corresponding setup for an a.c. potential drop setup [3.10]. There are two main operational differences between ac and dc potential drops. By using ac excitation it is posisble to condition the output from the probe using a phase sensitive detector. This enables noise and thermal voltages to be almost entirely rejected as only signals in phase with the excitation are measured. The second difference is that, depending on the permiability of the test substrate, the current tends to flow mostly in the vicinity of the surface. This skin effect can concentrate the current to a degree where the current density required for accurate readings of around $.1A/mm^2$ can be achieved with an excitation of the order of one amp. In a dc potential drop setup, since the field is uniform with depth, currents may need to be of the order of 10^2A to give comparable surface sensitivity. The dc setup will however, be inherently more

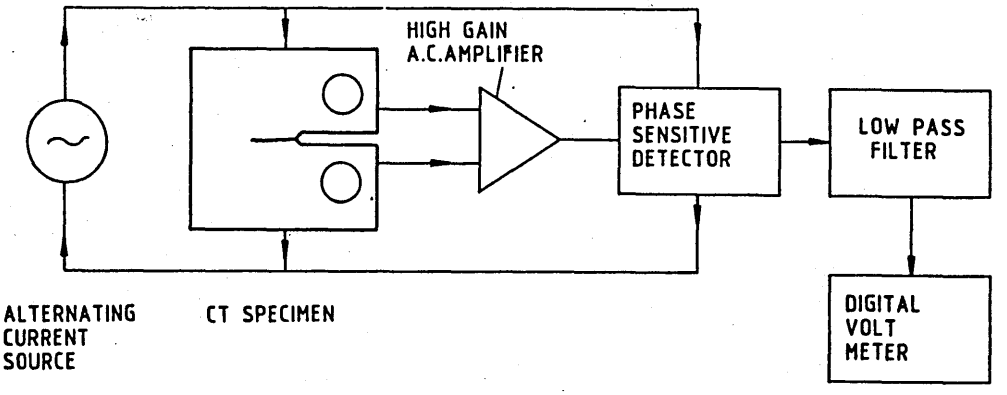

FIGURE 3.10 A.C. potential drop setup

sensitive to sub-surface defects. Doubtless in time multi-frequency potential drop equipment will become available, giving the benefits of each approach, as well as some degree of through thickness flaw location.

Compliance Techniques

Compliance techniques are very widely used in the measurement of crack growth rates. Essentially as cracks propagate through a component it becomes less stiff. Measurements of displacement as a function of load will give a measure crack size, though this will represent an average dimension rather than a precise depth in any case where the crack front shape or the number of cracks is likely to vary. In addition, very small cracks give very small changes in compliance so that, in practice, the technique is problematical for cracks shorter than 5 per cent of the specimen thickness for conventional displacement measuring techniques. The technique is hence not well suited to the study of the propagation of cracks within the shotpeened residual stress field.

Optical Methods

These methods vary from inspection with the naked eye to the use of microscopic examination and the use of contrast enhancing systems. However, in the present work emphasis has been placed on popular laboratories techniques.

Typically, for the examination of cracks in standard fracture mechanics specimens, a travelling microscope attached to a vernier scale is used to focus on the crack-tip and follows its progress. The ease with which a crack can be viewed depends upon the following parameters:-

(i) the extent of plastic deformation and the resulting blurring of the image,

(ii) the presence of surface oxidation which makes the detection of fine cracks against the dull background of the oxidised

surface difficult. This is most common in high temperature fatigue testing,

(iii) the intensity of illumination, and

(iv) the testing frequency. In cases involving high frequency fatigue testing, it is recommended to use stroboscopic illumination.

Clearly, optical methods will allow the measurement of surface cracks, and a reliable indication of average crack length will only be obtained if the crack front is relatively straight through the thickness of the specimen. Crack extension of 0.1 mm can be detected readily, but the reliability of precisely locating the crack-tip by this means is probably no better than $\pm$ 0.4 mm. An advantage of this technique is that crack extension is obtained directly without prior calibration. However, it has the disadvantage of being manual and operator dependent.

The optical method may be assisted by the use of contrast enhancing dyes as mentioned in Section 3.2.1. Visual tests are inexpensive, simple, fast to perform and very flexible. Some experience, however, is needed for the efficient identification and tracking of surface cracks. The surface under inspection must be clean and well illuminated. Again, it is important to note that die penetrants can, in certain circumstances, influence the propagation of fatigue cracks.

Components are frequently not amenable to microscopic examination and it is common practice to cast replicas of the surface which may then be inspected subsequently either optically or in a scanning electron microscope. One of the most widely used techniques is to soften cellulose acetate sheet in acetone, form it over the surface in question, allow it to dry and harden and then peel it off before it is completely hard. Figure 3.11 shows such a replica of partially covered shot-peened surface viewed in transmition optically. It is important to note that as the replica hardens, it shrinks. This means that features on the replica will be somewhat smaller than on the original surace. Making a replica of a fatigue crack usually involves interrupting the load sequence, possibly leaving the component in

tension to hold any cracks open, hence making them more visible. Such interruptions have been shown to affect the propagation of fatigue cracks. [3.11]

FIGURE 3.11 Replica of a partially peened surface

3.3 A NOVEL STROBOSCOPE USING LIGHT EMITTING DIODE LAMPS FOR THE INSPECTION OF FATIGUE CRACKS

SUMMARY

In the study of the propagation of fatigue cracks in components it is often extremely undesirable to interrupt the test sequence in order to inspect cracks as this frequently affects their propagation. Stroboscopic illumination can be used to circumvent this problem. This report describes a novel strobe system which was designed developed and used for the microscopic examination of rotating or oscilating components. The stroboscope utilises ultra high intensity light emitting diode lamps which proved ideal for the illumination of the small areas required for this application. The finished strobe equipment proved itself to be both highly flexible and capable of good resolution whilst being compact and inexpensive.

INTRODUCTION

The growth of fatigue cracks is often strongly influenced by intermissions in cyclic loading. Material relaxation, creep, corrosion, hydrogen embrittlement and even changes in temperature and temperature gradient will contribute to changes in the growth of a crack after a rest period. Hence the continuous monitoring of cracks without the need to interrupt the load sequence, is of great significance to the study of fatigue crack propagation.

In laboratory fatigue testing, travelling microscopes are frequently used to locate and size cracks. For microscopic stroboscopy, it is only necessary to illuminate a small area. It is however necessary to ensure that the duration of the flash is short so that the necessary resolution for microscopy is achieved.

Traditional stroboscopes, using gas discharge tubes suffer from a number of disadvantages in situations such as these where high power

output is not required. They are generally expensive on account of the cost of the major components. Their bulk, weight and power consumption severely compromise their portability and the physical size of the lamp makes them inflexible.

Most commercial stroboscopes are not designed with this application in mind and so would require major modifications and/or supplementary equipment to facilitate this mode of operation. In addition to these limitations, the stray light, fragile bulbs and dangerous voltages used in conventional strobes causes a number of potential hazards, especially in circumstances where specimen failure is likely to result in flying debris and sudden specimen movement.

With the afore-mentioned limitations associated with traditional strobes, it was decided to develop a new system specifically designed for examining small areas of poor accessibility. It was felt that with the electrical devices available at that time a solution could be found quickly and economically. Considering all the available light sources, light emitting diodes seemed to offer the greatest potential as they fulfilled the desired task. Preliminary testing of these lamps demonstrated that they could be overdriven to give acceptable brightness levels without lamp life becoming unreasonably short. The development of the circuitry to drive the lamps was then undertaken and careful consideration was given to the final design to ensure ease of use, good performance, reliability and flexibility.

PRINCIPLE OF OPERATION

The strobe would typically be connected to a machine or a rig in such a way that it could be triggered once during each cycle of the machines operation. This would be achieved by making use of some sensor from which the strobe could be triggered. Since the sensor will trigger the strobe at the same point in the cycle each time, a simple strobe responding to the trigger with an instantaneous flash of light would only be able to show that one instant in the cycle. By arranging the flash to occur at a variable timed interval after the triggering event, different stages within the cycle may be visualised.

The circuit used to drive the strobe must then respond in such a way that whilst it may be triggered by some regular event associated with the movement of the component, it must be possible to retard the flash by a controllable amount. In the system discussed here, the triggering event occurs when the incoming signal from the sensor crosses its mean whilst moving from a positive to a negative value in the cycle. This process initiates a delay after which the flash occurs. This is shown schematically for a trapezoidal input wave form shown in Fig. 3.12.

DESIGN OF DEVICE

Having established the feasibility and basic method of operation, the more important design considerations were considered with a view to manufacturing a prototype. It was required that the device should be as simple as possible to operate but without containing any complex circuitry which would extend the time required to develop and build the device. It was also desirable to ensure that the unit was compact and tolerant to electrical and mechanical abuse and contained standard inexpensive, easily replaced components. The operation of the device permits a number of options, and care was taken to ensure that these can easily be made use of with a simple system of controls and possible connections to ancillary equipment. These options include external d.c. powering of the unit, supplying power at $\pm$15V to external sensors, using the device as a conventional self-triggering strobe of variable frequency, or using the device as a general purpose delay for gating signals or creating sequencies.

A list of specifications defining the required inputs, outputs and operational characteristics was drawn up. These were chosen to ensure flexibility and compatibility with ancilary equipment and power sources as well as give a suitable level of performance in terms of image resolution. These are summarised in Appendix 3.3.1

By selecting to build the device into a die cast box both mechanical ruggedness and effective screening were assured. In order to simplify operation, five controls were felt desirable; this being the minimum number allowing complete control of the device. Two potentiometers were used to control the delay and flash time, both being affected by

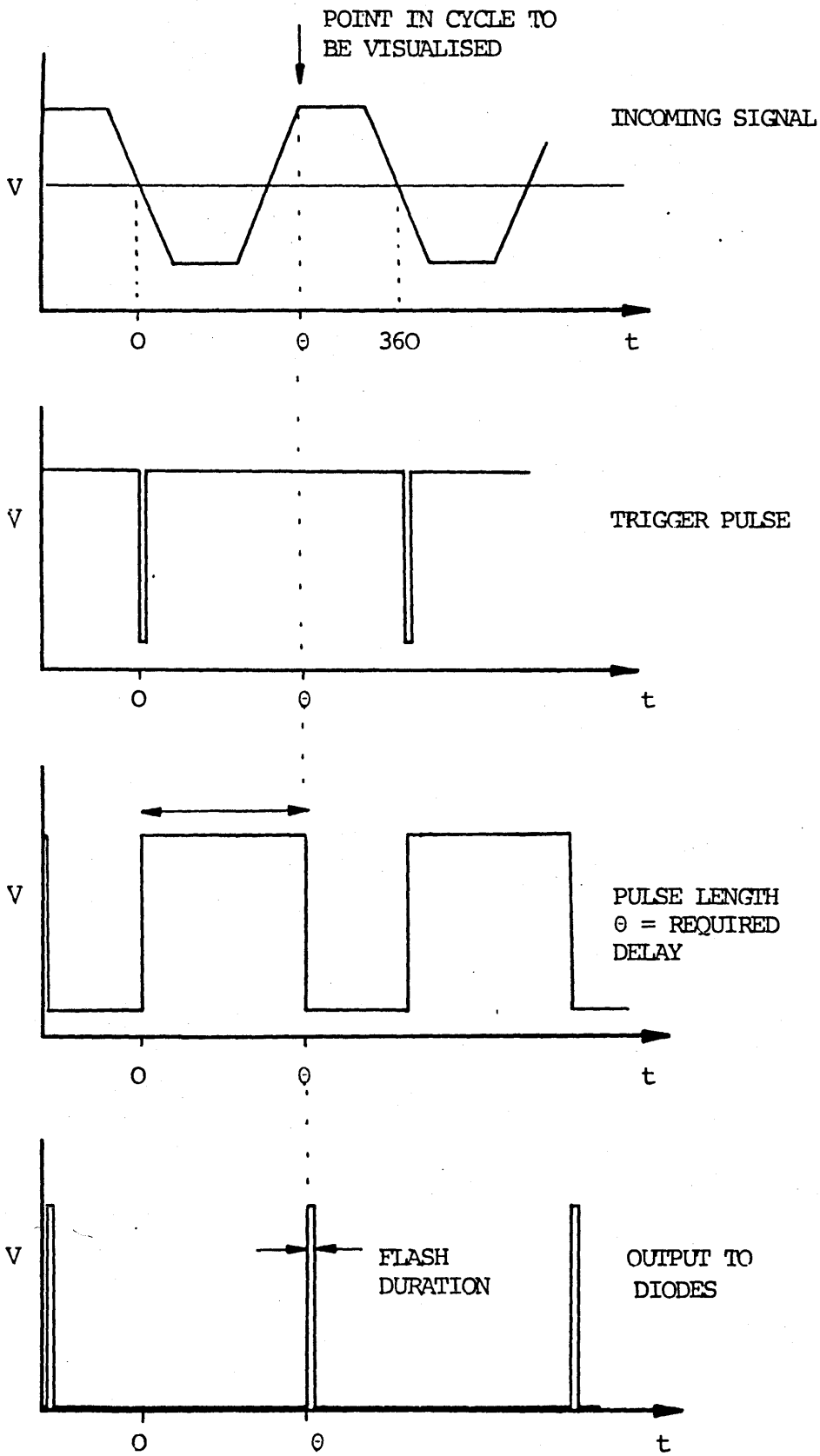

FIGURE 3.12 Basic principle of operation of the strobe

a range switch which gives a ten to one increase in each for use at lower frequencies. In addition to these controls a mode switch allows the lamps to be lit continuously to facilitate setting up and fault finding, and an on/off switch. The prototype was fitted with an indicator lamp to show whether or not the unit was correctly powered up and also whether an adequate trigger signal was present. This was achieved by the use of a bi-coloured light emitting diode, which was wired to show green for on and red in the presence of a suitable signal. The interior and basic construction of the prototype is depicted in Figure 3.13.

The interconnections necessary to ensure ease of use and good flexibility were organised as follows:

Mains Connector - "Euro Style" 6A 3pin connector including fuse holder with a (250 mA) fuse fitted.

Input Socket - Isolated B.N.C. Socket.

Output Terminal - Pair of 4 mm socket/binding terminals.

User Socket - Five pin DIN socket. This permits the unit to be driven by an external d.c. supplying ($\pm$15V). It also allows external circuitry to be driven by the unit's power supply.

The user socket also carries the input and output signals so that sensors, or ancilary lamp systems could be connected using a single plug lead. The option also exists to connect the output to the input in such a way that the unit acts as an oscillator of frequency equal to the inverse of the delay time, permitting the unit to be used as a regular strobe for the determination of frequency.

The device utilises two monostable type delays. Their respective functions are to generate the delay after which the flash occurs and to control the duration of the flash. Both delays are controllable by the Operator. It was decided to use two 555 timer integrated circuits as they offered the necessary performance, are easily obtained and simple to use. The other active elements in the circuit used were a 741 type operational amplifier

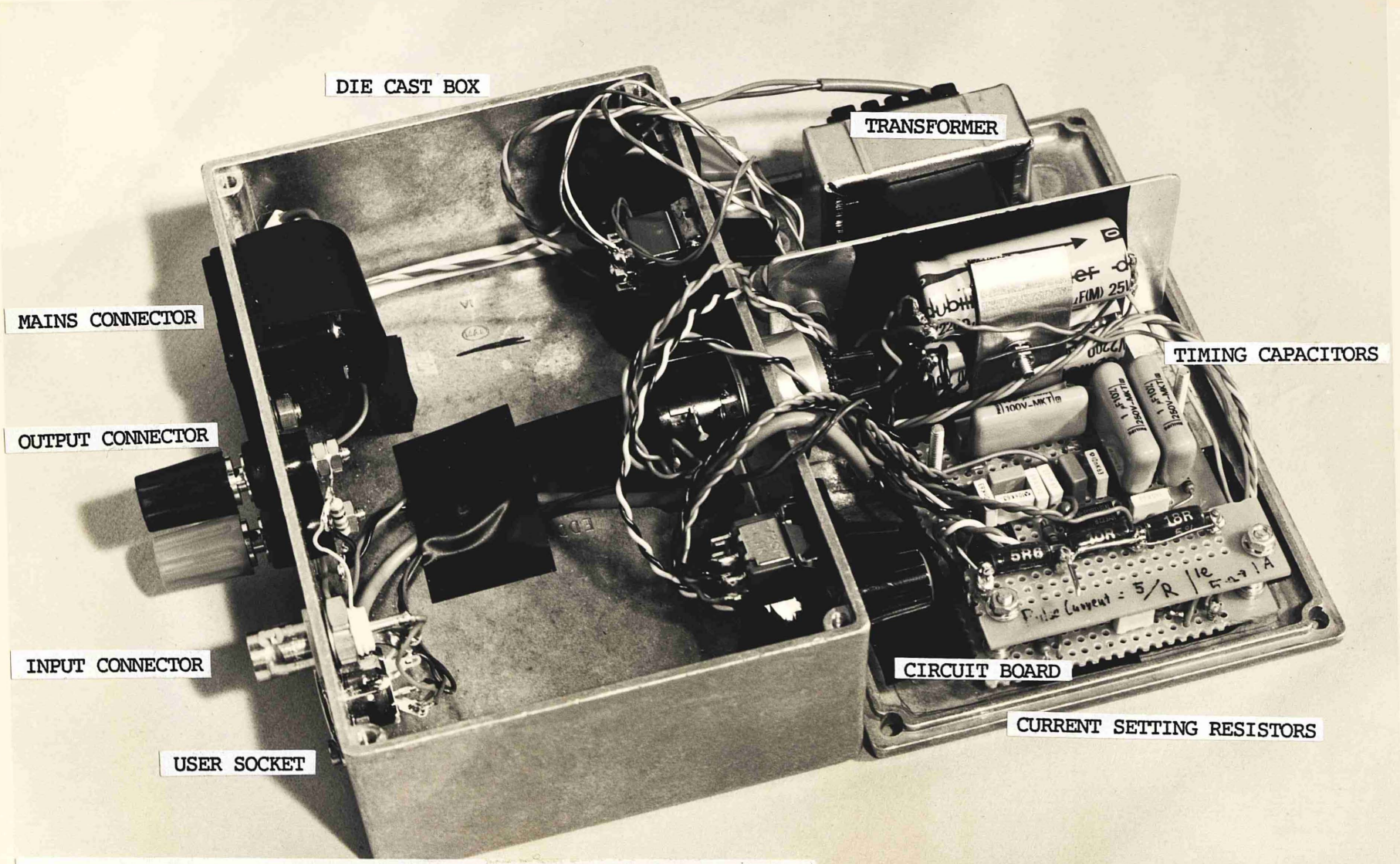

FIGURE 3.13 Interior and construction of the prototype strobe

used as a Schmitt trigger to generate the triggering impulse when the input waveform crosses its mean, a transistor used as a pulse shaper to eliminate width effects from the triggering impulse and a power transistor used as a constant current source to drive the lamps.

CIRCUIT DESCRIPTION

Input Stage

The two 1μF capacitors designated C1 and C2 in Fig. 3.14 completely decouple the input so that no d.c. offsets can interfere with the operation of the device. In addition, C1 in conjunction with the R1 also provides a low frequency cut-off (-3dB) at 3 Hz thus defining the lower end of the bandwidth of the front end.

The capacitor C3 in conjunction with the resistor R2 defines the upper end of the front end bandwidth at 1.5 KHz. This bandwidth gave good immunity to noise whilst allowing triggering from a variety of different wave forms over the entire useful range of the device.

The diodes D1 and D2 protect the operational amplifier from excessive inputs and the entire front end will cope safely with input differential RMS voltages of up to 200V. The operational amplifier and R3 and R4 form a Shmitt trigger with a 0.1V hysteresis giving a clean trigger pulse from slow moving or noisy inputs.

Indicator

The status indicator in the control unit is a bi-coloured light emitting diode D3 and D4. It is used here to indicate whether the unit is powered up and switched on, and whether or not trigger pulses of suitable amplitude are present at the input. When the unit is on but with the transistor TR1 off, as is the condition with no input present, the green side D3 glows. If trigger pulses are present then C4 charges up, switching TR1 on and shorting out the green side D3, meanwhile the red side D4 glows on account of the trigger pulses and the discharge of C4 so that the indicator turns from green to red when pulses are present. C4, R5 and R6 define the time constant of the pulse sensor circuit (20ms). Preliminary testing indicated that this set up gave a clear indication of the unit's status even at low

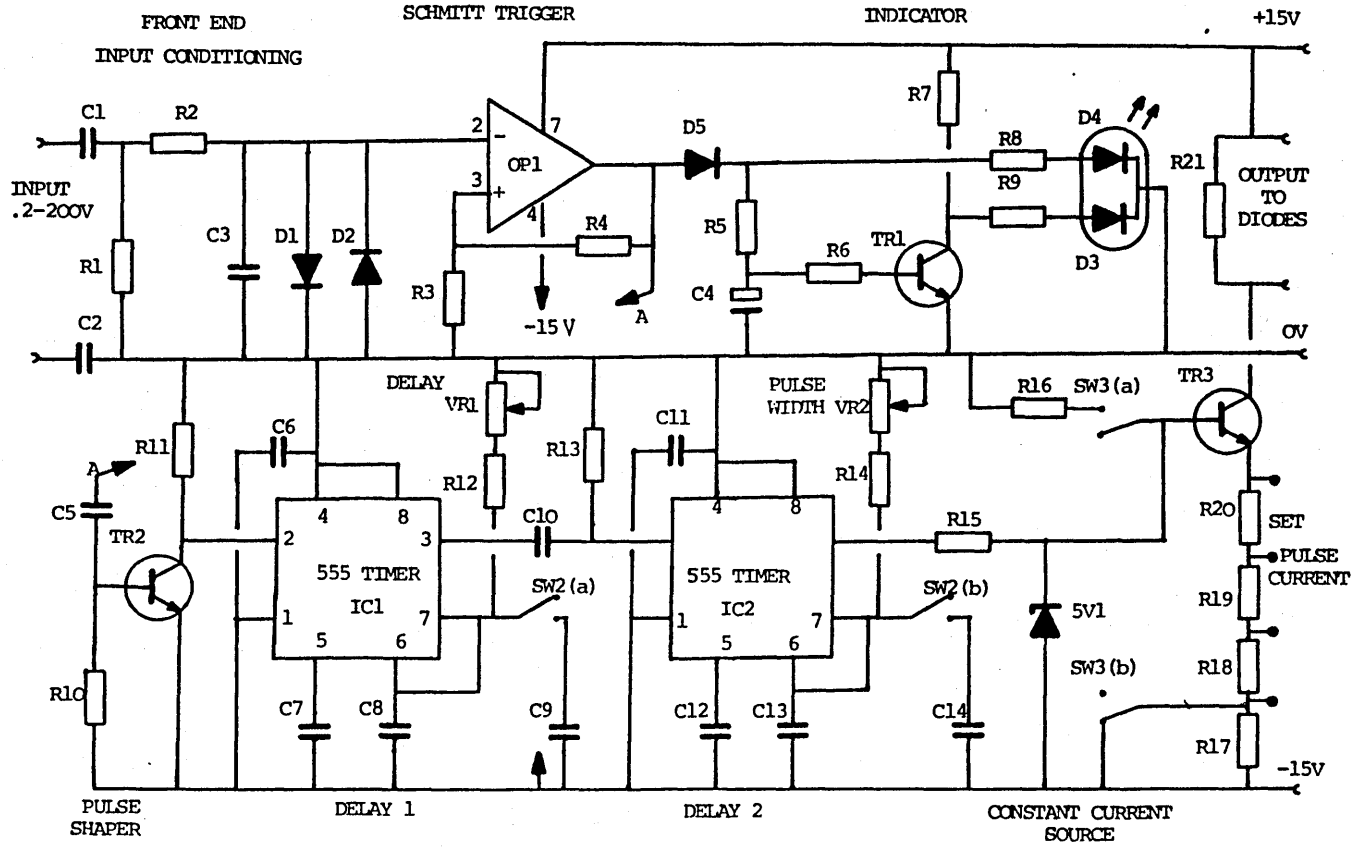

FIGURE 3.14 Circuit diagram of the strobe

trigger frequencies of 5 Hz, where the indicator shows alternatively flashing red and green.

Pulse Shaper

The transistor TR2 acts as a pulse shaper to give the first monostable (Delay One) a short trigger pulse 10μs so that the pulse length of the incoming signal does not affect the time delay.

Dual Mono Stables

The first monostable is used to set the delay between the arrival of the trigger pulse and the strobe flash, while the second monostable (Delay Two) is used to determine the length of the strobe pulse. Both delays are independently varied via the variable resistors VR1 and VR2, respectively. The range selector switch SW2 changes both delays by a factor of ten.

Constant Current Source

The final stage of the unit consists of a constant current source which for the duration of the lamp flash drives the lamps with a current defined by the effective emitter resistor and the voltage across Zener diode ZD1. This enables any number of lamps (up to a certain limit) to be connected in series without the need to make further adjustments. The number of lamps which can be driven depends on the total supply voltage range. In the present case, using $\pm$ 15V, twelve lamps could be satisfactorily operated.

Method of Operation

The unit must first be connected to a source of electrical power, e.g., 240V a.c. or $\pm$5-20V d.c. When correctly powered, the indicator will become

green when the power switch is switched into the active mode. The controls are depicted in Fig. 3.15.

Light emitting diode lamps will need at some stage, to be connected to the unit. As explained earlier, any number from one to twelve may be connected together in series and run of the unit without making adjustments. If too

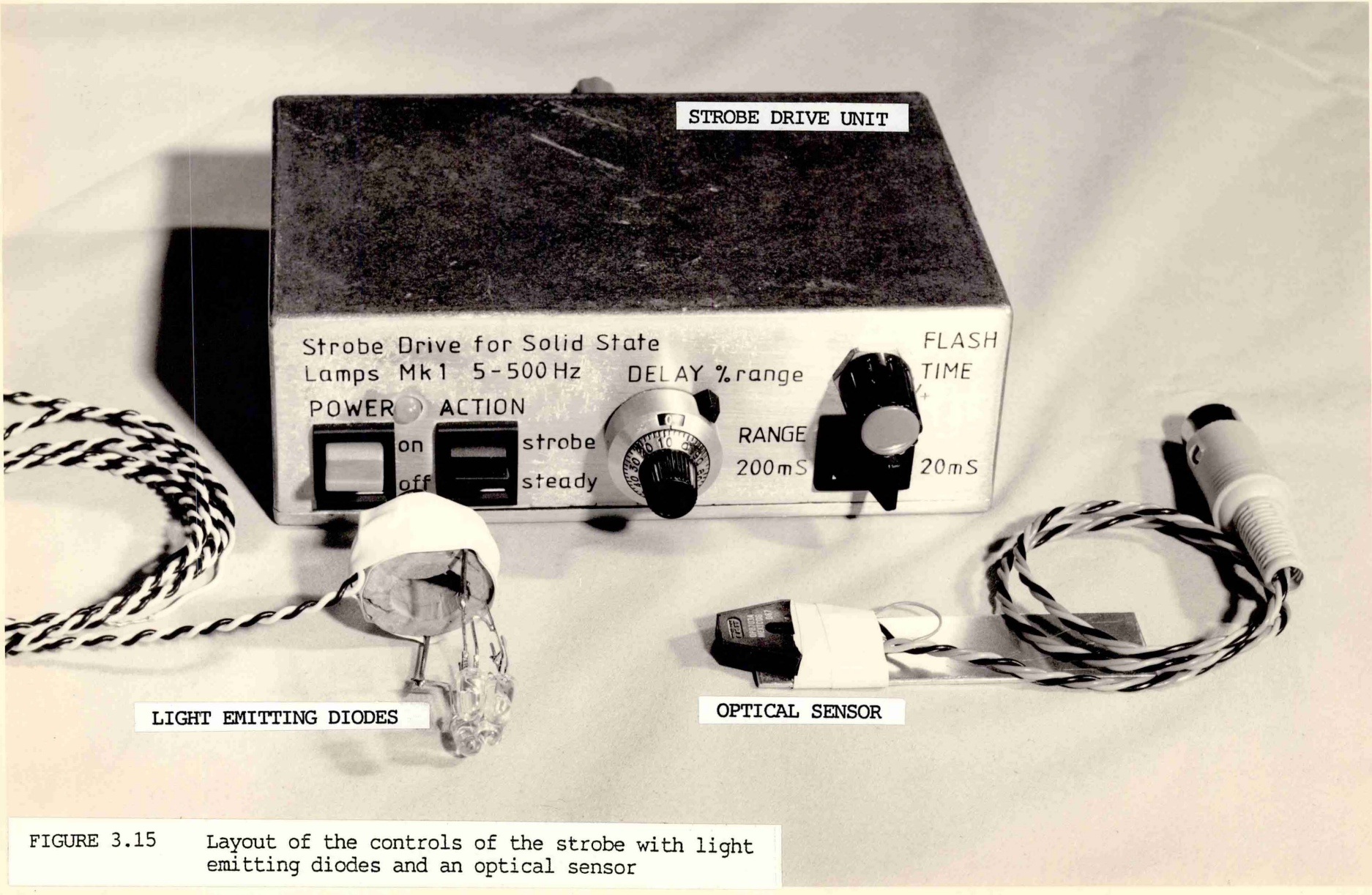

FIGURE 3.15 Layout of the controls of the strobe with light emitting diodes and an optical sensor

many lamps are connected then they will simply fail to illuminate. Fig. 3.16 shows the correct connection of the diodes.

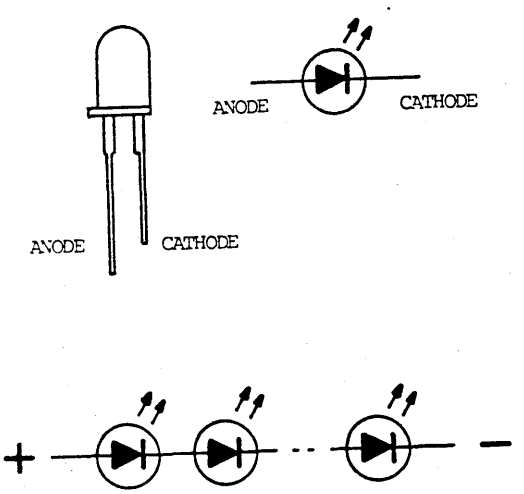

FIGURE 3.16 Correct connection of light emitting diodes

The current used to drive the diodes is set internally by a network of resistors which are arranged to give a variety of pulse currents. High currents give greater brightness but the lamps may not give adequate life.

Having connected the diodes to the output terminals it should be possible to illuminate them by selecting the 'steady' mode using the mode switch as depicted in Fig. 3.15. In the steady mode, the diodes will glow at normal brightness, i.e., they are receiving a continuous current of 20mA. This subjective brightness level should not be greatly exceeded when the diodes are being driven stroboscopically. The steady mode can be used to safely position the diodes and to assist in deciding upon the number of diodes to be used.

The final stage of the setting up is to feed the trigger or synchronisation signal into the strobe drive unit. If a suitable electrical signal is available, it may be connected via the BNC connector. If not, a variety of passive or active sensors may be connected directly to the unit via the 'USER' socket. Fig. 3.18 shows how optical or commutating sensors can be effectively connected for this purpose. When a suitable trigger signal is present at the input of the unit the power/status indicator will turn from green to red.

In order to use the strobe, we now select the appropriate range, 20ms for frequencies of $\geq$50Hz and 200ms for lower frequencies. It is now possible to set the delay control and the flash time control to minimum and switch the device to 'Strobe' mode. The flash time may then be increased until a suitable image can be seen. The delay may then be adjusted in order to examine different stages in the cycle. The delay control is directly calibrated so that the fully anticlockwise position reading 010 corresponds to 1% of the selected range and fully clockwise 1010 corresponds to 101% of the selected range i.e., a setting of 460 on the 20ms range corresponds to 46% x 20ms = 9.2ms.

It is worth noting that when the delay time exceeds the cycle time the unit will cease to flash on each cycle but will flash every second or third cycle as trigger pulses are ignored whilst the delay is in operation.

The resolution of the image will depend on the flash time. Whilst short flash time will give a limited brightness there will be little smearing of the image associated with specimen movement during the flash period.

Figs. 3.17(a) and 3.17(b) show a typical experimental set up involving a rotating bend fatigue test rig fitted with an optical sensor to provide the synchronisation of the signal, a travelling microscope fitted with four light emitting diodes and the prototype drive unit.

CONCLUSIONS

In response to problems associated with the use of conventional gas discharge type strobes, an alternative system utilising solid state light emitting diodes has been successfully developed and tested. The prototype proved reliable, inexpensive and easy to use whilst offering good microscopic resolution on components with surface speeds of $1ms^{-1}$ and good brightness levels making it ideally suited for the monitoring of cracks in a variety of differing situations.

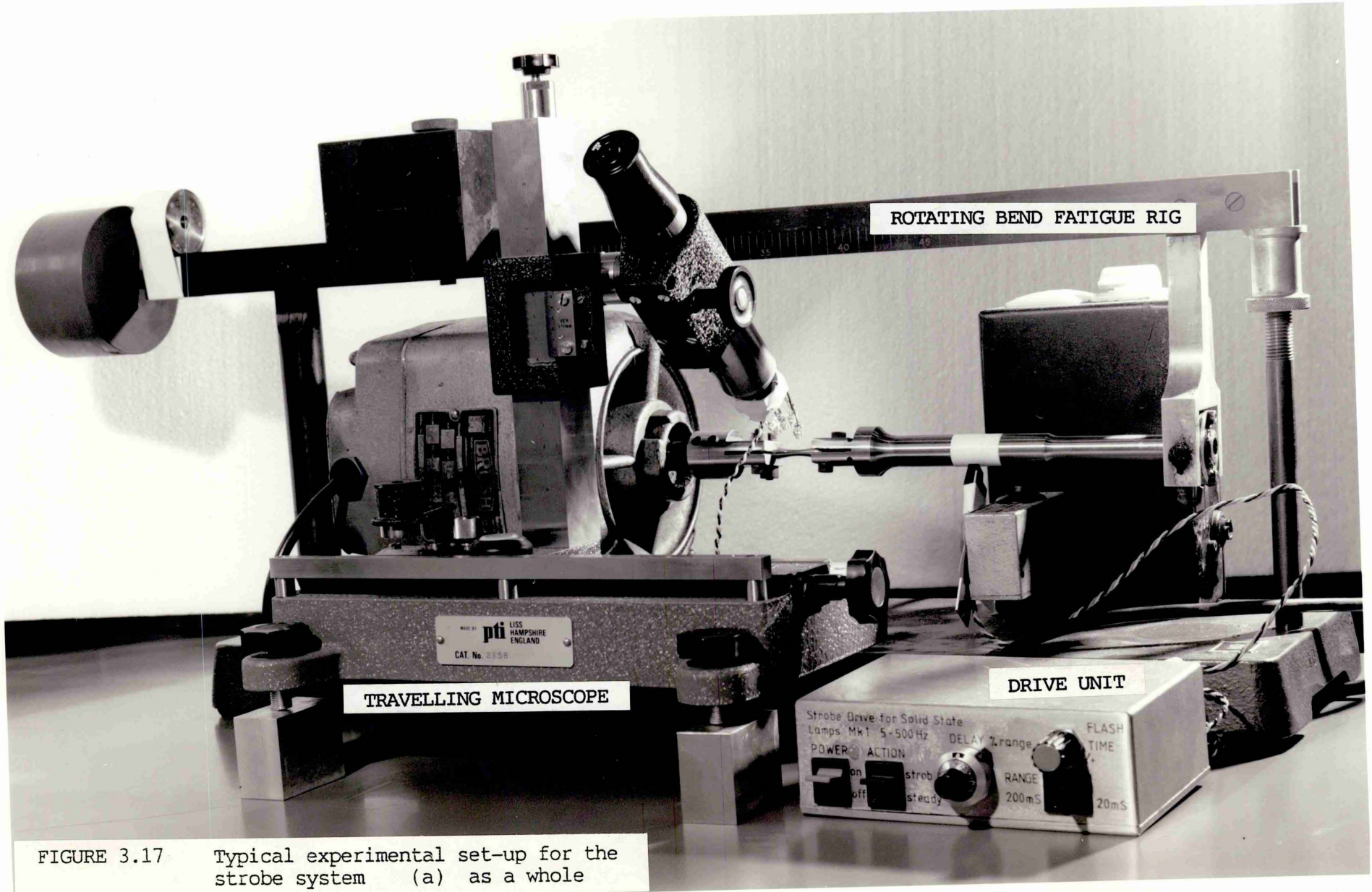

FIGURE 3.17 Typical experimental set-up for the strobe system (a) as a whole

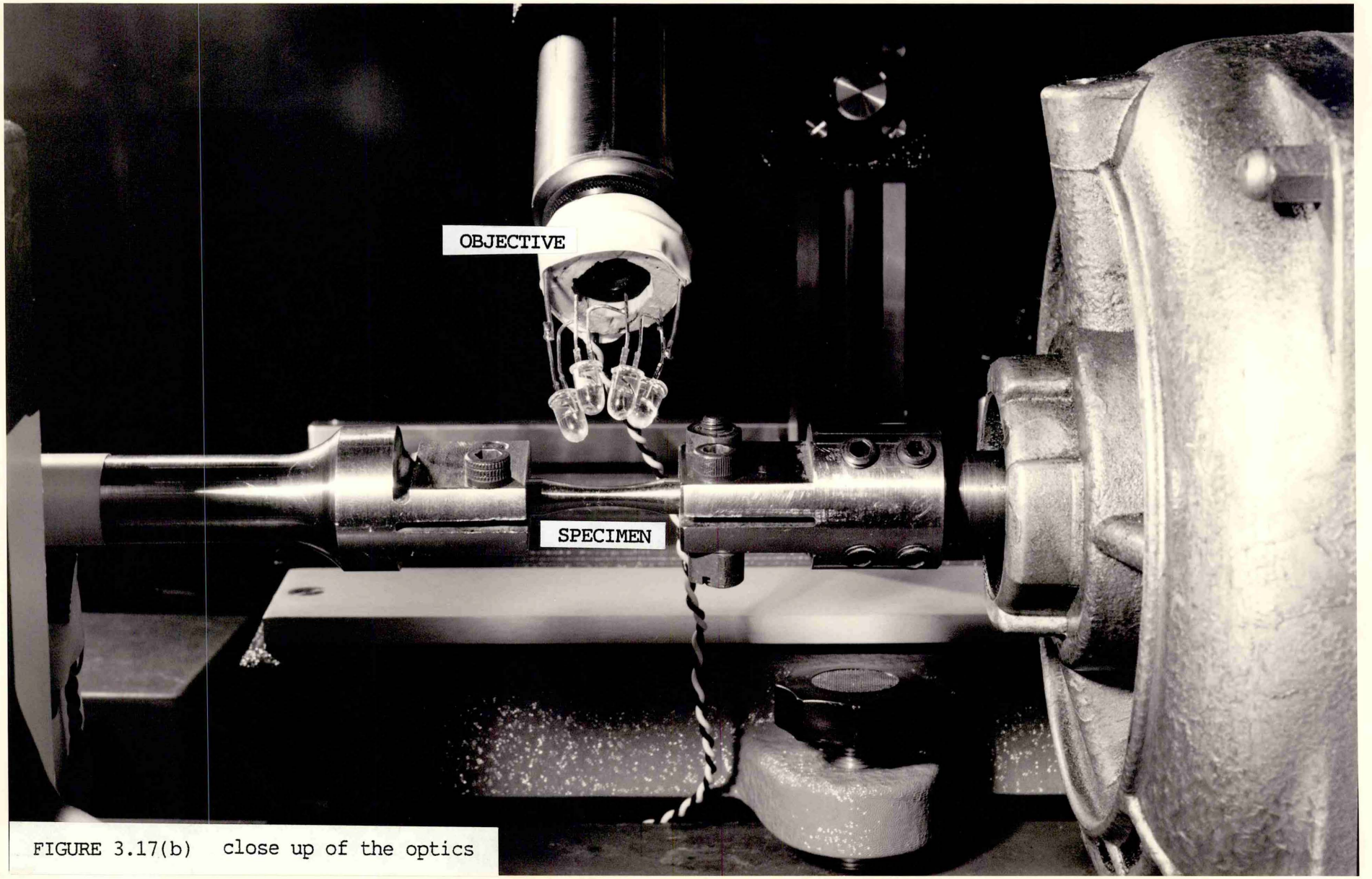

FIGURE 3.17(b) close up of the optics

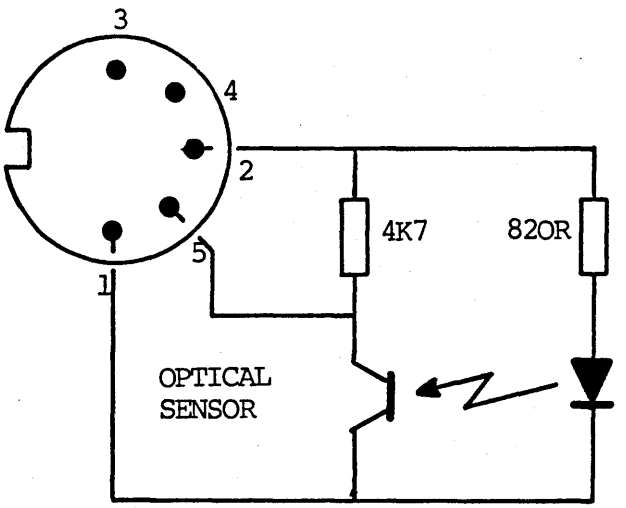

USER SOCKET PIN LAYOUT

PIN	FUNCTION
1	-15 Volts
2	0 Volts
3	+15 Volts
4	Output
5	Input

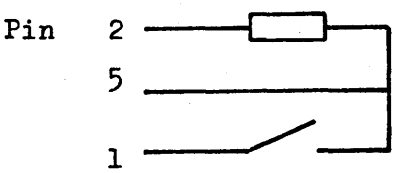

47K

COMMUTATOR
SENSOR

Commutator or
rReed switch

FIGURE 3.18 Connection of optical sensor to the strobe

APPENDIX 3.3.1

SPECIFICATIONS

INPUTS	Sensitivity: .2V peak to peak. Maximum input: 1kV peak to peak, 200V RMS. Bandwidth: 3Hz to 1.5kHz (-3dB). Isolation: Fully floating.
OUTPUTS	Internally adjustable constant current of .2A to 2A. Maximum Output Voltage: 24V.
SUPPLY	Mains or d.c. Mains Input: 120/240V a.c.-50/60Hz at 6VA d.c. Input: ±6 to ±20V.
DIMENSIONS	145 x 47 x 95mm excluding projections. 145 x 49 x 130mm including projections.
WEIGHT	800g.
ANCILARIES	3½ metre mains lead. Selection of Light Emitting Diodes. Optical Sensor.

APPENDIX 3.3.2

LIST OF COMPONENTS

Resistors

R1	100K	.6W	R13	8K2	.6W
R2	100K	.6W	R14	1K	.6W
R3	470R	.6W	R15	200R	.6W
R4	100K	.6W	R16	300R	.6W
R5	1K	.6W	R17	300R	.6W
R6	10K	.6W	R18	5R6	1.0W
R7	500R	.6W	R19	10R	1.0W
R8	1K	.6W	R20	18R	1.0W
R9	500R	.6W	R21	1K	.6W
R10	8K2	.6W			
R11	8K2	.6W			
R12	1K	.6W			

Capacitors

C1	1μF	Polyester	400V	C8	181μF	Polyester	63V
C2	1μF	Polyester	400V	C9	1.64μF	Polyester	63V
C3	1μF	Polyester	63V	C10	1μF	Polyester	63V
C4	10μF	Electrolytic	24V	C11	2μF	Polyester	63V
C5	1μF	Polyester	63V	C12	10μF	Polyester	63V
C6	2μF	Tautalum	24V	C13	10μF	Polyester	63V
C7	10μF	Polyester	63V	C14	100μF	Polyester	63V

Semi Conductors

IC1	741 Operational Amplifier
IC2&3	555 Timer Circuit
TR1&2	BC 1832L
TR3	BD 131
D1-3	4001 Type Silicon Diodes
D4&5	Common cathode type tri-coloured light emitting diode
ZD1	5.1V 400mW Zenner diode

Miscellany

VR1	100K linear 10 turn potentiometer
VR2	47K logarithmic 270° potentiometer
Power Supply	Unregulated $\pm$15 volt employing on/off switch SW1, a 12-0-12 volt 6VA transformer, full wave bridge rectifier and two 2000μF smoothing capacitors
SW2&3	Double pole double throw switches.

3.4 SHOT-PEENING

The process relies on inducing plasticity into the surface of the component whilst the core of the component remains elastic. This is achieved by bombarding the component with a stream of near spherical particles. These may be cast steel shots, rounded-off cut wire, glass or ceramic beads. Steel shots and cut wire are currently the most resilient media available and are widely used to achieve high intensities of peening. Glass and ceramic beads break up rapidly when used to achieve high intensities, but they do offer the possibility of lightly peening non-ferrous materials without the risk of ferrous contamination. Where high intensities of peening are required in non-ferrous materials, it is common to first peen the component with steel shot and then to re-peen it lightly with glass or ceramic beads. This is believed in the industry to both decontaminate the surface and further improve the extreme surface residual stresses. It also gives the surface a brighter appearance.

The acceleration of the peening media is achieved either by a centrifugal peening wheel or by feeding the media into a jet of air. Peening wheels are generally used for high volume, low cost peening applications where some variability in the quality of peening is permissible. Air peening systems are generally much more precisely controlled and can generate more reproduceable results. Their productivity though is generally much lower. Figure 3.19 illustrates schematically, the components of a peening system.

The residual stresses generated by shot-peening tend to cause thinner components to bow such that the peened surface becomes larger than before. This effect is widely used to form precise curvatures in large components. Wing panels, spars and fuselage panels are commonly peen-formed. Conversely, slightly warped but otherwise acceptable forgings and castings may be "peened-straightened" in the same way.

For consistent and effective peening the process must be closely controlled. The variables having the most significant effect on the effectiveness of peening are as follows:

- the size and size distribution of the media

- its hardness and density

- the velocity and obliquity with which the media impacts the component
- the cleanliness of the component and the media
- the shape of the media
- the coverage, i.e., the proportion of the area of the component which has been impacted.

These basic variables are usually considered in terms of the process variables such as nozzle or wheel type, air pressure or wheel rotational speed, media flow rate, exposure time, nozzle or wheel to workpiece distance and media quality, etc. [3.12].

Effect and Assessment of peening

Shot-peening generally induces three obvious changes in the condition of a component:

(i) a change in the residual stress field in the component

(ii) a change in the degree of work hardening in the surface of the component

(iii) the original surface finish will be modified by the plastic indentations.

The change in residual stresses is produced by the local nature of the deformation produced by the impingement. Whilst the bulk of the material remains elastic, the material immediately adjacent to the point of an impact yields, tending to spread out a little. When the shot rebounds, the component unloads, placing the yielded material in compression. In thin components, this unloading can manifest itself in a measurable curvature. This curvature forms the basis for one of the most widely used methods of indicating the severity of peening, known as the Almen strip.

The Almen strip is a small strip of spring steel which is used as a standard for purely comparative measurements of the severity or "intensity" of peening. Precise details of the strips and the methods by which they should be used are given in [3.5]. The basis of the test is to subject an Almen strip to the media stream until its curvature reaches a near limiting value. This curvature is then quoted as a measure of the intensity of peening.

The change in hardness of the surface is easily, albeit destructively, evaluated by standard indentation techniques like Vickers microhardness. The hardness change is in fact the result of several factors, namely: dislocation density and sub-structure, the residual stress field and the phase constitution [3.13].

Whilst the depth and shape of the indentations produced by shot-peening can potentially reveal much about the severity of peening, examinations of peened surfaces are usually limited to an examination of "coverage", i.e., the proportion of the surface actually covered by indentations. Image analysis facilities can give some indication of coverage but the results can be misleading if the prior surface finish was poor.

Equipment Used

The equipment used for peening specimens in conjunction with this study is depicted in Fig. 3.20. It consists of a media handling system featuring dual pressure vessels for continuous operation, and a single nozzle blast cabinet with motor driven lances and component handling equipment. The peening media is introduced into the air current at the base of the media handling system. This is achieved by allowing the media to fall through an adjustable orafice from the lower pressure vessel which is periodically re-charged with recovered media via the second pressure vessel. The recovery system uses a large venturi to suck used media from the base of the peening cabinet into a whirlwind chamber where sound media is separated from dust and fractured or sub-size media. The dust laden air is drawn through filters before it exits from the system via the venturi whilst sound media falls to the base of the whirlwind chamber where it is periodically admitted to the upper pressure vessel which acts as a pressure lock between the recovery system and the high pressure system.

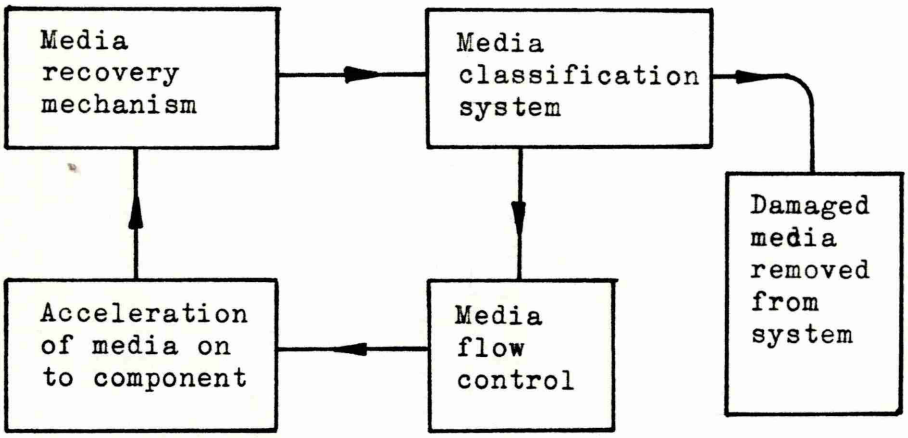

FIGURE 3.19 Schematic representation of a shot-peening system represented from the point of view of the media

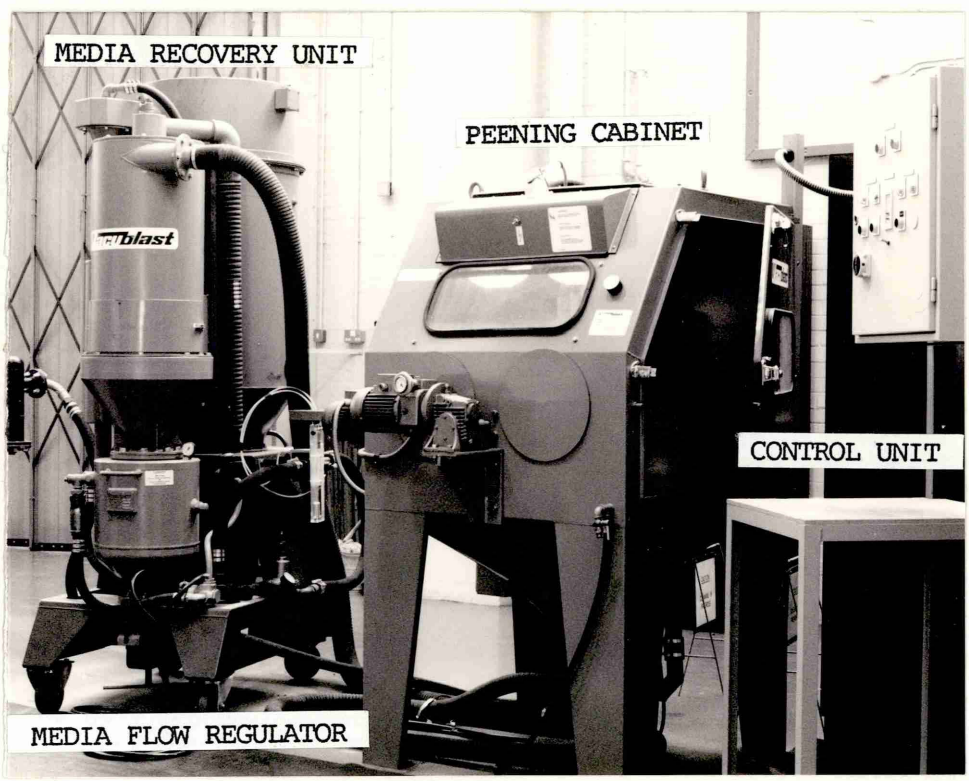

FIGURE 3.20 Peening eqipment used

The media used was a medium hard S230 shot. This was conditioned before use by using it to peen a hard target for a time adequate for the media to be re-circulated in the system three times, using a nozzle pressure of 320KPa (45 psi). This is somewhat higher than the pressures used for peening specimens, ensuring minimum shot working and media instability during peening.

A sample of the conditioned shot was prepared for metallurgical examination and hardness testing. The shots were mounted in an edge retaining Bakelite and polished down to a diametral section. A hardness survey of the media indicated that over 80% of the shots were in the hardness range 550 to 700 MPa, using a micro Vickers indentor with a 1 Kg load and an indent period of 15 seconds. The mean hardness was 656 MPa.

The sectioned shots were then etched in 2½ Nital and examined metallographically. They possessed a fine martnesitic microstructure with evenly distributed carbides and type II (rounded) Manganese Sulphide inclusions. Their overall shape and structural integrity was good. Fig. 3.21 shows a typical micro-structure and Figure 3.22 shows the types if misshapen shots present.

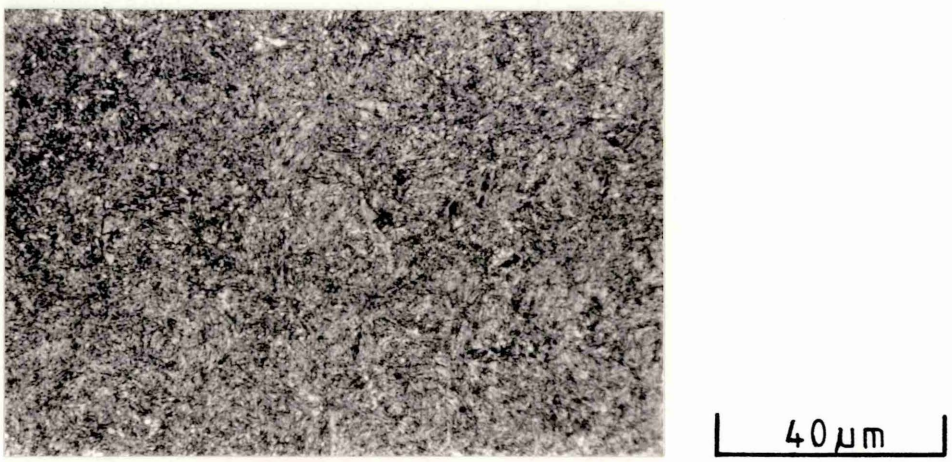

FIGURE 3.21 Shot microstructure

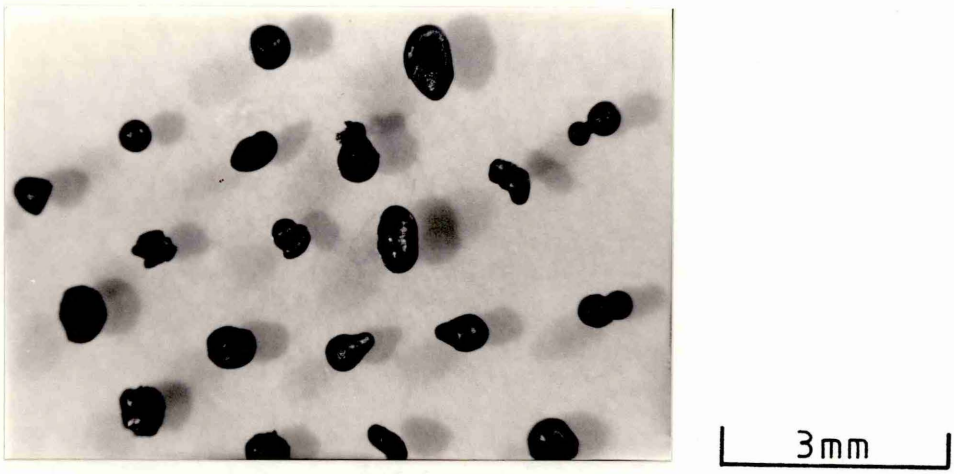

FIGURE 3.22 Shot geometry showing some misshapen shots

An Almen curve was generated for the conditions used to peen the fatigue specimens. It indicates that the specimens were peened to beyond Almen saturation. The saturation curves are depicted in Fig. 3.23.

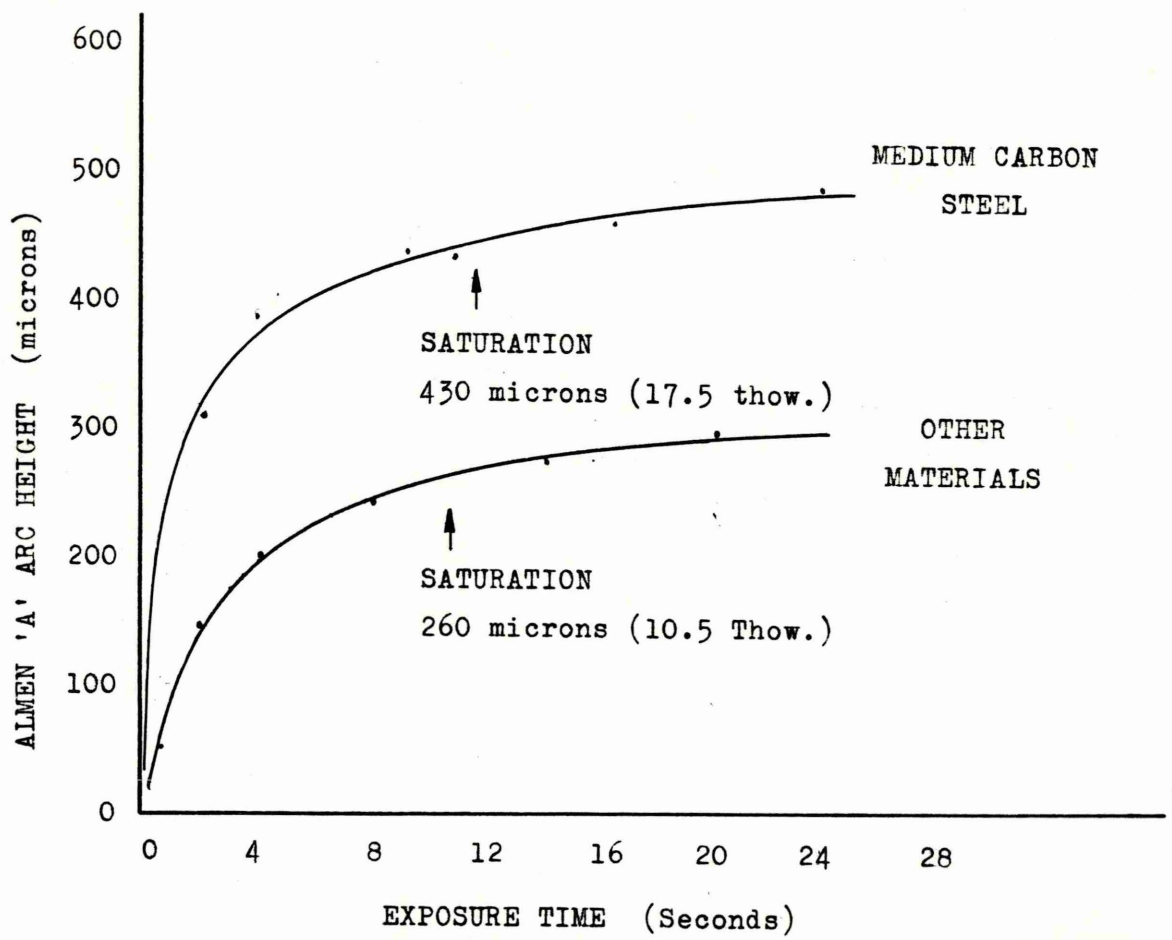

FIGURE 3.23 Almen arc height

3.5 RESIDUAL STRESS MEASUREMENT

A large number of residual stress measuring techniques exist [3.14]. Whilst many of these are very interesting they have not yet found widespread usage for one reason or another. These techniques include Neutron diffraction, which requires a beam of slow neutrons (from a nuclear reactor) [3.15], Positron Annihilation [3.16], Ultrasonics [3.6], [3.17 [3.18], Acoustic Emission [3.7] [3.19], Barkhousen noise [3.20], and Indentation methods [3.21].

Three techniques have however, become well established and are in regular scientific and engineering use. Two of these, the hole drilling and dissection techniques, rely in relieving the residual stresses by metal removal, and thirdly the x-ray diffraction technique uses changes in the lattice spacing to evaluate residual elastic strains.

3.5.1 X-Ray Diffraction

This method relies on the atomic structure of the material under investigation. At its most basic level, the equilibrium positions of planes of atoms within any crystalline structure is a function of the composition temperature and the state of stress. When the structure is being subjected to compression in one direction, the lattice spacing will be decreased. Since x-ray diffraction can be easily used to measure lattice parameters, residual stresses can be computed from x-ray diffraction data. References [3.22] and [3.23] give more specific information on the experimental and data interpretation aspects of x-ray residual stress measurements.

The method may be used non-destructively just on the surface of the component, but this yields only a value of surface residual stress. In order to survey residual stresses as a function of depth, it is necessary to remove layers of material by for instance, electropolishing, and performing an additional measurements. In this investigation, such an electrolytic layer removal technique was used to measure residual stresses as a function of depth. The equipment used for the measurements was a Rigau Strainflex computerised goiniometer system which also gave a direct reading of x-ray peak breadth, which is related to the diffracting domain size, which reflects the degree of "deformation" in the material. More particular information on the test parameters used is given in Chapter Five.

3.5.2 Hole Drilling

The hole drilling technique relies upon the relaxation of residual strains which occurs when a small hole is introduced into a residually stressed component. This can be recorded by means of strain gauges in the vicinity of the hole [3.24]. This method requires that a strain gauge rosette of suitable design is fixed to the component in the area of interest, and that these gauges must then be connected to suitable excitation and monitoring equipment, and measurements made before the hole is begun. The drilling of the hole typically involves the use of an ultra high speed end mill or an abrasive machining jig, though in principle other techniques could be used. The important consideration is that the creation of the hole should not introduce significant levels of residual stress as these will undermine the assumption of elastic unloading due to the presence of the hole. In practice only low levels of residual stress are recorded in stress free samples indicating that the residual stresses associated with ultra high speed milling and abrasive machining are low in comparison to other sources of variation and error involved in the technique.

Some hole drilling measurements were done in connection with the current studies. The equipment used is depicted in Fig. 3.24. It consists of a jig, an optical alignment and measuring microscope and an air abrasive machining drill employing an off-centre saphire nozzle. In order to ensure good hole geometry the machining nozzle is fitted slightly off axis, and rotated around the drill axis whilst drilling is in progress. The displacement of the nozzle from the axis determines the radius of the hole drilled so that a single nozzle can be used to drill holes of differing size.

Whilst the technique was principally developed to measure residual stresses of magnitude independent of depth, numerical correction techniques allow data from incrementally drilled holes to be used to give residual stress profiles of σ_1 and σ_2 with depth [3.25].

Full details of the techniques employed are given in [3.26]. The measurements made were used to corroborate x-ray diffraction measurements.

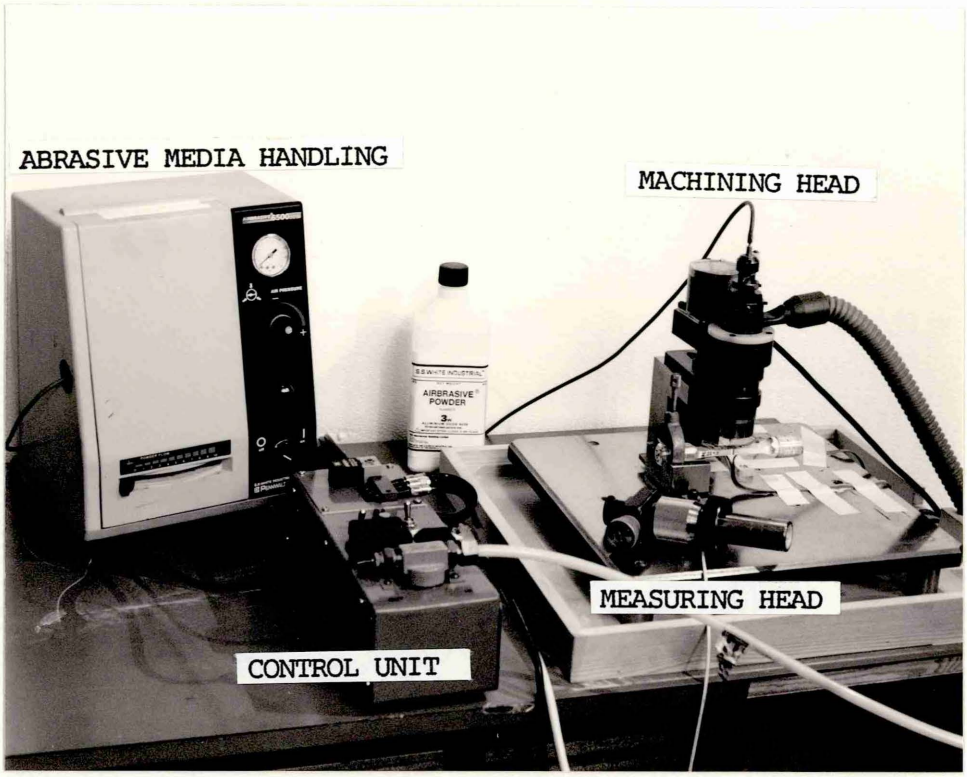

FIGURE 3.24 Hole drilling residual stress measuring equipment

3.5.3 Dissection Technique

This technique utilises the change in shape of a component when a residually stressed layer of material is removed. It is hence only usable on thin components which will show measurable changes in curvature or shape when a residually stressed layer is progressively removed. It is, however, a very simple technique to use and requires only simple and inexpensive hardware. In the current investigation this technique was used to measure residual stresses in thin tokens of material subjected to different peening parameters and after exposure to elevated temperatures.

In the current investigation, the strip specimens were protected on one face with P.V.C. tape to prevent the back face from being dissolved, and then the front face of the strip was subjected to attack by strong acid or alkali, electrolytically in the case of steels, particularly stainless. The electrolytic cell used is shown in Fig. 3.25. It consists of the specimen, and electrode to connect with the specimen, and a perforated cathode, all submerged below the level of the electrolyte. The current source used was a conventional battery charger.

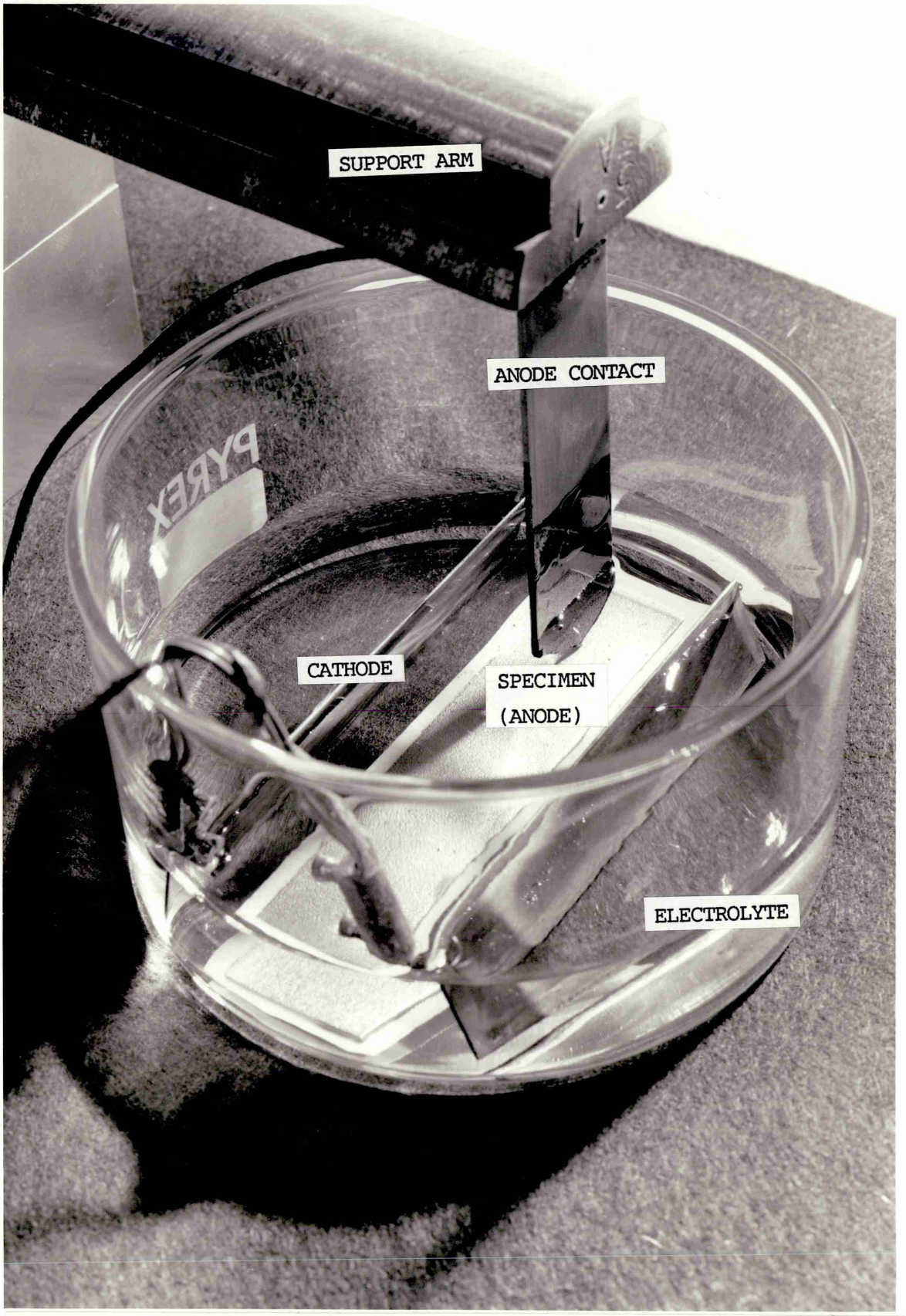

FIGURE 3.25 Dissection technique for measuring residual stress.

LIST OF FIGURES

3.1 Rotating bend configurations

(a) Three point bend

(b) Four point bend

3.2 Large rotating bend rig used in investigation

3.3 Calibration specimen

3.4 Schematic of a servo-hydraulic uniaxial test machine

3.5 Servo-hydraulic test machine used in investigation

3.6 Ultrasonic flaw detection

(a) Simple setup giving 'A' scan readout

(b) Setup utilising multiple probes to size a crack in a C.T. specimen

3.7 Schematic acoustic emission setup

3.8 Basic eddy current setup

3.9 D.C. potential drop setup

3.10 A.C. potential drop setup

3.11 Replica of a partially peened surface

3.12 Basic principle of operation of the strobe

3.13 Interior and construction of the prototype strobe

3.14 Circuit diagram of the strobe

3.15 Layout of the controls of the strobe with light emitting diodes and an optical sensor

3.16 Correct connection of light emitting diode

3.17 Typical experimental set-up for the strobe system

(a) as a whole
(b) close up of the optics

3.18 Connection of optical sensor to the strobe

3.19 Schematic representation of a shot-peening system represented from the point of view of the media

3.20 Peening equipment used

3.21 Shot microstructure

3.22 Shot geometry showing some misshapen shots

3.23 Almen arc height

3.24 Hole drilling residual stress measuring equipment

3.25 Dissection technique for measuring residual stress.

REFERENCES

[3.1] British Standards Institution Guidance on some methods for the derivation of acceptance levels for defects in fusion welded joints. P.D. 6493, 1980.

[3.2] Schijve, J., Four lectures on fatigue crack growth, Engineering Fracture Mechanics, Vol. 11, No. 1, 1979, pp 165-222.

[3.3] Duggan, T.V., and Byrne, J., Fatigue as a design criterion, Macmillan Press Ltd., London, 1979.

[3.4] Frost, W.E., Marsh, K.J., and Pook, L.P., Metal Fatigue, Clarendon Press, Oxford, 1974.

[3.5] Hammond, D.W., The mechanics of peening and re-peening partially fatigued components, M.Phil. Dissertation, Cranfield Institute of Technology, 1986.

[3.6] Szilard, J., Editor, Ultrasonic testing: non-conventional testing techniques, Pub. John Wiley and Sons, 1982.

[3.7] Nichols, R.W., Acoustic emission, Applied Science Publishers Ltd., London, 1976.

[3.8] Sabbagh, H.A., and Sabbagh, D.L., Inversion of eddy-current data and the reconstruction of flaws using multi-frequencies, in International Advances in Non-destructive Testing, Vol. 10, Ed. Warren J. McGonnagle, Gordon and Breach Science Publishers, S.A.1984, pp 267-307.

[3.9] Clark, G., Fatigue at low growth rates in a maraging steel. Fatigue Engng. Mater. Struct. Vol.9, No.2, 1986, 131-142.

[3.10] Su, X., Gu, M., and Yan, M., A simplified residual stress model for predicting fatigue crack growth behaviour at cold worked fastener holes, Fatigue Engng., Mater. Struc. Vol.9, No.1, 1986, pp 57-64.

[3.11] Brown, R., and Smith, G.C., A note on the influence of rest periods on the fatigue endurance of a titanium alloy, Fatigue Engng. Mater. Struct. Vol.7, No.3, 1984, pp 229-235.

[3.12] Meguid, S.A., Notes on shot peening used at short courses at Cranfield Institute of Technology, 1987.

[3.13] Mutoh, Y., Fair, G.H., Noble, B., and Waterhouse, R.B., The effect of residual stresses induced by shot-peening on fatigue crack propagation in two high strength aluminium alloys, Fatigue Fract. Engng. Mater. Struct. Vol.10, No.4., 1987, pp 261-272.

[3.14] Mordfin, L., Measurement of residual stresses: problems and opportunitues in Residual Stress for Designers and Metallurgists, Ed. Larry J. Vande Walle, American Society of Metals, 1981, pp 189-210.

[3.15] Krowitz, A.D., Burune, J.E., and Schmank, M.J., Measurements of stress in the interior of solids with neutrons. Proc. Residual Stress and Stress Relaxation. Sagamore Lake Placid, 1981, Ed. E. Kula and V. Weiss, Plenum Press, New York, 1982, pp 139-156.

[3.16] Reno, R.C., Swartzendraber, L.J., and Bennett, L.H., Positron annihilation effects of defects in titanium, Non-Destructive Testing International, Vol.12, No.5, 1975, pp 224-228.

[3.17] Hsu, N.N., Acoustical birefringence and the use of ultrasonic waves for experimental stress analysis, Experimental Mechanics, Vol.14, No.5, 1974, pp 169-177.

[3.18] Hirao, H., Fukuoka, H., Toda, H., Sotani, Y., and Suzki, S., Non-destructive evaluation of hardening depth using surface-wave dispersion patterns. Journal of Mechanical Working Technology, Vol.8, 1983, pp 171-179.

[3.19] Briggs, A., An introduction to scanning acoustic microscopy, Oxford University Press, 1985.

[3.20] Ono, K., Shabata, M., and Kwan, M.M., Determination of residual stress by magneto mechanical acoustic emission in Residual Stress for Designers and Metallurgists, Ed. Larry J. Vaude Walle, American Society of Metals, 1981, pp 223-243.

[3.21] Simes, T.R., Mellor, S.G., and Hills, D.A., A note on the influence of residual stress on measured hardness. Journal of Strain Analysis, Vol.19, No.2, 1984, pp 135-137.

[3.22] Maeder, G., Lebrun, J.L., and Spranel, J.M., Present possibilities for the x-ray diffraction method of stress measurement, N D T International, October 1981, pp 235-247.

[3.23] Cullity, B.D., Elements of x-ray diffraction, Addison Wesley, New York, 1956.

[3.24] Kabiri, M., Measurement of residual stresses by the hole drilling method; Influences of transverse sensitivity of the gauges and relieved strain coefficients, Experimental Mechanics, Vol.24, No.3, pp 252-296.

[3.25] Rasul, T., Effect of pre- and post- processing upon shot peening residual stress. Ph.D. Thesis, Cranfield Institute of Technology, 1988.

CHAPTER FOUR

THREE-DIMENSIONAL FINITE ELEMENT ANALYSIS OF CIRCUMFERENTIALLY-CRACKED BODIES

SUMMARY

4.1 Background

4.2 Interactive Modelling

4.2.1 Model Creation and Mesh Definition
4.2.2 Model Checking
4.2.3 Simulation of Cracked Bodies using the Finite Element Method

4.3 Finite Element Approach

4.4 Determination of Stress Intensity and Stress Concentration Factors

4.5 Finite Element Results

SUMMARY

A comprehensive three-dimensional finite element analysis is made of cylindrical components containing cracks using the interactive solid modelling facility of SDRC-GEOMOD. Both stress concentration and stress intensity factors were evaluated for different cracked geometries, and the relation between k_t and K_I was derived for different crack depths.

The present chapter was initiated because of its importance to the fatigue testing of the cylindrical specimens described in Chapter Three. Specifically, the relationship between K_I and a, the crack dpeth, is of great use in evaluating crack growth rate data which can subsequently be used in design.

4.1 BACKGROUND

Stress-intensity factor solutions are of great value in the design of engineering components. Cylindrical components are in common use in engineering applications. The current literature indicates that a very restricted number of solutions exist for cylindrical components. This is partly due to the complexities of a three-dimensional analysis, see references [4.1, 4.2 and 4.3].

In view of the above, it was decided to examine circumferentially-cracked components using the finite element approach. This was deemed necessary in view of the importance of these solutions to the investigation.

4.2 INTERACTIVE MODELLING

Current sophisticated finite element packages employ powerful pre- and post-processing facilities for the interactive preparation of data. SDRC-GEOMOD is one of such packages. It is commonly used by the aerospace industry. With it, the user can interactively generate the appropriate nodes and elements, impose the necessary restraints and other boundary conditions ready for the analysis. The pre- and post-processors of the SDRC package are known collectively as SUPERTAB.

4.2.1 Model Generation and Mesh Definition

The solid modelling facility of the SDRC package, known as GEOMOD, was used to interactively generate the three-dimensional geometry of the cylindrical component depicted in Fig. 4.1.

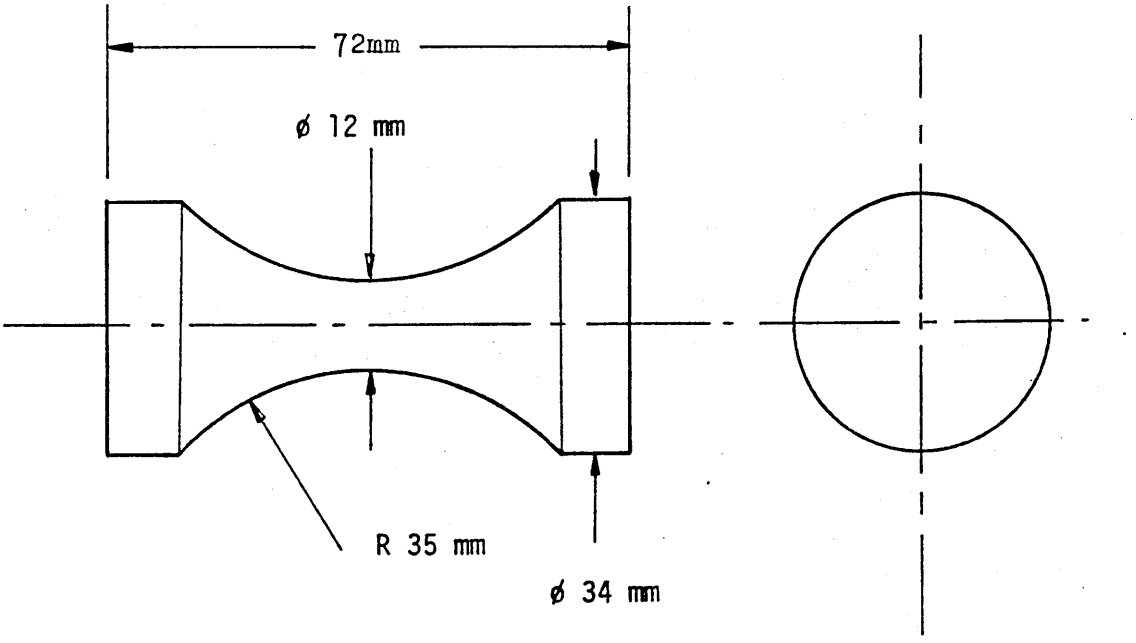

Figure 4.1 Geometry of the three-dimensional solid model

This geometry was then transferred to the pre-processor, SUPERTAB, for mesh definition. Two approaches can be followed to create the mesh:

(i) mapped mesh generation, and
(ii) enhanced mesh generation.

In the present work, it was thought appropriate to use the mapped mesh generation facility to enable the creation of elements with known aspect ratios so as to maintain accuracy in relation to the induced cracks. This mapped mesh generator allows elements to be concentrated into the regions of interest by biasing the mesh.

In view of the symmetry of the component about the x and y planes, only one-quarter of the model was considered in the analysis. Fig. 4.2 shows a typical example of a discretised model of the cylindrical configuration, with a bias towards the outer surface at one end, enabling the use of a finer mesh in the vicinity of the crack.

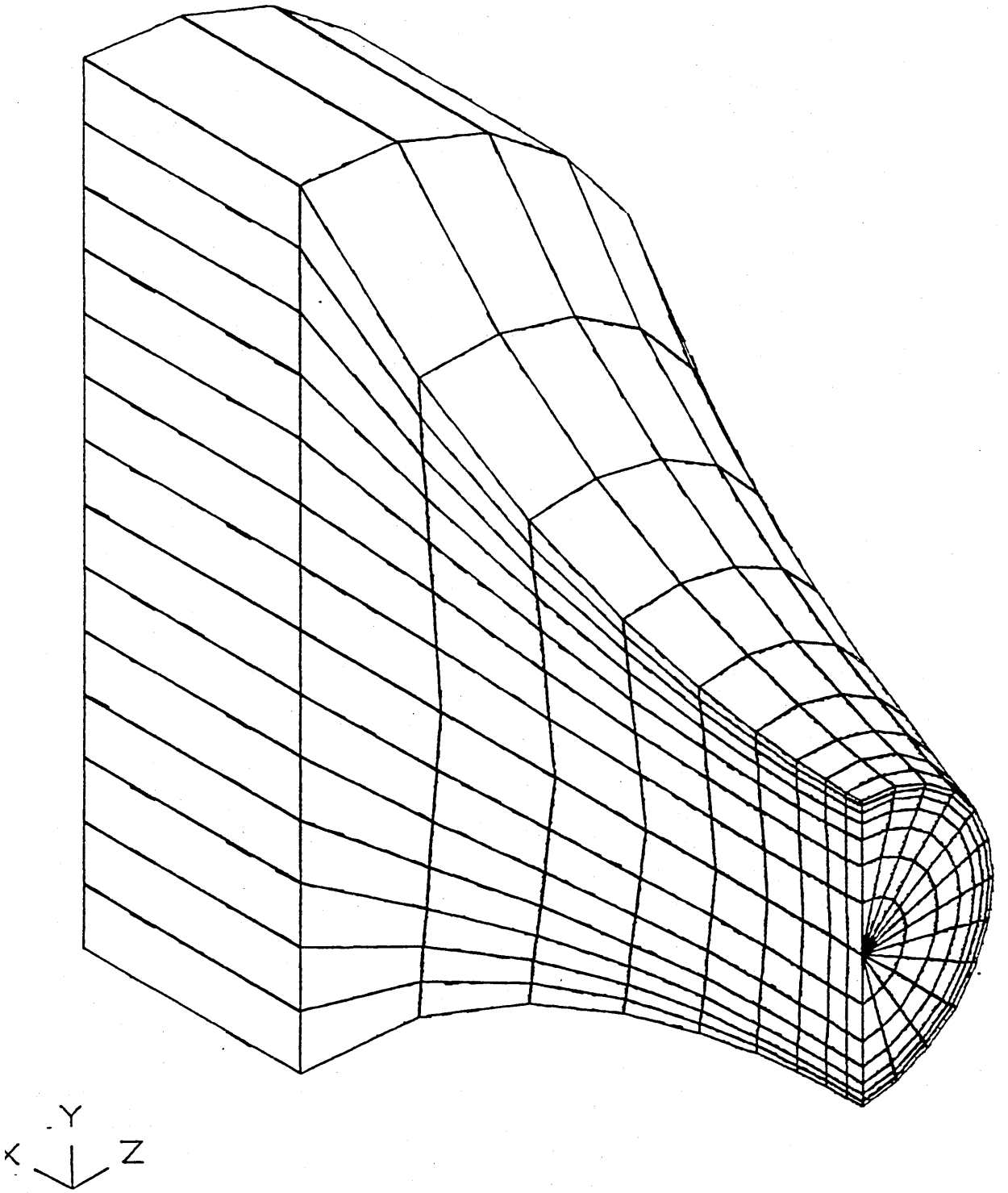

FIGURE 4.2 Discretised model

Eight noded linear brick elements were used to model the body and a total of 840 elements and 1012 nodes were used. The applied couple was simulated by the application of two equal and opposite forces acting at the extremities of the shoulder of the component. The appropriate restraints were then imposed on the model.

4.2.2 Model Checking

The model described was then checked before submission to the analysis program. The following checks were made:

(i) coincident nodes
(ii) coincident elements
(iii) element distortion
(iv) free-edge continuity

4.2.3 Simultion of Cracked Bodies using the Finite Element Method

In this study cracks were simulated by omitting restraints on the nodes near the outer circumference. The biasing of the mesh ensured that the large transitions in displacement and stress fields experienced in the vicinity of the crack tip were evaluated with a fine mesh whilst most of the model had a more coarse mesh. The mesh, and the elements used were a compromise between cost, accuracy and the time available for this part of the study.

Fig. 4.3 shows the model containing a crack, ready for analysis.

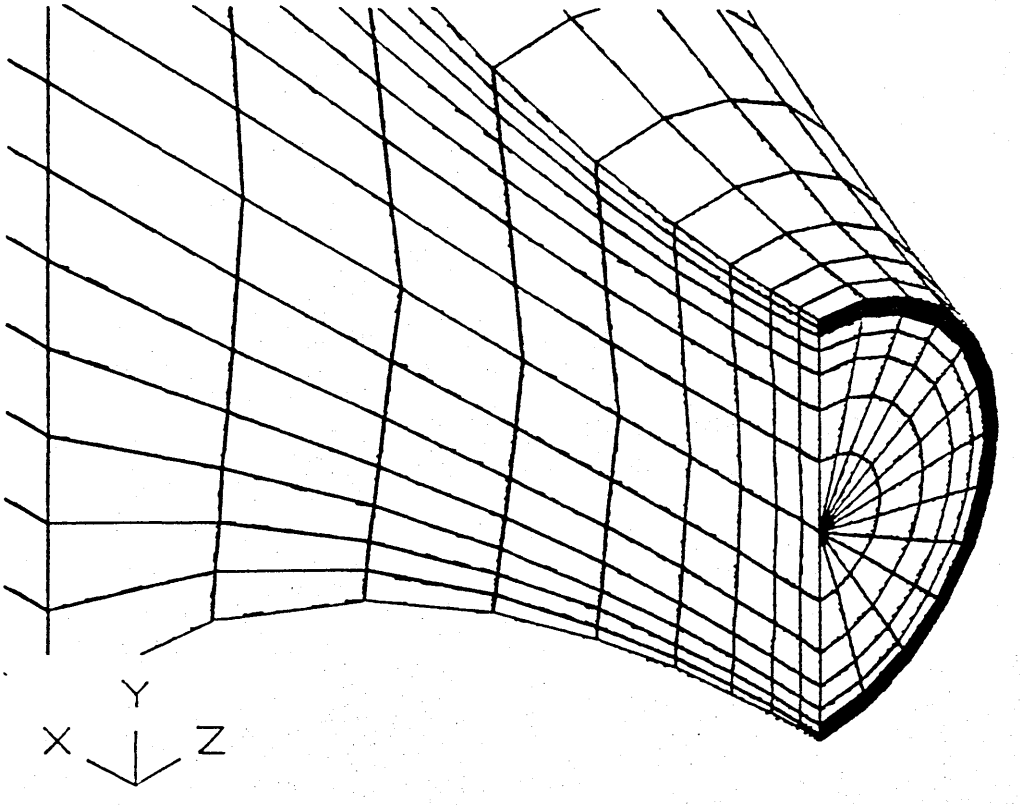

Figure 4.3 Completed model showing crack face elements shaded

4.3 THE FINITE ELEMENT APPROACH

The basic steps in any structural finite element solution are summarised as follows:

(i) sub-division of the domain into a number of smaller sub-domains or "finite elements", defining nodal points which connect the sub-domains.

(ii) evaluation of element stiffness and load terms $[\underset{\sim}{K}^{e}]$ and $[\bar{F}^{e}]$.

(iii) assembly of the global element stiffness matrices to obtain a piecewise continuous function for the entire domain thus generating global stiffness and load matrices, as follows:

$$\left[\underset{\sim}{K} \right] = \sum_{i=1}^{n} \left[\underset{\sim}{K}^{e} \right]$$

$$\left[\underset{\sim}{F} \right] = \sum_{i=1}^{n} \left[\underset{\sim}{F}^{e} \right] \qquad (4.1)$$

Where n = number of elements

(iv) solution of the resulting set of simultaneous equations for the unknown nodal displacements:

$$\left[\underset{\sim}{K} \right] \cdot \left[\underset{\sim}{u} \right] = \left[\underset{\sim}{F} \right] \qquad (4.2)$$

4.4 DETERMINATION OF STRESS INTENSITY AND STRESS CONCENTRATION FACTORS

The finite element solution yields nodal displacements and nodal forces. In order to use these results they need to be simplified to the linear elastic fracture mechanics parameters K_I and K_t, the stress intensity and stress concentration factors.

This transposition can be accomplished by reference to the work of Sih and Liebowitz [4.4]. Fig. 4.4 defines the co-ordinates referenced in equations (4.1) to (4.11).

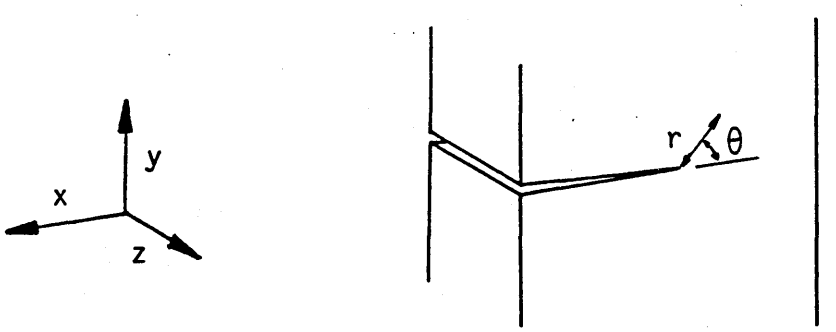

Figure 4.4 Co-ordinate system for equations (4.1) to (4.11)

Displacements in the x,y and z directions are referenced as displacements u,v and w respectively.

Sih and Liebowitz showed that the displacements u,v and w may be written in terms of stress intensity factors K_I, K_{II} and K_{III}:

$$u = \frac{1+\nu}{4E}\sqrt{\frac{2r}{\pi}}\left\{K_I\left[(5-8\nu)\,\mathrm{Cos}\,\frac{\theta}{2} - \mathrm{Cos}\,\frac{3\theta}{2}\right]\right.$$

$$\left. + K_{II}\left[(9-8\nu)\,\mathrm{Sin}\,\frac{\theta}{2} + \mathrm{Sin}\,\frac{3\theta}{2}\right]\right\} + O(r) \qquad (4.3)$$

$$v = \frac{1+\nu}{4E}\sqrt{\frac{2r}{\pi}}\left\{K_I\left[(17-8\nu)\,\mathrm{Sin}\,\frac{\theta}{2} - \mathrm{Sin}\,\frac{3\theta}{2}\right]\right.$$

$$\left. - K_{II}\left[(3-8\nu)\,\mathrm{Sin}\,\frac{\theta}{2} + \mathrm{Sin}\,\frac{3\theta}{2}\right]\right\} + O(r) \qquad (4.4)$$

$$w = \frac{K_{III}}{\sqrt{2\pi r}}\,\mathrm{Cos}\,\frac{\theta}{2} + O(r) \qquad (4.5)$$

The corrresponding stress field in the vicinity of the crack-tip may be expressed so:

$$\sigma_x = \frac{K_I}{\sqrt{2\pi r}}\,\mathrm{Cos}\,\frac{\theta}{2}\left[1-\mathrm{Sin}\,\frac{\theta}{2}\,\mathrm{Sin}\,\frac{3\theta}{2}\right]$$

$$- \frac{K_{II}}{\sqrt{2\pi r}}\,\mathrm{Sin}\,\frac{\theta}{2}\left[2+\mathrm{Cos}\,\frac{\theta}{2}\,\mathrm{Cos}\,\frac{3\theta}{2}\right] \qquad (4.6)$$

$$\sigma_y = \frac{K_I}{\sqrt{2\pi r}} \cos\frac{\theta}{2}\left[1+\sin\frac{\theta}{2}\sin\frac{3\theta}{2}\right]$$

$$+ \frac{K_{II}}{\sqrt{2\pi r}} \sin\frac{\theta}{2}\left[\cos\frac{\theta}{2}\cos\frac{3\theta}{2}\right] + \theta(r) \qquad (4.7)$$

$$\sigma_z = \nu\,(\sigma_x + \sigma_y) \qquad (4.8)$$

Where E = Young's modulus

ν = Poisson's ratio.

For the purposes of this study, equations (4.4) and (4.7) may be simplified to the following:

$$v = \frac{2\,(1-\nu^2)}{E}\sqrt{\frac{2r}{\pi}}\,K_I \qquad (4.9)$$

$$\sigma_y = \frac{K_I}{\sqrt{2\pi r}} \qquad (4.10)$$

By the extrapolation of finite element results these expressions were used directly to evaluated $_{KI}$ for the cracked geometry.

Stress concentration factor K_t values for the various geometries were evaluated using the following expression:

$$k_t = \frac{\sigma_{y\ max}}{\sigma_{ynom}} \qquad (4.11)$$

Where $\sigma_{y\ max}$ is σ_y in the vicinity of the crack-tip and $\sigma_{y\ nom}$ is the value σ_y would be in an uncracked component of the same general dimensions under the same external load.

4.5 FINITE ELEMENT RESULTS

In order to examine the accuracy of the current solution, the results were compared with the most appropriate solutions available. Fig. 4.5 is a graph of K_I vs a for the current soltution, but also showing the solutions of Benthem and Koiter [4.2] and Harris [4.3].

Fig. 4.6 represents, in an exaggerated form, the displacement of the loaded model.

Figure 4.7 is a representation of the approximate level of σ_y in the plane of the crack.

Both the displacement and stress approaches to evaluating K_I and k_t gave good agreement.

Whilst the current analysis was necessary, on account of the absence of a completely suitable solution in the literature, approximate comparisons can be made by considering the work of Benthem and Koiter [4.2] and Harris [4.3]. Fig. 4.5 shows both the current solution for the precise geometry used, and solutions based on the aforementioned authors for circumferentially cracked cylindrical components in bending.

Fig. 4.6 shows an exaggerated displacement graphic which the post processing facilities of the IDEAS package can be used to generate. Another means of displaying qualitatively the outcome of a finite element analysis is a contour plot as depicted in Fig. 4.7 for the axial component of stress. It is even possible to use colour contouring to highlight areas of high stress or strain though this is hardly necessary on such simple geometries as those dealt with here.

The computing of stress intensity factors from the output of an analysis, it is possible to use either nodal displacement or averaged element stress data. The good agreement obtained between the two methods indicated that some faith could be placed in the results.

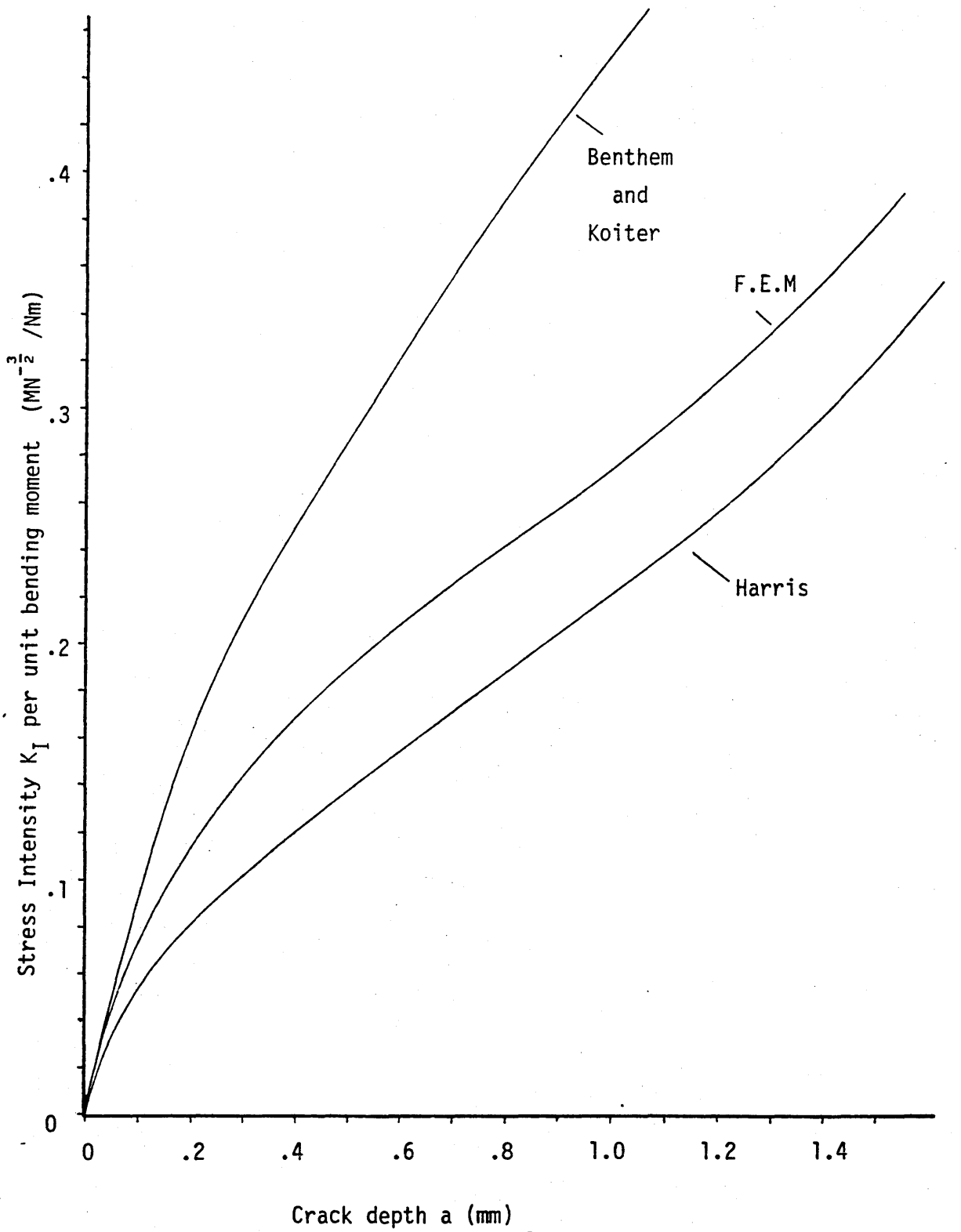

Figure 4.5 Graph of K_I versus a for the current solution, and the solutions of Benthem and Koiter and Harris.

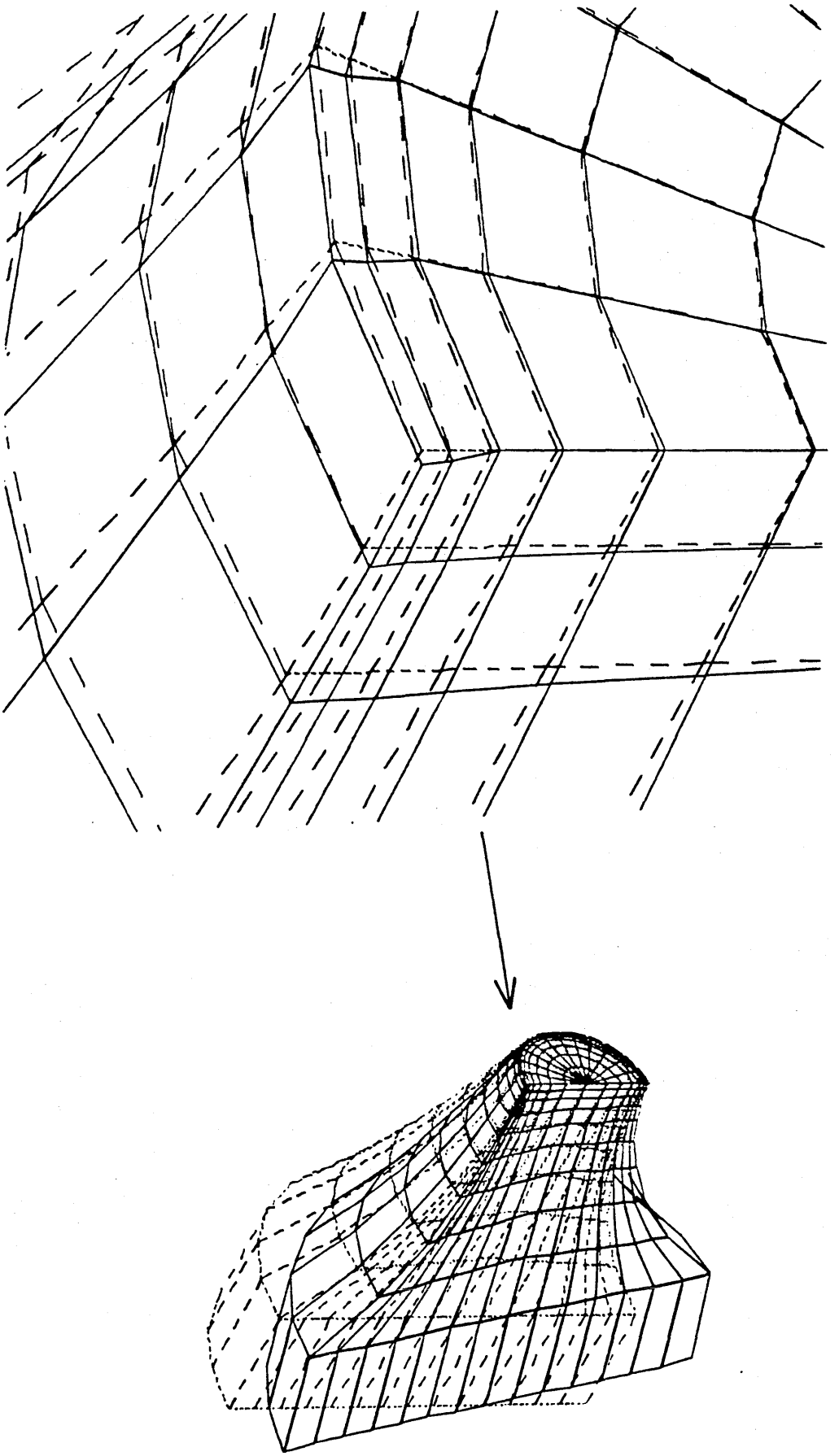

FIGURE 4.6 Exaggerated representation of model displacement

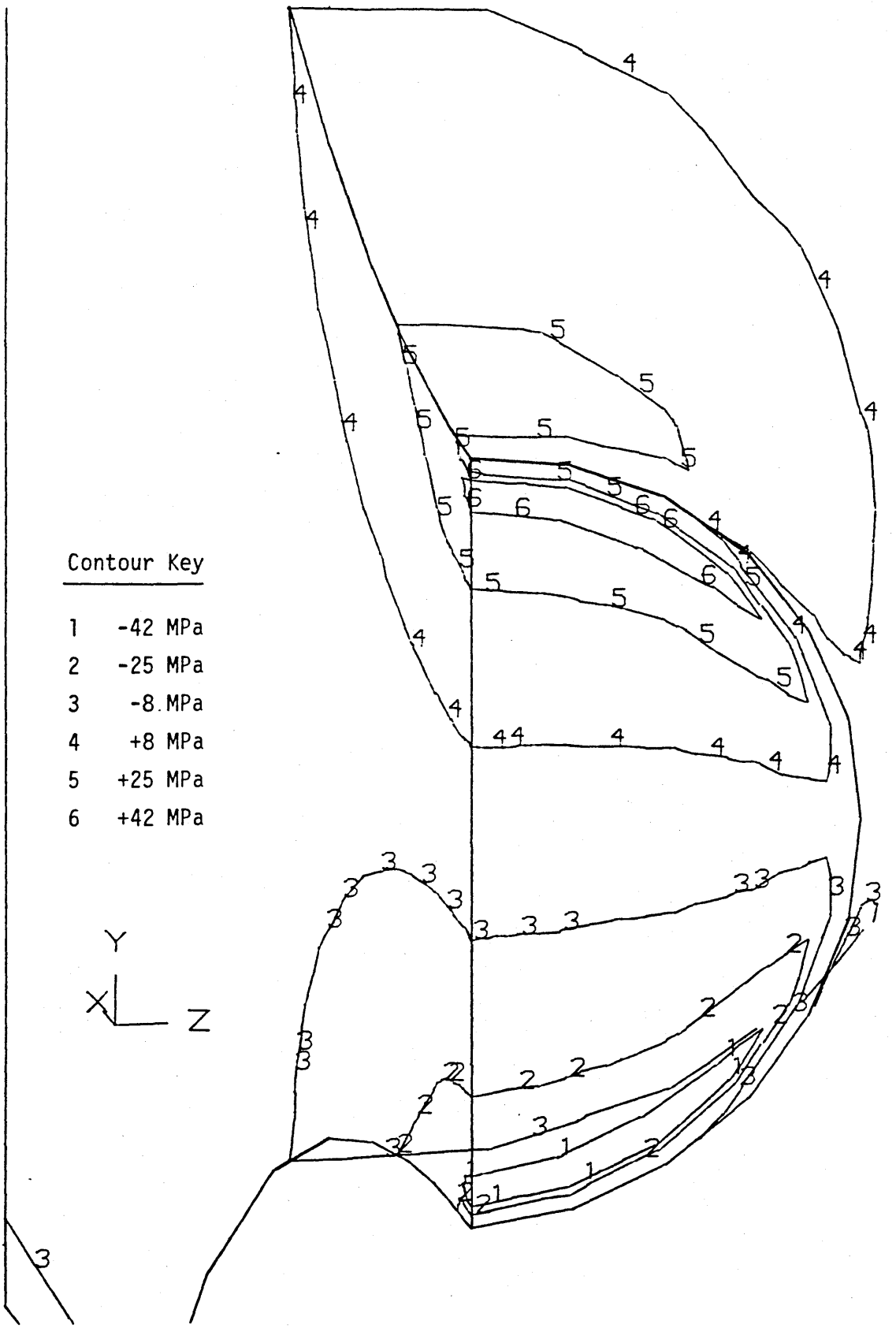

Figure 4.7 Representation of the approximate level of stress in the plane of the crack.

LIST OF FIGURES

Fig. 4.1 Geometry of the three dimensional solid model

Fig. 4.2 Discretised solid model

Fig. 4.3 Completed model showing crack face elements

Fig. 4.4 Co-ordinate system for equations (4.1) to (4.11)

Fig. 4.5 Graph of K_I versus a for the current solution, and the solutions of Benthem and Koiter and Harris

Fig. 4.6 Exaggerated representation of the model deformation

Fig. 4.7 Representation of the approximate level of stress in the plane of the crack

LIST OF REFERENCES

[4.1] Matthec, C., Mordwietz, P., and Munz, D., Stress intensity factors of sickle shaped cracks in cylindrical bars, International Journal of Fatigue, Vol. 7, No. 1, 1985, pp 45-47.

[4.2] Benthem, J.P., and Koiter, W.T., Asymptopic approximations to crack problems, in methods of analysis and solutions of crack problems, ed. G.C.Sih, Noordhoft International Publishing, 1973, pp 131-173.

[4.3] Harris, D.O., Stress intensity factors for hollow circumferentially notched round bars, Journal of Basic Engineering, March 1987, pp 49-54.

[4.4] Sih, G.C., and Liebowitz, H., Mathematical theories of brittle fracture, Fracture Vol. 2. Acadmic Press, 1968.

CHAPTER FIVE

FATIGUE CRACK PROPAGATION IN THE PRESENCE OF SHOT-PEENING RESIDUAL STRESSES

SUMMARY

This investigation examines the respective effects of peening and re-peening upon the fatigue fracture behaviour of metallic components in the presence of shot-peening residual stresses. Specifically, the work is devoted to highlighting the beneficial effects of compressive surface residual stresses, their relaxation and the associated crack initiation and propagation behaviours of two contrasting materials. Accordingly, room temperature rotating bending fatigue tests were conducted on cylindrical specimens made in aluminium zinc alloy and medium carbon steel. These specimens were first peened and then partially fatigued to a "known" proportion of their anticipated fatigue life. A number of these specimens were then repeened and tested to ultimate fracture; the remainder were used for supplementary tests.

The above tests revealed a substantial fatigue life improvement for both the steel and aluminium specimens. However, when re-peened, after being partially fatigued, only the steel specimens showed further life enhancement. Residual stress measurements using x-ray diffraction techniques and fratography using scanning electron microscopy and optical methods were employed, at different stages of the work, to elucidate this discrepancy.

5.1 INTRODUCTION

Residual stresses are introduced in metallic components either intentionally by the use of surface treatment such as shot-peening and its derivatives, or unintentionally by most metal forming and metal cutting and fabrication processes such as forging, rolling, milling and welding, etc. These processes introduce residual stresses as a result of inhomogeneous plastic deformation due to mechanically or thermally induced loads. It is also interesting to note that a crack

may indeed generate its own residual stress field, both in front and in the wake of its tip.

Justification for the study of residual stresses, and the processes which induce them lies in the fact that these stresses have been found to profoundly affect the fatigue fracture behaviour of metallic components. For example, in the case of shot-peening, the introduction of compressive residual stresses at and near the exposed surface layers of the component results in improving the lifetime of the component considerably, see, e.g., Refs.[5.1] to [5.6]. Conversely, the introduction of thermal tensile residual stresses in weldments may drastically reduce the service life of such components. It is recognised by many researchers, see, e.g., Refs.([5.7] to [5.9]) that regions of compressive residual stresses retard fatigue crack growth and may even arrest cracks, while tensile residual stress regions produce the opposite effect, see, e.g., Refs. [5.10] and [5.11].

A few investigators ([5.12] to [5.15]) have demonstrated that these residual stresses are not permanent, but tend to diminish as a function of time, temperature, load history and metal removal in the form of either wear or corrosion.

This study, which is part of a major investigation into fatigue fracture in the presence of residual stresses, is devoted to highlighting the interaction between compressive surface residual stresses and the lifetime of two contrasting materials; aluminium zinc alloy and medium carbon steel. The work was then extended to assess the potential of re-peening treatment for the restoration of faded residual stresses and the consequent fatigue life improvement. Accordingly, two aspects of the material behaviour under constant amplitude cyclic loading were examined; as follows:

(i) the extent of fading of the residual stress profile due to partial fatigue, and

(ii) the extent of fatigue life enhancement associated with re-peening treatment after partial fatigue.

For this purpose, room temperature rotating-bend fatigue tests were conducted on peened and re-peened cylindrical components made from the aforementioned materials.

5.2 EXPERIMENTAL ANALYSIS

5.2.1 Selection of Test Materials and Specimen Preparation

The materials tested were aluminium zinc alloy designation 7075 and medium carbon steel designation 080M40, formerly known as En8. Both materials are typical of many engineering alloys in that they possess high inclusion contents associated with the initial cast. This, together with the fact that these materials possess different crystal structures and use different strengthening mechanisms has prompted our current choice.

The 7075 aluminium zinc alloy, of the constituents provided in Table 1, was tested in the T7351 condition, i.e., overaged for optimum stress corrosion resistance and given a controlled plastic deformation to reduce prior residual stresses. Its microstructure is depicted in Fig. 5.1. On the other hand the 080M40 medium carbon steel, of the constituents also given in Table 5.1, possessed a ferritic-pearlitic structure with no directionality effect, as shown in Fig. 5.2. The mean grain size for the steel and aluminium specimens was found to be 100μm and 70μm, respectively, giving approximately 10^4 grains across the reduced section of the specimen. The mechanical properties of the tested materials, which are listed in Table 5.2, were averages of five tests. Finally, the hardness measurements indicated a random distribution of comparable values across the examined section.

Preliminary experiments were conducted on these materials in order to determine the specimen dimensions. The design requirement of notch and overall dimensions of the specimens were dictated by the need to ensure (i) elastic loading conditions, (ii) rigidity during dynamic loading, (iii) no distortions resulting from the peening treatment, and (iv) the number of the grains existing across the reduced section was sufficient, so that the experimentally determined properties were representative of polycrystalline material behaviour. As a

Table 1: Details of Composition of Tested Materials

Material	Element (wt%)												
	Fe	C	Mn	Al	Zn	S	Si	Ti	Cu	Mg	Cr	Zr	P
080M40 Steel	Bal	.43	.79	-	-	.012	.20	-	-	-	-	-	.022
7075 Aluminium	.19	-	.05	Bal.	5.98	-	.10	.054	1.28	2.52	.20	.05	-

Table 2: Details of Mechanical Properties of Tested Materials

Material (MPa)	σ_y (.1%) (MPa)	σ_{UTS} (MPa)	ε_f %	H_v (MPa)
808M40 Steel	400	550	22	246
7075 Aluminium	462	526	11	256

FIGURE 5.1 Microstructure of 080M40 Medium Carbon Steel. (Etched: 2½% Nital)

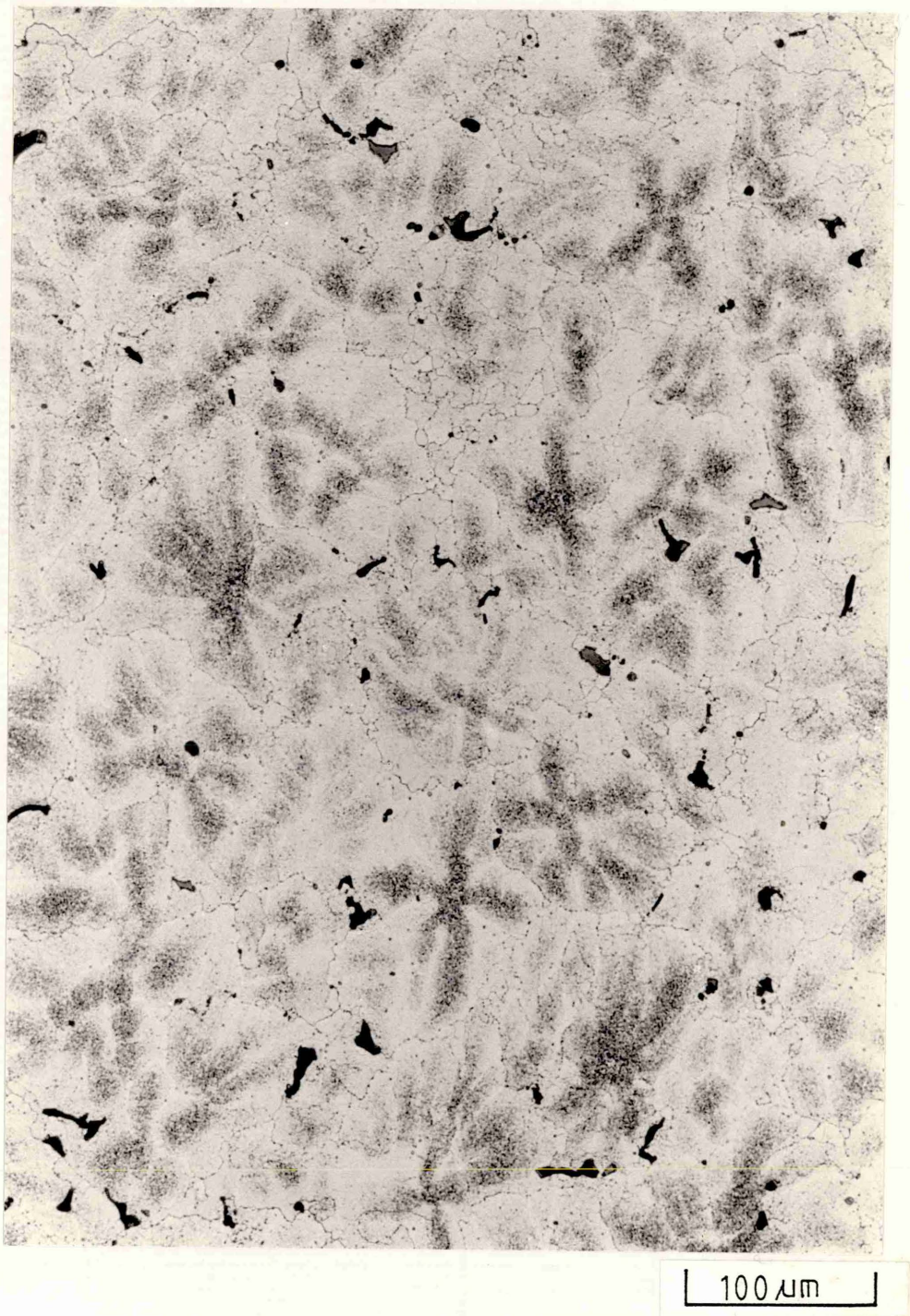

FIGURE 5.2 Microstructure of 7075 T7351 Aluminium Zinc Alloy. (Etched: Keller's)

compromise, it was decided to select the dimensions given in Fig. 5.3. Finite element and photoelastic analysis indicated that $k_t = 1.1$. In Order to minimise experimental scatter and ensure repeatability, a complete manual of the manufacturing procedure was laid down, and guidelines given in [6] were followed. Relevant machining details are given in Table 5.3.

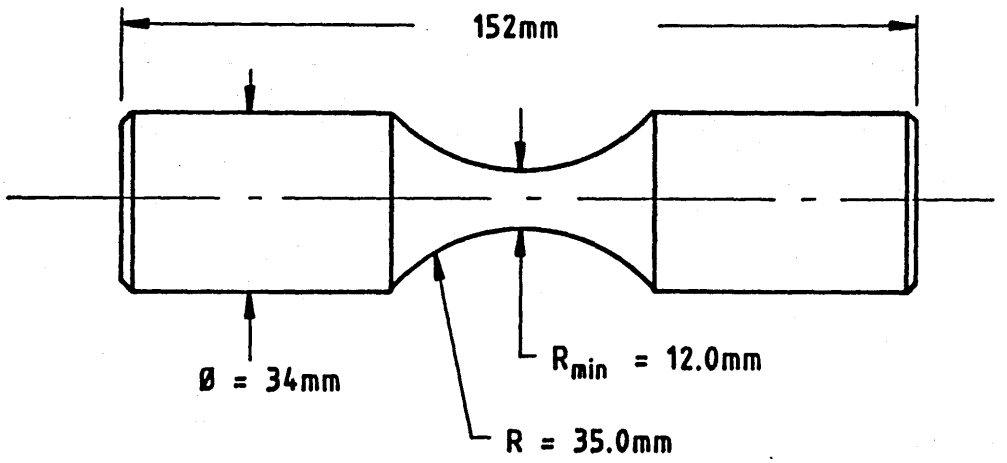

FIGURE 5.3 Geometry of rotating bend specimen

Table 3: Details of Machining Parameters

Material	Feed Rate μm/rev	Speed rev/min	Depth of Final Cut μm	Tools Used	Surface Finish R_a (μm)
080M40 Steel	8	900	400	Tungsten Carbide	0.3
			200	Tungsten Carbide	
			20	Aluminium Oxide-Cloth	
7075 Aluminium	70	1100	500	Tungsten Carbide	0.7
			100	Tungsten Carbide	
			80	Tungsten Carbide	
			50	Tungsten Carbide	

5.2.2 Equipment and Procedure

The experimental programme conducted utilised specially built four-point rotating-bending fatigue testing equipment, and a direct pressure air-peening system. This testing machine was equipped with an automatic cut-out circuit, digital revolution counter and a remote emergency shut-down facility. Linear strain-gauge bridges were installed in one of the flexure shafts and these, in turn, were connected to a series of slip rings, brushes and signal pick-up points. Adequate slip rings were also made available for picking-up the signals from strain-gauged specimens during the initial calibration of the testing machine.

The rotating bend machine was initially calibrated by strain-gauging one of the specimens and both static and dynamic calibrations were carried out. During the dynamic calibration use was made of a digital storage oscilloscope not only to measure the magnitudes of the resulting bending stresses, but also to monitor the wave-form during testing.

The shot-peening system used in the present investigation is fully described in [5.5]. The shot-size used was determined by prevalence of its use in industry. Current shot-peening specification recommends the use of peening intensities between 0.25 - 0.40mm (0.010 - 0.016) A (Almen Intensity) for the test materials. It was therefore decided to use the peening parameters described in Table 5.4 for both peening and re-peening treatments.

Table 4: Details of Peening Parameters

Material	Shot	Air Pressure (kPa)	Stand Off Distance (mm)	Duration (S)	Impacts/ mm^2	Mean Plastic Indent Diameter (μm)	Corres-ponding Almen Arc Height(A) (mm)
80M40 Steel	S230	200	150	60	200	160	0.45
7075 Alum-inium	S230	70	150	40	150	190	0.27

5.2.3 Measurement Techniques Used

Crack Monitoring

During testing, cracks were monitored using a "crack-micro-gauge type U7G-300 series" which is an ACPD field measuring device used with a 10mm probe. Some checks were made using optical methods employing contrast enhancing dies and using the replica technique.

Crack profiles for fatigued un-peened, peened and re-peened specimens were obtained: firstly, by examining beach marks left by the dye on the fractured surfaces and secondly, by examining valleys using optical and electron microscopy techniques.

Residual Stress Measurements

X-ray diffraction measurements were made on the as machined shot-peened and shot-peened partially-fatigued specimens. The technique, which is summarised, e.g., in Refs. [5.18] and [5.19], provides information on the residual stresses and microstructural deformation in the surface layers. Depth profiles were measured by the controlled removal of successive layers of the surface of the material by electropolishing. All measurements were made at the centre of the stress raiser region using the conditions described in Table 5. The x-ray residual stress results were found comparable with results obtained by the use of the hole-drilling technique.

5.2.4 Experimental Programme

The experimental work consisted of preliminary and main test programmes. The preliminary tests involved the determination of the σ_a-N curves for peened and un-peened specimens with the view of establishing the improvement in the fatigue life due to peening for varying applied alternating stress, σ_a, and to establish the appropriate fatigue load for the main test programme in order to ensure: (i) essentially elastic loading conditions, thus yielding high cycle fatigue testing, (ii) avoidance of endurance (or fatigue) limit, and (iii) appropriate testing time. As a compromise, it was decided

to select a test load which will yield comparable fatigue lifetime between the aluminium and the steel specimens.

The main test programme was conducted using previously-peened partially fatigued specimens. Examination of cracks as well as residual stress measurements were performed during the different stages of the tests using the above-mentioned techniques. As a result of these measurements, σ_a-N curves for peened and un-peened specimens were established together with the response of the material to the re-peening treatment. Furthermore, the change in the residual stresses profiles was measured.

Attention was also devoted to the development and behaviour of cracks in the presence of residual stresses during different stages of the current fracture process.

Table 5: Details of X-Ray Measurement Conditions

Equipment	Rigaku Strainflex
Target	Cr
Filter	V
Diffraction planes Aluminium	(311)
Steel	(211)
Irradiated area	5 x 4 mm^2
Incident angles	0, 15, 25, 35, 45°
Geometry	Side inclination
Method	$\sin^2\psi$
Stress constant K^* Aluminium	165 MPa
Steel	113 MPa

$$K^* = \frac{E}{2(1+\nu)} \cdot \frac{\pi}{180 \tan\theta}$$

5.3. ANALYSIS OF RESULTS AND DISCUSSIONS

5.3.1 Preliminary Test Results

The fatigue testing programme conducted was designed to reveal information about the behaviour of cracked bodies in the presence of residual stress, and also to assess the life improvement due to re-peening. Once basic fatigue lifetime data had been established, a single load was selected for subsequent testing. This corresponded to a total fatigue life of the order of 10^5 cycles. Such a requirement is between the extremes of LCF where residual stress relaxation might be expected to be very rapid and HCF where relaxation may or may not be prevalent. Such regime also coincides with a number of industrial applications, e.g., aeroengine compressor and turbine discs, undercarriage components materials handling equipment, pressurised parts, etc.

Figs. 5.4(a) and 5.4(b) show the σ_a - N curves for peened and un-peened specimens for both materials. The results clearly indicate the beneficial effects of the peening treatment. For example, at a test stress of 400 MPa, the steel specimens showed an improvement of 200% in fatigue life. Similarly, at a test stress of 230 MPa, the aluminium specimens showed an improvement of 500% in fatigue life. We believe that the comparatively modest improvement in the steel specimens is attributed to

(i) the relatively high alternating stress, σ_a, used, and

(ii) the use of completely reversed bending with R = -1; the residual stress pattern tends to fade out more rapidly under high alternating stresses [5.3], [5.5] and [5.17].

The σ_a-N curves for the steel specimens also indicate that the improvement in the fatigue life could still be achieved even for an alternating stress, σ_a, exceeding the initial uniaxial yield stress of the material, σ_y. This could be explained by the fact that the work-hardened layer attains a new higher flow stress.

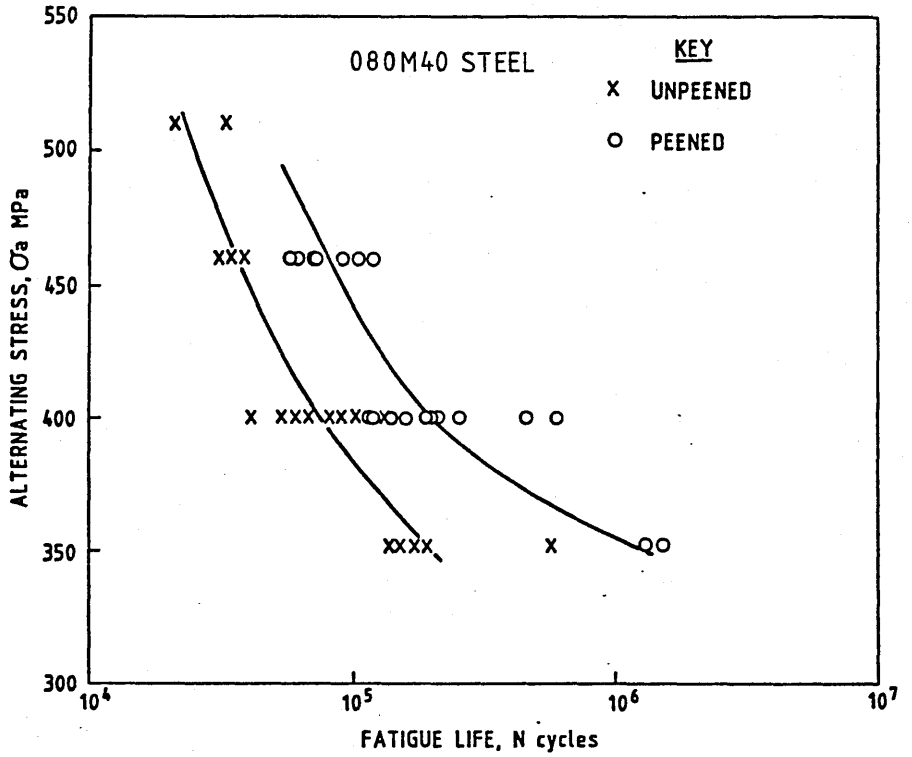

(a) 080M40 Medium Carbon Steel

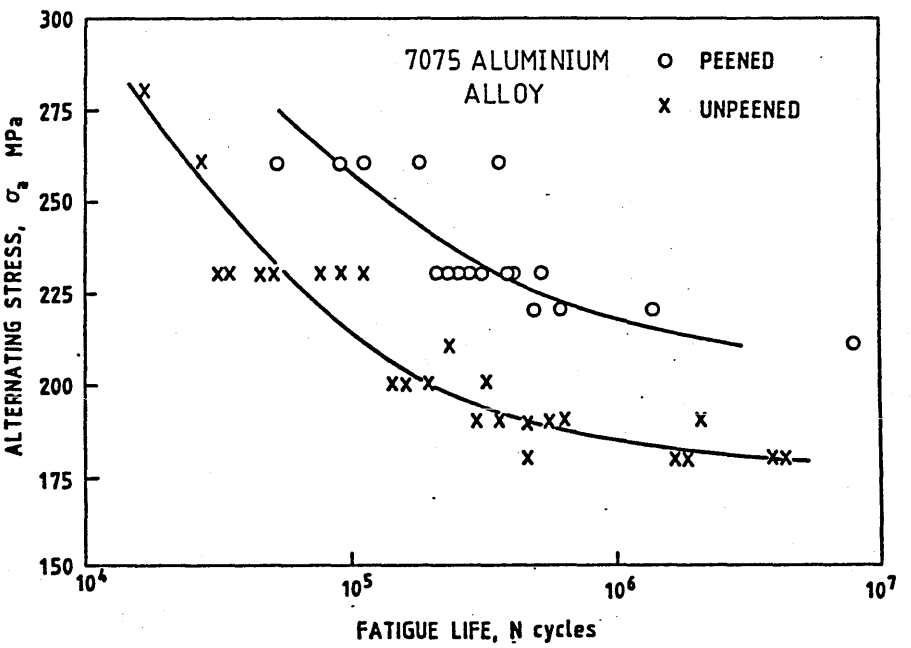

(b) 7075 Aluminium Alloy

FIGURE 5.4 O_a- N Curves for tested material

5.3.2 Main Test Results

These results are divided into three main sections; as follows:

(i) the effect of re-peening treatment,
(ii) relaxation of residual stresses, and
(iii) crack profile studies.

THE EFFECT OF RE-PEENING TREATMENT

In this case, peened specimens were tested for part of their estimated shot-peened fatigue lives N_p, then re-peened and re-tested to complete fracture. The results obtained from the testing of the two materials are given in Fig. 5.5.

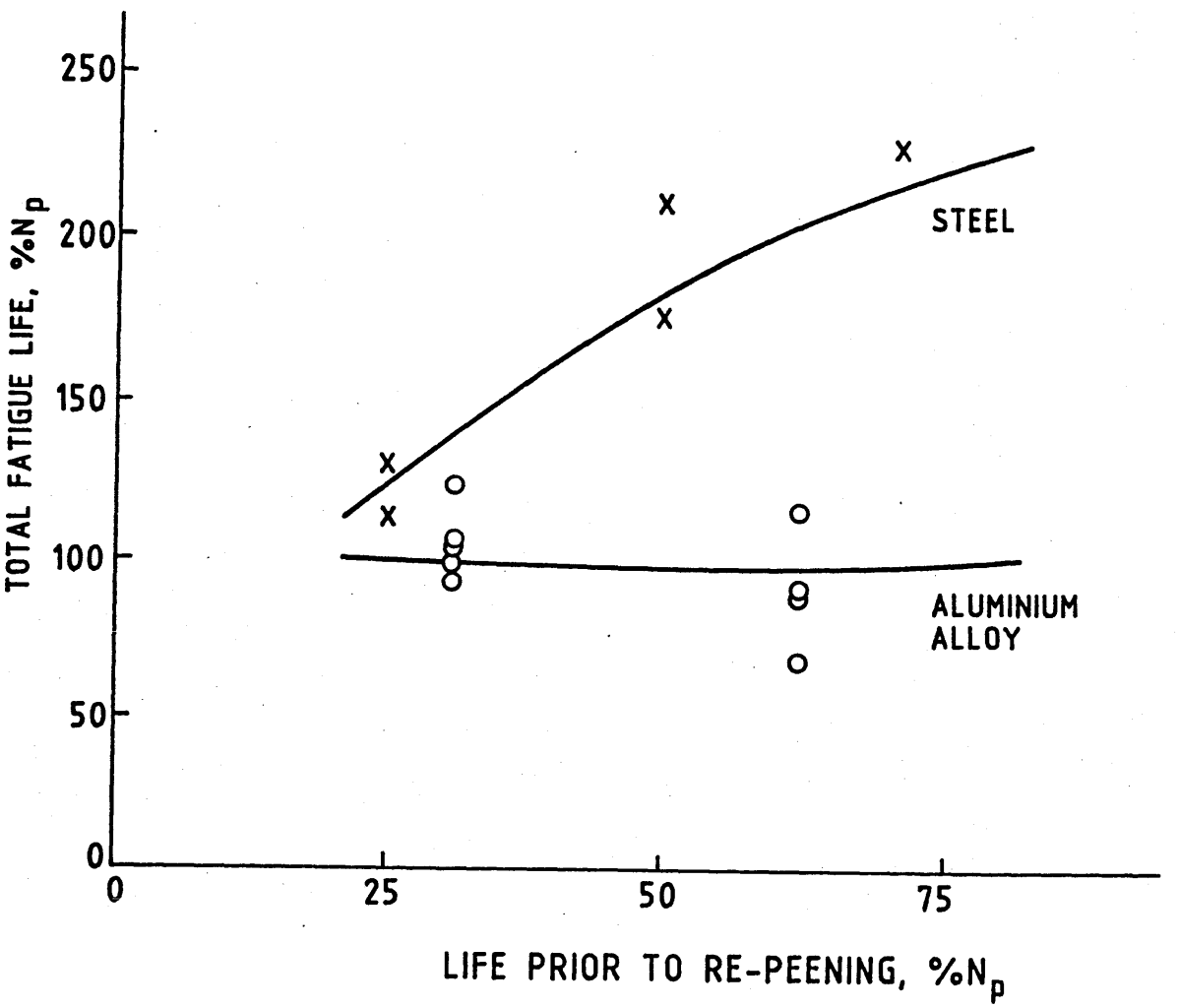

FIGURE 5.5 Fatigue life enhancement due to re-peening

These results reveal the following. In the case of the steel specimens, further enhancement of the life was achieved by re-peening. This, however, was not the case for the aluminium specimens. Typically, re-peening of the steel after being partially fatigued by 70% of its mean fatigue life, showed complete rejuvenation. Surprisingly, however, the re-peening of the aluminium specimens did not show any improvement.

RELAXATION OF RESIDUAL STRESSES

In view of the contrasting response of the materials to the re-peening treatment, residual stress measurements were conducted to assist in the interpretation of the results. Accordingly, x-ray diffraction measurements were performed on both materials at various stages of the testing sequence.

Figs. 5.6(a) and 5.6(b) show the original residual stress profiles for specimens in the two materials after peening and before fatigue testing. These results are provided in Tables 5.6 and 5.7. These profiles are typical of those found in peened components, with the maximum compressive residual stress occurring below the surface with magnitudes comparable to half the yield stress of the material see, e.g., Refs. [5.20] to [5.23]. In the steel specimens, a maximum compressive residual stress of 440 MPa was measured at a depth of 15μm. In the aluminium specimens these figures were 200 MPa and 40μm, respectively.

Figs. 5.7(a) and 5.7(b) show the changes in the residual stress profiles in specimens which have been partially fatigued by 75% of their anticipated life. In Fig. 5.7(a), for the steel specimens, two features are apparent:

(i) shallowing of the profile, and

(ii) diminution of the general magnitudes of the residual stresses as a result of cyclic loading.

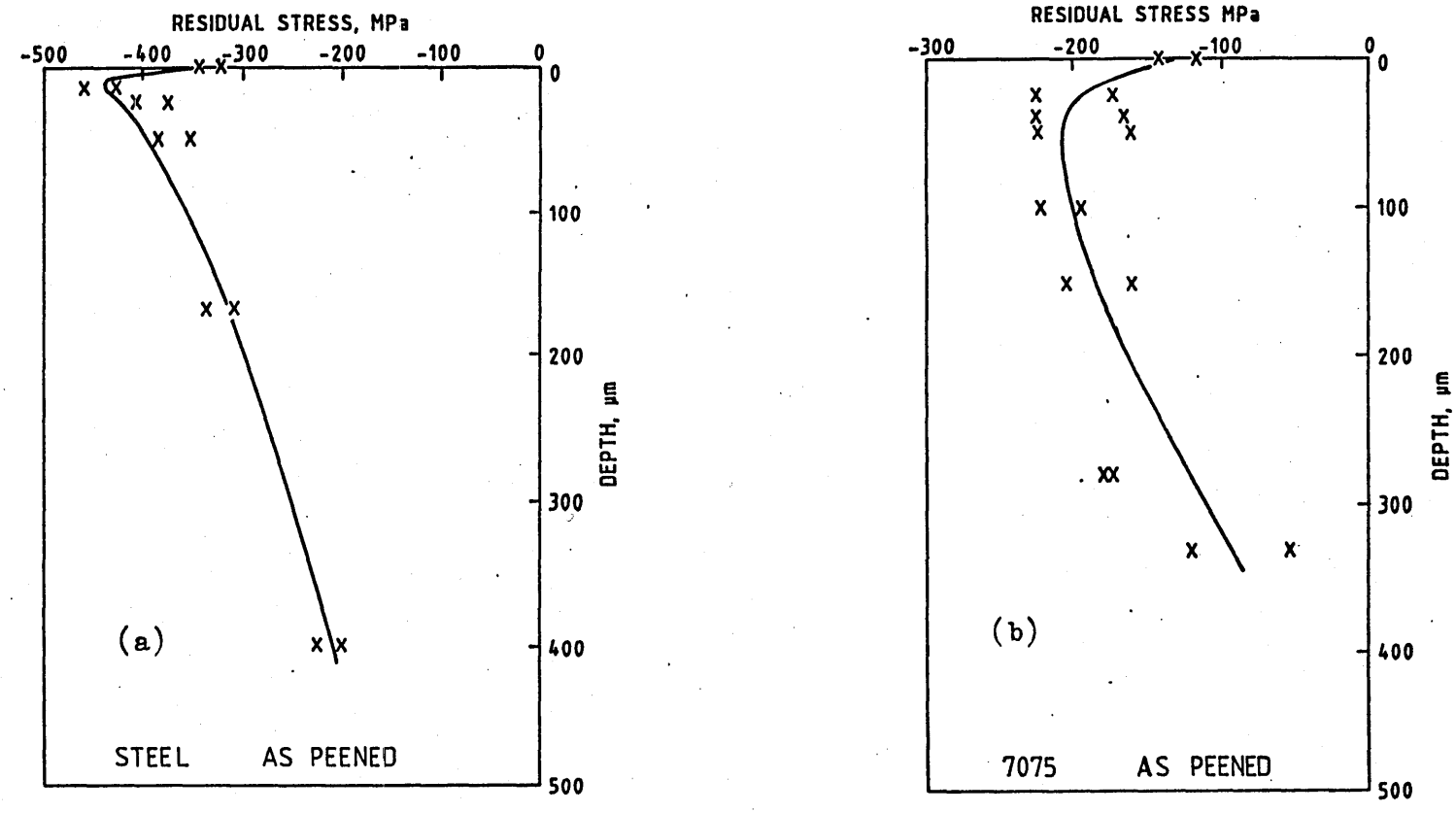

FIGURE 5.6 Residual stress profiles of the peened specimens prior to fatigue testing

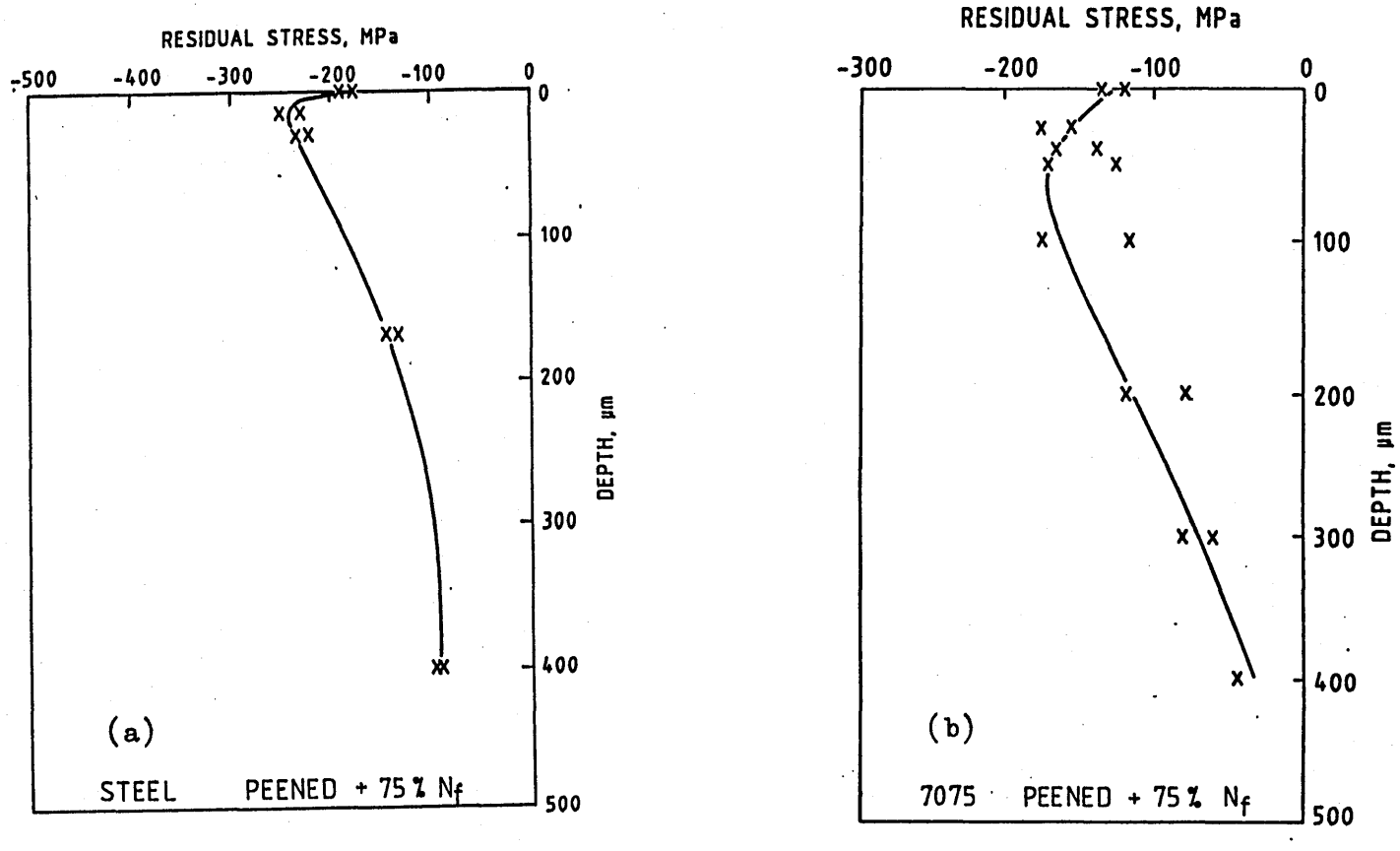

FIGURE 5.7 Residual stress profiles of the peened specimens after being fatigue tested to 75% of their anticipated life

Table 6: Details of Residual Stress Profile in Peened Specimens

Material	Depth below Surface (μm)	Residual Stress (MPa)	Peak Breadth FWHM (2θ°)
080M40 Steel	0	- 333 ± 11	3.24 ± .09
	15	- 443 ± 16	2.86 ± .06
	25	- 391 ± 16	2.71 ± .06
	50	- 368 ± 16	2.43 ± .04
	170	- 322 ± 14	2.16 ± .03
	400	- 210 ± 12	1.90 ± .04
7075 Aluminium	0	- 129 ± 13	2.17 ± .13
	25	- 199 ± 26	2.08 ± .10
	40	- 195 ± 30	2.02 ± .08
	50	- 192 ± 31	1.99 ± .07
	100	- 208 ± 14	1.82 ± .07
	150	- 182 ± 22	1.64 ± .20
	280	- 176 ± 3	1.48 ± .05
	330	- 92 ± 38	1.50 ± .14

Table 7: Details of Residual Stress Profile in Peened and Partially Fatigued Specimens

Material	Depth below Surface (μm)	Residual Stress (MPa)	Peak Breadth FWHM (2θ°)
080M40 Steel	0	- 184 ± 7	3.09 ± .06
	15	- 239 ± 10	2.79 ± .02
	15	- 227 ± 6	2.70 ± .04
	30	- 210 ± 12	2.64 ± .03
	100	- 139 ± 6	2.36 ± .04
	300	- 93 ± 2	1.97 ± .02
7075 Aluminium	0	- 128 ± 8	2.10 ± .11
	25	- 165 ± 10	2.01 ± .13
	40	- 155 ± 17	1.94 ± .18
	50	- 148 ± 23	1.89 ± .22
	100	- 145 ± 29	1.84 ± .15
	200	- 98 ± 20	1.52 ± .08
	300	- 70 ± 10	1.33 ± .16
	400	- 20 ± 24	1.44 ± .12

The aluminium results as depicted by Fig. 5.7(b) did not show marked change in the profile and any possible change lies within the scatter band of the measurements.

In addition to these profiles, further measurements were made of the maximum residual stress as a function of the proportion of the expired peened life for both materials. These results are given in Tables 5.8 and 5.9 and Figs. 5.8(a) and 5.8(b). They support the observation made above regarding the re-peening treatment of the aluminium. Fig. 5.8(a) indicates that the maximum residual stress in the steel specimens is reduced by 50% of its previous value after having been fatigued for 75% of its estimated shot-peened fatigue life.

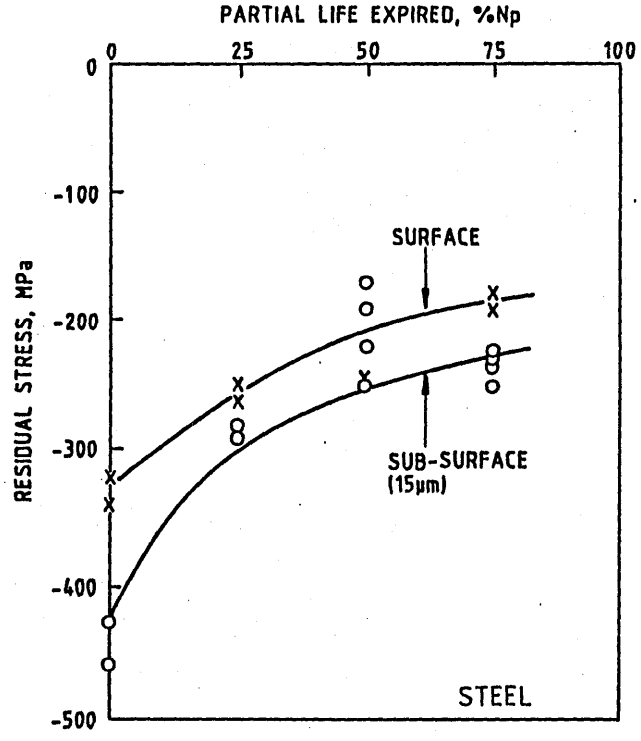

(a) Medium carbon steel

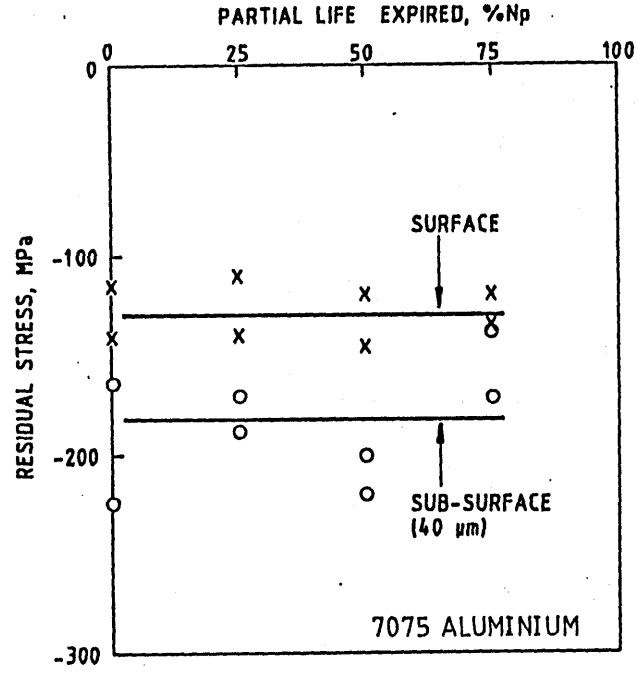

(b) Aluminium alloy

FIGURE 5.8 Surface and subsurface residual stresses as a function of fatigue life expired for partially fatigued peened specimens

Table 8: Residual Stress Measurements, Surface and Sub-Surface as a Function of Partial Peened Fatigue Life Expired for the Steel Specimens

Condition	Residual Stress (MPa)		Peak Breadth FWHM (2θ°)	
	Surface	15μm Sub-Surface	Surface	15μm Sub-Surface
Peened	-333 ± 11	-443 ± 16	3.24 ± .09	2.86 ± .06
Peened + 25% N_p	-257 ± 7	-286 ± 4	3.22 ± .07	2.74 ± .06
Peened + 50% N_p	-222 ± 22	[-180 ± 10] [-233 ± 14]	3.00 ± .03	[2.71 ± .02] [2.63 ± .01]
Peened + 75% N_p	-184 ± 7	[-239 ± 10] [-227 ± 6]	3.09 ± .06	[2.79 ± .02] [2.70 ± .04]

Table 9: Residual Stress Measurements, Surface and Sub-Surface as a Function of Partial Peened Fatigue Life Expired for the Aluminium Specimens

Condition	Residual Stress (MPa)		Peak Breadth FWHM (2θ°)	
	Surface	40mm Sub-Surface	Surface	40μm Sub-Surface
Peened	-129 ± 13	-195 ± 30	2.17 ± .13	2.02 ± .08
Peened + 25% N_p	-125 ± 15	-180 ± 9	2.12 ± .07	2.05 ± .06
Peened + 50% N_p	-133 ± 13	-211 ± 10	2.15 ± .11	2.02 ± .10
Peened + 75% N_p	-128 ± 8	-155 ± 17	2.10 ± .11	1.94 ± .18

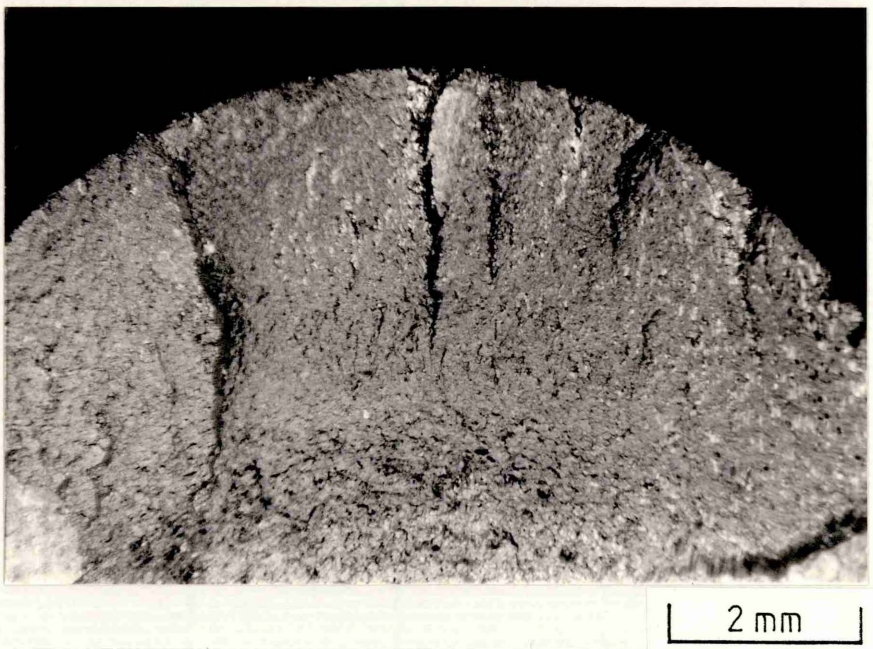

FIGURE 5.9 Typical Fracture Surface of an Un-Peened 080M40 Medium Carbon Steel Specimen.

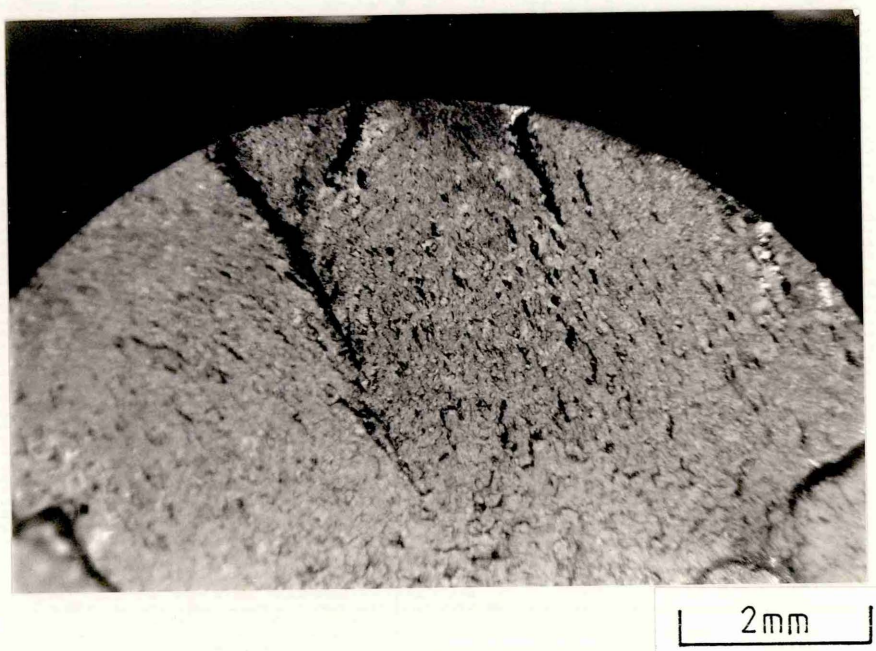

FIGURE 5.10 Typical Fracture Surface of a Peened 080M40 Medium Carbon Steel Specimen.

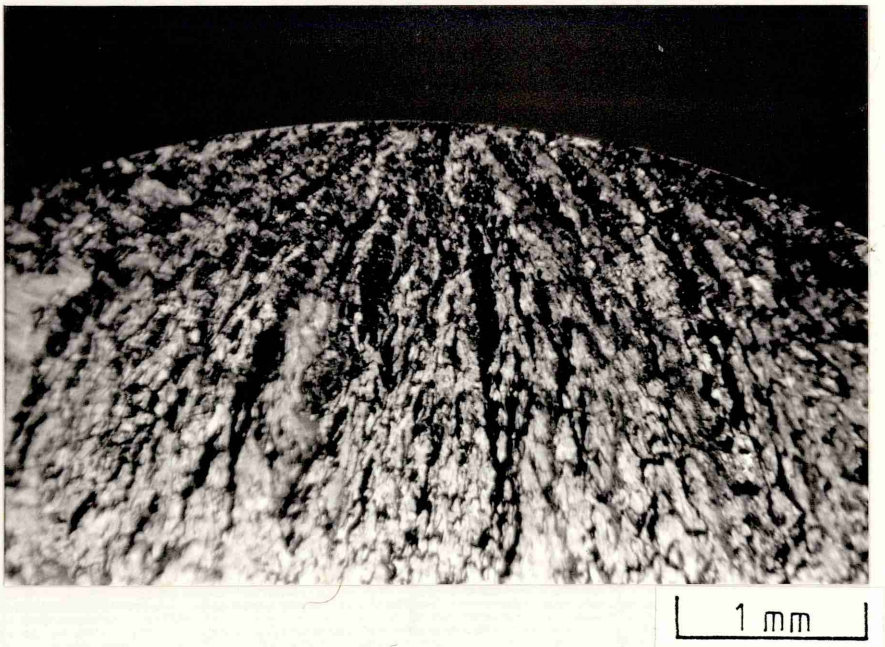

FIGURE 5.11 Typical Fracture Surface of an Un-Peened 7075 Aluminium Alloy Specimen.

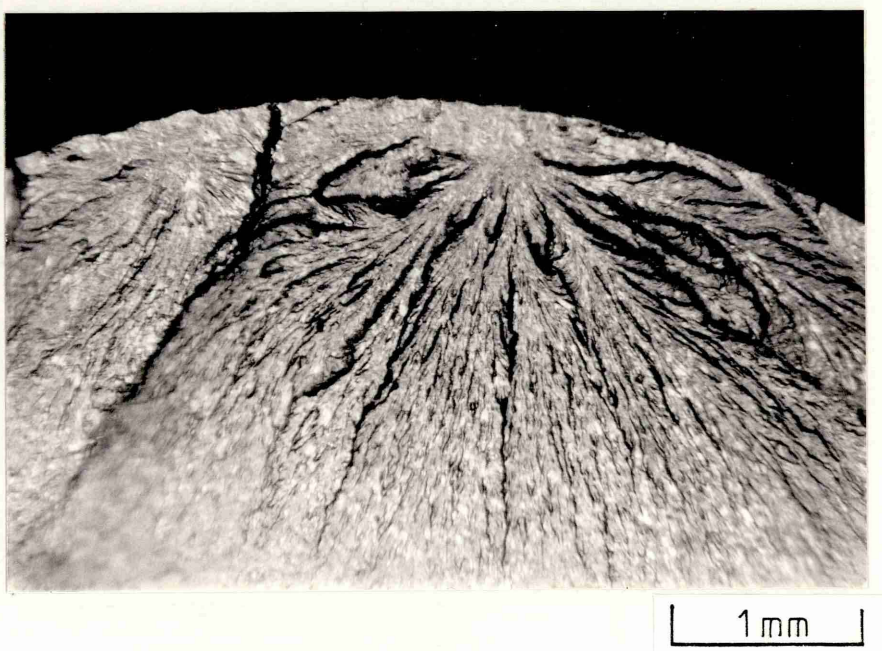

FIGURE 5.12 Typical Fracture Surface of a Peened 7075 Aluminium Alloy Specimen.

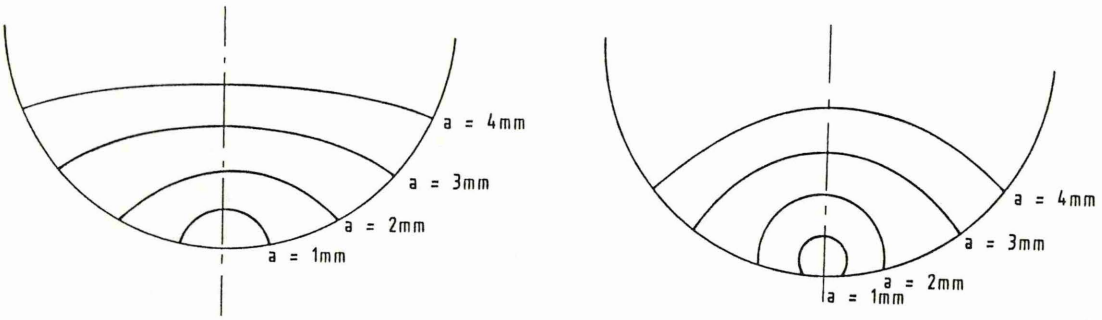

(a) Unpeened (b) Peened

FIGURE 5.13 Idealised Representation at the Crack Profile in the 7075 Aluminium Alloy Specimens

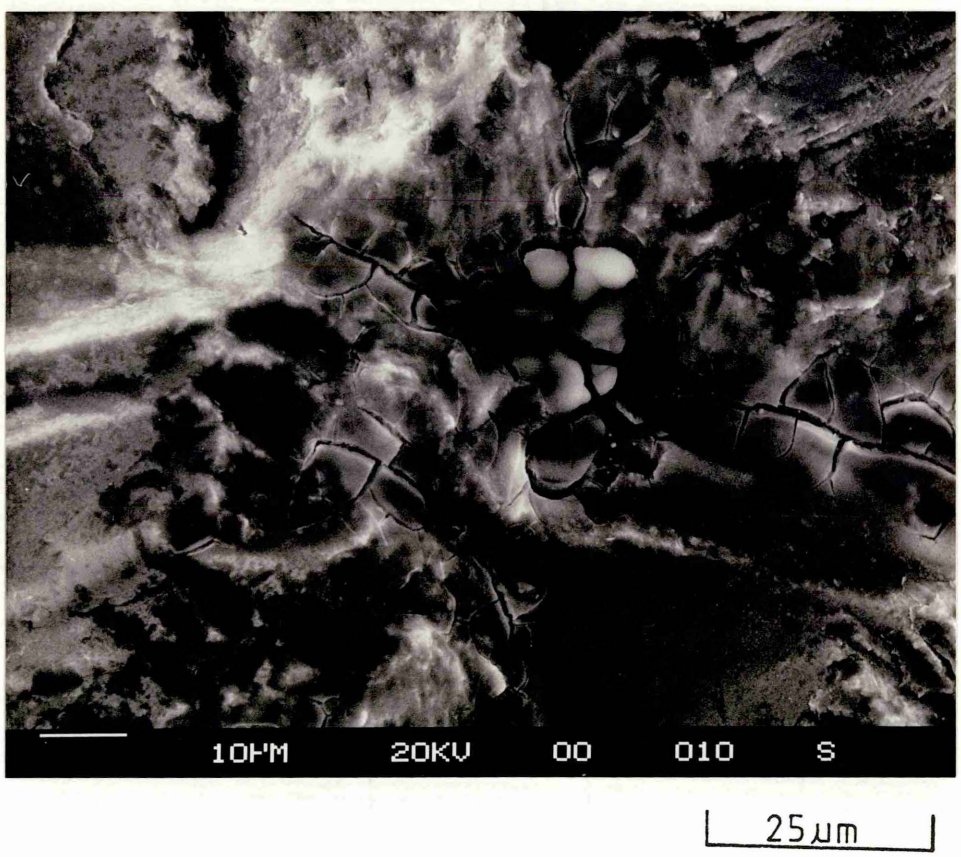

FIGURE 5.14 Electron micrograph of an Inter-metallic Inclusion in a 7075 Alloy Specimen

CRACK PROFILE

In order to augment the above findings, attention was paid to the prominent features of cracks associated with the fatigue behaviour of these two materials in the presence of residual stresses. Figs. 5.9 and 5.10 show typical fracture surfaces for the un-peened and peened fatigued aluminium specimens, while Figs. 5.11 and 5.12 show the same for the steel specimens.

In the detailed analysis of the aluminium results, it was observed that whilst all of the un-peened specimens showed surface initiation-related features, 50% of the peened ones showed subsurface initiation related features similar to those depicted in Fig. 5.10. This suggests that the presence of the compressed layer at or near the exposed surface layers promotes subsurface crack initiation in this situation. An idealisation of crack profiles in peened and unpeened fatigued specimens was generated by the examination of a large number of fracture surfaces, which is shown in Fig. 5.13. The results demonstrated a tendency towards elliptical cracking except in the initial stages of the peened specimens. Again, this may be attributed to the large initial compressive surface residual stress and the location of the initiation site.

Finally, it is worth pointing out that close examination of the fractured surface in SEM revealed the presence of crack-like defects associated with inter-metallic inclusions, as depicted in Fig. 5.14. These may well act as initiation sites, both surface and subsurface, in the peened and un-peened conditions. In the case of the steel, however, no subsurface cracks were observed.

5.4 CONCLUSIONS

The present investigation was mainly devoted to examining the effect of re-peening partially fatigued components on two dissimilar materials; 7075 aluminium alloy and 080M40 medium carbon steel. Rotating bend fatigue tests supported by residual stress measurements,

and crack profile analysis were conducted. The results reveal the following:

(i) The peening treatment enhances the fatigue life of both materials appreciably. This is due to the presence of compressive residual stresses in the vicinity of the exposed surface layers.

(ii) The re-peening of partially fatigued components showed a marked effect on the steel specimens but not on the aluminium. This may be related to the low degree of residual stress relaxation observed with 7075 aluminium alloy as compared with the 080M40 medium carbon steel.

(iii) The peening treatment promoted subsurface crack initiation in the aluminium alloy. However, this was not observed in the steel. Clearly, the occurrance of subsurface crack initiation will influence the effectiveness of the surface compressive residual stresses resulting from the re-peening treatment.

CAPTIONS TO FIGURES

Fig. 5.1 Microstructure of 080M40 Medium Carbon Steel.
(Etched: 2½% Nital)

Fig. 5.2 Microstructure of 7075 T7351 Aluminium Zinc Alloy.
(Etched: Keller's)

Fig. 5.3 Geometry of Rotating Bend Fatigue Specimen.

Fig. 5.4 σ_a-N Curves for Tested Materials:
(a) 080M40 Medium Carbon Steel, and
(b) 7075 Aluminium Alloy.

Fig. 5.5 Fatigue Life Enhancement Due to Re-Peening

Fig. 5.6 Residual Stress Profiles of the Peened Specimens prior to Fatigue Testing:
(a) 080M40 Medium Carbon Steel, and
(b) 7075 Aluminium Alloy.

Fig. 5.7 Residual Stress Profiles of the Peened Specimens after being Fatigue Tested to 75% of their Anticipated Life:
(a) 080M40 Medium Carbon Steel, and
(b) 7075 Aluminium Alloy.

Fig. 5.8 Surface and Subsurface residual stresses as a Function of Fatigue-Life Expired for Partially Peened Specimens:
(a) 080M40 Medium Carbon Steel, and
(b) 7075 Aluminium Alloy.

Fig. 5.9 Typical Fracture Surface of an Un-Peened 7075 Aluminium Alloy Specimen.

Fig. 5.10 Typical Fracture Surface of a Peened 7075 Aluminium Alloy Specimen.

Fig. 5.11 Typical Fracture Surface of an Un-Peened 080M40 Medium Carbon Steel Specimen.

Fig. 5.12 Typical Fracture Surface of a Peened 080M40 Medium Carbon Steel Specimen.

Fig. 5.13 Idealised Representation of the Crack Profile in the 7075 Aluminium Alloy Specimens:
(a) Un-Peened, and
(b) Peened.

Fig. 5.14 Electron Micrograph of an Inter-Metallic Inclusion in a 7075 Aluminium Alloy Specimen.

LIST OF TABLES

Table 5.1 Details of Composition of Tested Materials

Table 5.2 Details of Mechanical Properties of Tested Materials

Table 5.3 Details of Machining Parameters

Table 5.4 Details of Peening and Re-Peening Treatments

Table 5.5 Details of X-Ray Measurements Conditions

Table 5.6 Details of Residual Stress Profiles in Peened Specimens

Table 5.7 Details of Residual Stress Profiles in Peened and Partially Fatigued Specimens

Table 5.8 Surface and Subsurface residual stresses as a Function of the Fatigue Life Expired for partially peened 080M40 Medium Carbon Specimens

Table 5.9 Surface and Subsurface residual stresses as a Function of the Fatigue Life Expended for the partially peened 7075 Aluminium Alloy Specimens

REFERENCES

[5.1] S.A. Meguid, C.B. Chee, The Effect of Peening and Re-Peening upon Partially-Fatigued Components. Journal of Mechanical Working Technology, 8, pp 129-146, 1983.

[5.2] S.A. Meguid, J.A. Coufopanos, Elasto-Plastic Finite Element Studies of the Effect of Residual Stresses upon Double Edge-Cracked Plate. Engineering Fracture Mechanics. 23, No.4, pp 735-744, 1986.

[5.3] J.E. Campbell. Shot Peening for Improved Fatigue Properties and Stress Corrosion Resistance. Metals and Ceramics Information Center, Report MClC-71-02, Ohio, 1971.

[5.4] H.O. Fuchs (Editor) Proceedings of Second International Conference on Shot Peening. Chicago, American Shot-Peening Society, NJ, 1984.

[5.5] D.W. Hammond. The Mechanics of Peening and Re-Peening Partially-Fatigued Components. M.Phil Thesis, Cranfield Institute of Technology, 1986.

[5.6] G. Chadwick, Fatigue Performance of Shot-Peened Components and Related Finite Element Studies Incorporating Dynamic Elasto-Plasticity. Doctoral Thesis, Cranfield Institute of Technology, 1984.

[5.7] Masaaki Musumi and Masafumi Ohkuba, Deceleration of Small Crack Growth by Shot-Peening, International Journal of Materials and Product Technology, 2, No.1, pp 36-47, 1987.

[5.8] H. Berns, L. Weber. Influence of Residual Stresses on Crack Growth. Impact Surface Treatment, S.A. Meguid, (Editor), Elsevier Applied Science Publishers, London, pp 31-44, 1986.

[5.9] W. Elber, Effects of Shot-Peening Residual Stresses on the Fracture and Crack Growth Properties of D6AC Steel in Fracture Toughness and Slow Stable Cracking, ASTM-STP559, pp 45-58, 1974.

[5.10] G. Glinka, Effect of Residual Stresses on Fatigue Crack Growth in Steel Weldments under Constant and Variable Loads, ASTM-STP 677, pp 198-214, 1979.

[5.11] N.E. Frost, K.J. Marsh and L.P. Pook, Metal Fatigue, Clarendon Press, Oxford, 1974.

[5.12] M.R. James, The Relaxation of Residual Stresses During Fatigue, Residual Stress and Stress Relaxation, E. Kula and Volker Weiss (Editors), Plenum Publishing Corporation, N.Y., pp 297-314, 1982.

[5.13] V.M. Radhakrishnan and C.R. Prasad, Relaxation of Residual Stress with Fatigue Loading, Engineering Fracture Mechanics 8, pp 593-597, 1976.

[5.14] P.J. Neff, A Quantitative Evaluation of Surface Residual Stress and its Relation to Fatigue Performance, Residual Stress for Designers and Metallurgists, Ed. Larry J. Vande Walle, American Society of Metals, p 119-136, 1981.

[5.15] J.M. Potter and R.A. Millard, The Effect of Temperature and Load Cycling on the Relaxation of Residual Stresses. Advances in X-Ray Analysis, ed. H.G. McMurdie, 20, pp 309-319, 1977.

[5.16] American Society of Testing Materials, Manual on Fatigue Testing, ASTM-STP 91, ASTM, Philadelphia, 1949.

[5.17] British Standards Institution, Methods of Fatigue Testing: Rotating Bend Fatigue Tests, BS 3518, pt. 2, 1962.

[5.18] G. Maeder, J.L. Lebrun and J.M. Sprauel, Present Possibilities for the x-ray Diffraction Method of Stress Measurement, N.D.T. International, pp 235-247, 1981.

[5.19] B.D. Cullity, Elements of x-ray's Diffraction, Addison Welsey Reading, NY, 1956.

[5.20] E.B. Chee, Effect of Peening and Re-Peening on the Improvement of Fatigue Life of In-Service Components, M.Sc. Thesis, Cranfield Institute of Technology, 1982.

[5.21] J.J. Waisman and A. Phillips, Simplified Measurement of Residual Stresses. Experimental Stress Analysis, X1, No.2, pp 29-44, 1952.

[5.22] M.J. Chant, R.A. Griffiths, L. Miles, Comparison of Two Methods of Measuring Residual Stresses Arising from Surface Treatment. Journal of Mechanical Working Technology, 8, pp 181-191, 1983.

[5.23] W. Luo, B. Noble, R.B. Waterhouse, The Interaction between Shot-Peening and Heat Treatment on the Fatigue and Fretting Fatigue Properties of the High Strength Aluminium Alloy 7075, Impact Surface Treatment, S.A. Meguid (Editor), Elsevier Applied Science publishers, London, pp 57-67, 1986.

CHAPTER SIX

FATIGUE CRACK INITIATION AND PROPAGATION

SUMMARY

6.1 Introduction

6.2 Experimental

6.2.1 Materials Tested
6.2.2 Specimen Preparation
6.2.3 Fatigue Testing and Crack Detection

6.3 Results and Discussion

6.4 Conclusions

SUMMARY

This chapter presents and discusses results which relate to the initiation and growth of cracks in un-peened and peened components. The results cover the rotating bend testing discussed in Chapter Five, uniaxial fatigue testing performed on the 7075 aluminium alloy and supplementary results relating to other materials. The influence of peening on the initiation and propagation of fatigue cracks is demonstrated and discussed in the light of data already available in the literature.

6.1 INTRODUCTION

As previously discussed, fatigue failure may be divided into three regimes, the initiation of a crack, its propagation and final failure when the cracked component losses its ability to sustain the applied load. The nature of initiation processes has been studied in the literature but generally there is little work to bridge the gap between micro mechanisms and predictive continuum considerations. The degree of localised plastic deformation which precedes the appearance of a detectable crack is difficult to assess though efforts have been made in this direction [6.1]. Thus it is common to define the transition from initiation to propagation of a crack to the point at which the crack exceeds a particular size, possibly for instance the experimentalists threshold of detection [6.2].

An increased awareness of the role of fatigue propagation in short cracks overlap considerations of initiation and has to some extent caused investigators to consider initiaion as a process of the development and growth of short cracks where the process of initial crack formation is assumed to be rapid. [6.3] This approach may work well for severely notched components such as compact tension or centre notched plate specimens, or in notch sensitive materials - especially those containing incoherent microstructural inhomogeneities such as inclusions or inter metallic particles. This approach is though limited due to difficulty in predicting the behaviour of short cracks and it is more common to consider the mixed initiation and propagation model defined in Chapter Two [6.4].

In this investigation, whilst the importance of the microstructure on crack development is discussed it did not prove possible to study crack growth on the truely microstructural scale. The microstructure did, however, greatly influence the results, as did specimen geomeotry. The results discussed herein shed some light on the fundamental interactions relevant to fatigue in the presence of residual stresses and local work hardening.

6.2 EXPERIMENTAL ANALYSIS

6.2.1 Materials Tested

In addition to the 7075 aluminium zinc alloy and the 080M40 medium carbon steel which are described in Chapter Five, two other materials were tested, though in less detail. These are as follows:

300M Ultra high strength nickel-silicon-chromium molybdenum-vanadium steel as defined in MIL S 8844 CL3. The material also satisfies the requirements of the B.S.I. specification S155. The composition of the material is given in Table 6.1 and the results of a tensile test, done in accordance with BS970 are given in Table 6.2. This material is widely used in under-carriage components where a high strength to weight ratio is most beneficial. Its final heat treatment comprises of an oil quench, possibly a deep freezing opertion, and double tempering for three hours at 300°C. The bulk of the current material was deep frozen (-70°C) in the hope of circumventing retained austenite problems. Fig. 6.1 shows the microstructure of this material.

Titanium 6% aluminium 4% vanadium alloy. A small quantity of this alloy was supplied by Rolls-Royce. Its heat treatment was designed to mimic that of the roots of aero-engine compressor disks. Its structure which is depicted in Fig. 6.2 is an $\alpha+\beta$ structure and its hardness was 330-345 MPa Hv using a 1Kg load.

6.2.2 Specimen Preparation

The preparation of large aluminium alloy and medium carbon steel rotating bend specimens has been dealt with in Chapter Five. This

TABLE 6.1 Composition of 300M Ultra High Strength Steel

Element	C	S	Mn	p	S	Cr	Mo	Ni	Cu	Sn	Al	V
Weight Per Cent	.42	1.68	.77	.006	.001	.86	.40	1.76	.14	.013	.019	.08

TABLE 6.2 Mechanical Properties of 300M

Property Value	$\sigma_{.2\%}$ (MPa)	σ_{uts} (MPa)	ε_f (%)	Hardness (H_v)
Value	1770	2072	12.1	583-603

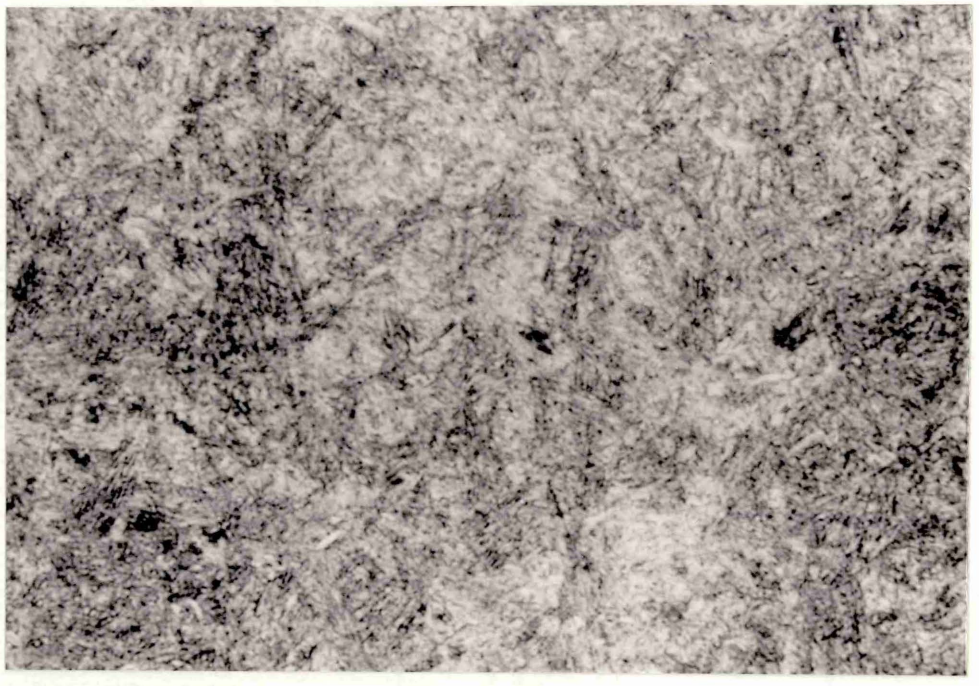

FIGURE 6.1 Microstructure of 300M, Etched 2½% Nital

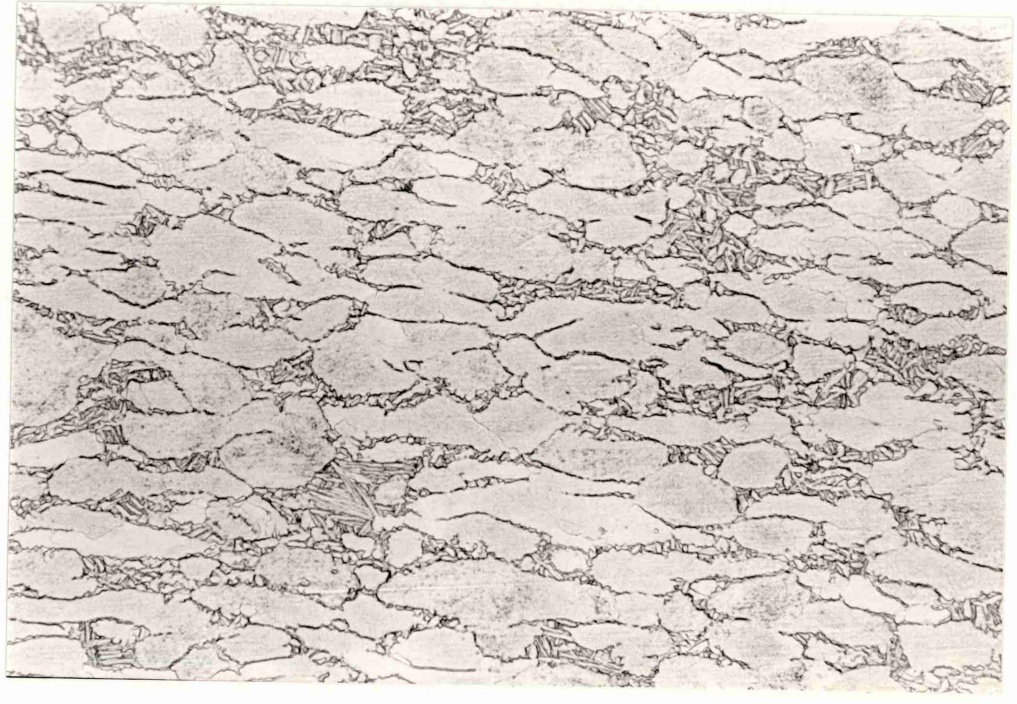

FIGURE 6.2 Microstructure of Ti6 AL4V Alloy, Etched Kellers

section details the manufacture of small rotating bend specimens in both the titanium and the aluminium alloys, large 300M rotating bend specimens and milled aluminium alloy specimens for uniaxial fatigue loading.

Small 7075 aluminium alloy rotating bend specimens

The dimensions of these specimens are given in Fig. 6.3. These specimens were made from the same stock of 7075 as the larger specimens and their alignment parallel to the axis of the bar was maintained. The finish machining was performed in the same way as the larger specimens and their alignment parallel to the axis of the bar was maintained. The finish machining was performed in the same way as the larger specimens except that the lathe's rotational speed was increased to produce similar cutting rates on the reduced diameter. The tool, feed rate and cutting depths are the same as those given in Table 5.3.

Peening the specimens was achieved by rotating them under the nozzle of the peening plant at a stand-off distance of 150mm using the same exposure time shot flow rate and shot speed as for the larger specimens. No significant distortion of the specimens occurred as a result of the peening.

Titanium 6AL 4V rotating bend specimens

The dimensions of these specimens were the same as the small aluminium alloy specimens except that the minimum diameter was reduced to 3.5mm since early tests in this material revealed a tendency for the specimens to fracture in the shank due to frettage at the point where the specimen entered the grips of the test machine. The machining details are given in Table 6.3.

The peening of these specimens was performed in the same way as for the small aluminium specimens except that they were exposed for 50% longer to compensate for the smaller area of individual shot impact craters giving rise to a slower rate of coverage build up.

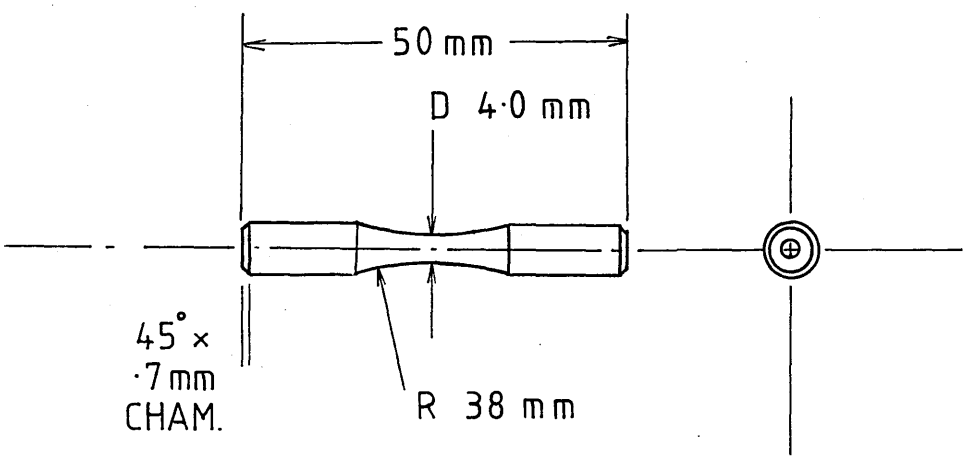

FIGURE 6.3 Dimensions of Aluminium Alloy Small Rotating Bend Specimens

TABLE 6.3 Machining Details for the Ti6 L4V Alloy

Cut	Feed Rate Microns/ Turn	Speed r.p.m.	Cut Depth Microns	Tool
Roughing	50	1100	300	Tungsten Carbide rad=4mm
Penultimate	20	1100	70	
Final	20	1100	30	

300M Ultra high strength steel rotating bend specimens

Two specimen geometries were tested in this material. They are depicted in Fig. 6.4. The introduction of a notch into some of the specimens was done to examine the influence of a notch on the effectiveness of the peening treatment in this highly notched sensitive material.

The specimens were rough machined to 3mm over size on diameter before final heat treatment and then finish machined in the finally tempered condition. The details of the machining treatment are given in Table 6.4.

7075 Alumium alloy uniaxial fatigue specimens

These specimens, of the same stock as the other 7075 specimens, were made in order to examine crack shape and growth rate, and also to permit the use of a non zero mean stress. The stress raiser they contain was designed to ensure specimen failure in the central portion of the specimen without giving rise to high stress gradients. In principle, residual stress measurements can easily be performed in the root of this shallow stress raiser though this has not been exploited. Fig. 6.5 gives the dimensions of the specimens and Table 6.5 gives the details of their machining.

6.2.3 Fatigue Testing and Crack Detection

Large rotating bend specimens, 7075 aluminium alloy and 080M40 medium carbon steel

The detailed testing procedure of these specimens is given in Chapter Five and [6.5].

Crack detection in the steel was performed using a.c. potential drop as it proved quite sensitive ferritic materials where the skin effect is more pronounced. The a.c. potential drop measurements in principle relate to the depth of cracks but cracks with greater surface length of multiple cracks will give greater readings for the same depth.

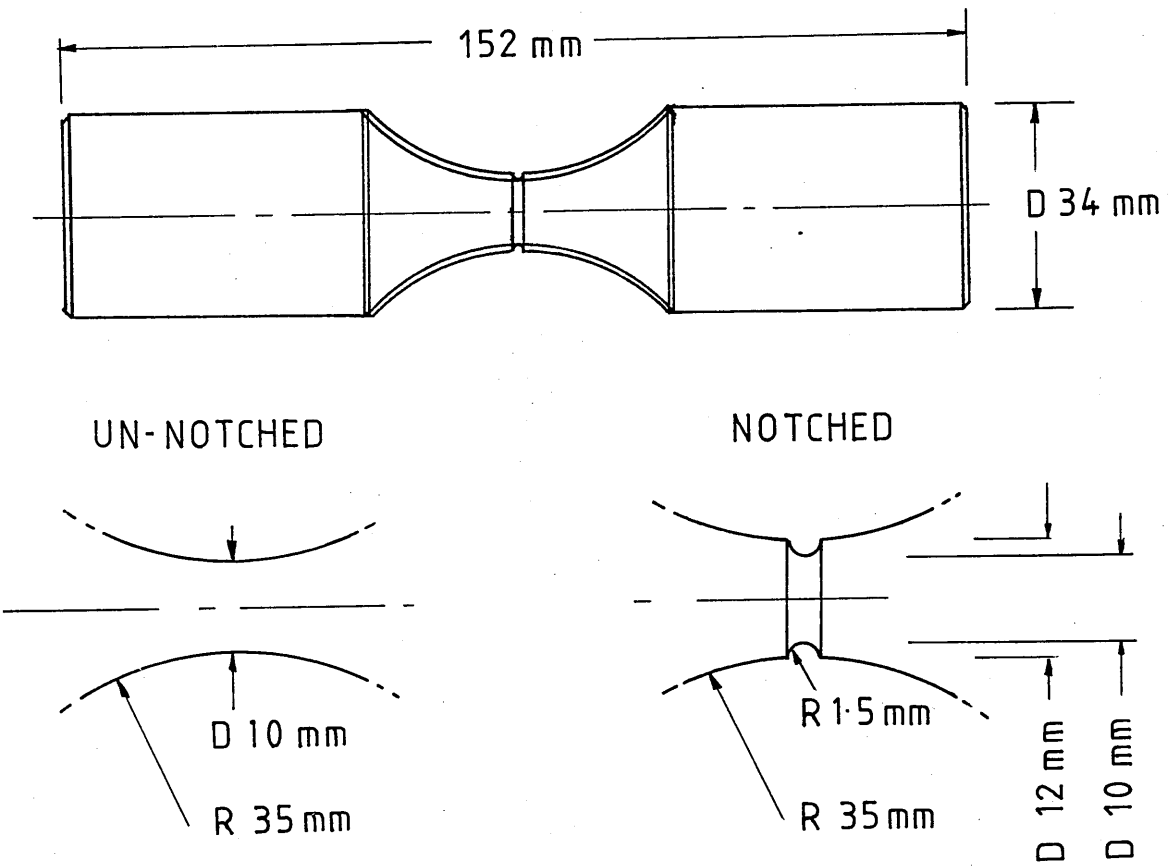

FIGURE 6.4 Dimensions of ultra high strength steel rotating bend specimens

TABLE 6.4 Machining Details for the 300m Specimens

Cut	Feed Rate Microns/ Turn	Speed r.p.m.	Cut Depth Microns	Tool
Roughing	50	1500	120	Tunsten Carbide rad=4mm
Penultimate	20	1100	90	
Final	20	1500	50	
Notch (where applicable)	Formed ≃ 50	200	1000	Tungsten Carbide rad=1.5mm

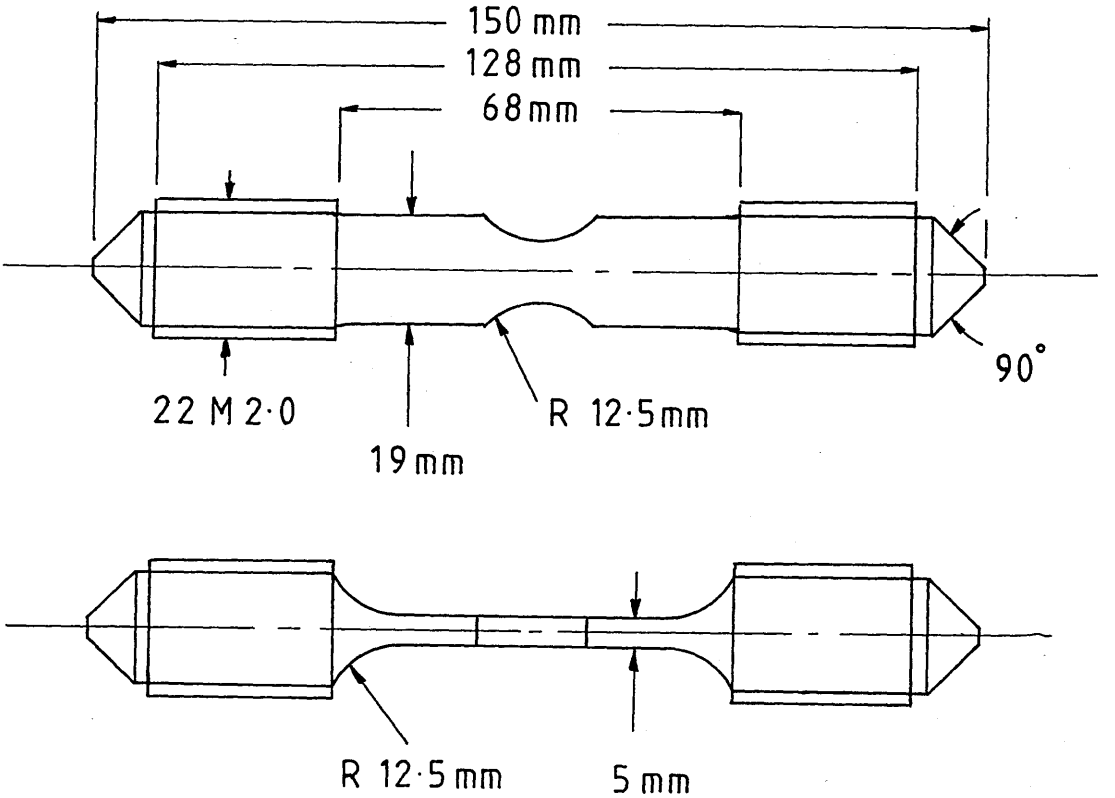

FIGURE 6.5 Dimensions of the 7075 Uniaxial Fatigue Specimens

TABLE 6.5 Machining Details for the 7075 Uniaxial Specimens

Cut	Feed Rate Microns/ Turn	Speed r.p.m.	Cut Depth Microns	Tool
Roughing	5000	1600	300	Double
Penultimate (side)	5000	1800	120	Edged
Final	2000	1800	70	End Mill rad=12.5mm
Penultimate (side)	20	900	80	Single Point
Final	20	900	50	Cutter rad=1.5mm

This was allowed for by calibrating the a.c. potential drop equipment on fatigue specimens containing fatigue cracks which were subsequently measured by fractography. Visual examination using "Zyglo" die penetrant was used on the aluminium specimens since it was found to be more sensitive than a.c. potential drop, the results from which were characteristed by a level of scatter corresponding to around .7mm in the aluminium. A comparison of the propagation of longer cracks both in the presence of the die penetrant and without it suggested that at crack propagation rates of $10^{-7}m^{-1}$ the penetrant did not significantly affect the crack propagation rate at the test frequencies utilised in this investigation. The die did, however, improve the sensitivity of the visual crack detection to the point where cracks with a surface length of .3mm could be located reliably. The presence of the die did not affect the total life of specimens so the initiation of cracks was also assumed to be largely unaffected.

Small rotating bend specimens

The smaller specimens were tested on a Krouse type three point bend rig as depicted in Fig. 3.1(a) in Chapter Three. No serious attempt was made to measure crack growth rate in these specimens as the stroboscope illumination system was not developed at the time of the testing and the rig passed through violent instability every time it was stopped and re-started. Specimen damage could in part be overcome by clamping the load cantilever prior to stopping and starting the motor, but lateral vibrations could not entirely be eliminated.

300M ultra high strength steel specimens

The high strength of these specimens, particularly the un-notched varient necessitated reducing the test frequency to 33Hz to avoid overheating the rig's bearings. This done, the testing of these specimens used the same procedures as the testing of the large aluminium and medium carbon steel specimens.

Crack detection proved most satisfactory on the un-notched variant of the specimen and die pentetrants were used as the results visual inspection revealed were more consistent than those provided by a.c. potential drop.

Uniaxial 7075 aluminium alloy specimens

Use was not made of die penetrants in these tests. Instead a travelling microscope was used in conjunction with the stroboscopic illumination system described in Chapter Three. It was, however, necessary to interrupt the testing in order to reposition the specimen in the load frame as the travelling microscope could only be used to view one side of the specimen at a time. In practice, a strong hand lens, used with stroboscopic illumination was employed to initially locate cracks as this could be used to examine the entire specimen without interrupting the load. When a crack was located, the test was then interrupted and the specimen moved to allow microscopic examination and measuring. In the case of corner cracks, which were prevelant, it was necessary to again interrupt the test for each crack measurement as two faces of the specimen at least needed to be viewed in the measuring microscope. It was found most effective to view cracks with a crack opening load present. In practice subjecting the specimen to load cycles of a low frequency, 1Hz allowed good visual discrimination between cracks and scratches and other indications. Preliminary testing using compact tension specimens confirmed that at crack growth rates of the order of 10^{-6}–10^{-8} m/cycle this material was not appreciably sensitive to test frequency.

A replication technique as described in Chapter Three was used to compare crack measurements made directly using the microscope with those recorded on the replica. The replica also provide a semi permanent record of the precise crack path on the specimen's surface.

6.3 RESULTS AND DISCUSSION

Stress Gradient Effects

The results of rotating bend fatigue tests on the 7075 aluminium zinc alloy and the medium carbon steel, using the larger specimen configuration are discussed to some extent in Chapter Five. Fig. 6.6, however, shows the S.N. curve for the 7075 material for both the large and the small specimen configurations in rotating bend fatigue. The results show clearly that in addition to a size effect contribution to

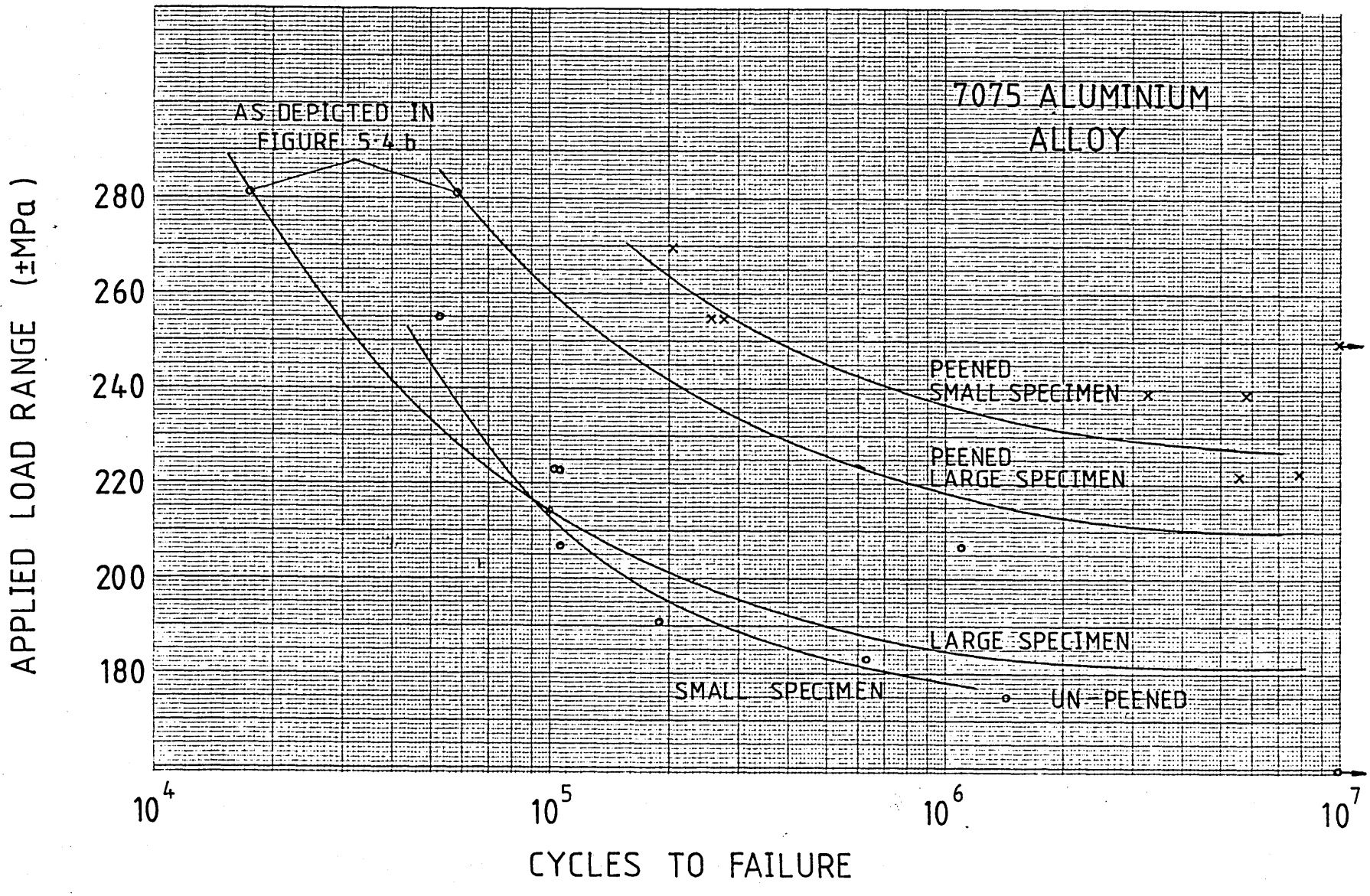

FIGURE 6.6 S.N. curve for the 7075 rotating bend specimens

the fatigue strength, the peening treatment gives a greater benefit in the case of the smaller specimens. This is in spite of the greater degree of specimen distortion due to peening that might be expected in the smaller specimens, though as mentioned previously no significant distortion could be measured. This effect is to be expected since the occurrence of sub-surface initiation makes the sub-surface stress level critical. The greater stress gradient associated with the smaller specimen will dictate that the sub-surface stresses will be lower than in the larger specimen. The uniaxial fatigue specimen generates within itself a stress gradient significantly lower than that in the larger rotating bend specimen, and it is significant as shown in Fig. 6.17 that peening did not induce an increase in the fatigue life of these specimens. Fig. 6.7 gives the fatigue life improvement as a function of stress gradient for the three specimen geometries at a load level of ±230MPa.

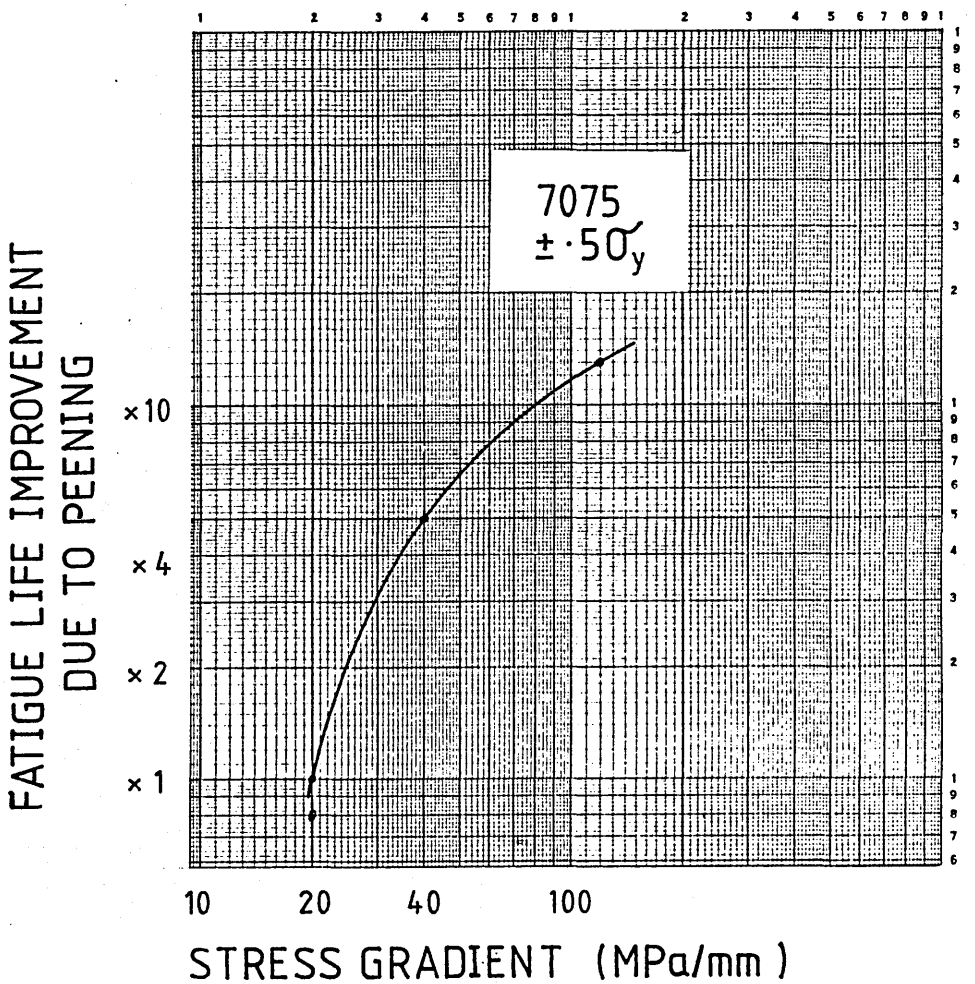

FIGURE 6.7 Fatigue life improvement due to peening as a function of applied stress gradient

Crack Propagation Effects in the 7075 and 080M40

Little attention was paid to the shape of cracks in the medium carbon steel since whether in peened or un-peened specimens they showed only modest variations in aspect ratio. They may then be characterised by their crack depth as measured by a.c.p.d. Crack depth versus cycle curves for typical specimens are given in Fig. 6.8. The relationship between crack depth and crack surface length in the aluminium rotating bend specimens was, however, less straight-forward as discussed in Chapter Five. Fig. 6.9 gives typical curves of crack surface length with cycles in the 7075. Fig. 6.10 gives the relationship between the crack surface length, 2c and the crack depth as for the medium carbon steel and the 7075 alloy. From this crack depth versus cycles data may be established for the 7075 alloy and using the stress intensity solution developed in Chapter Four crack growth rate as a function of the applied stress intensity range may be evaluated. This is given in Fig. 6.11 and Fig. 6.12. The complex variation of crack shape in the peened 7075 alloy specimens will lead to some uncertainty in the interpretation of such data and more faith may be put in the results gleaned from uniaxial fatigue testing where more consistent corner cracks were prevelant. The servo-hydraulic test machine was also more able to sustain accurate loading on cracked components than the rotating bend rigs, which tended to vibrate due to uneven specimen compliance.

300M material

The overall S.N. curve for the 300m ultra high strength steel specimens is given in Fig. 6.13.

Fig. 6.14 and Fig. 6.15 give crack propagation data for the 300M ultra high strength specimens.

Clearly peening these specimens has been relatively unsuccessful in terms of fatigue life improvement. It was also noted that a much higher density of cracks formed in the peened 300M specimens. The results tend to suggest that the initiation of cracks was occurring earlier in the peened 300M than in the as machined specimens.

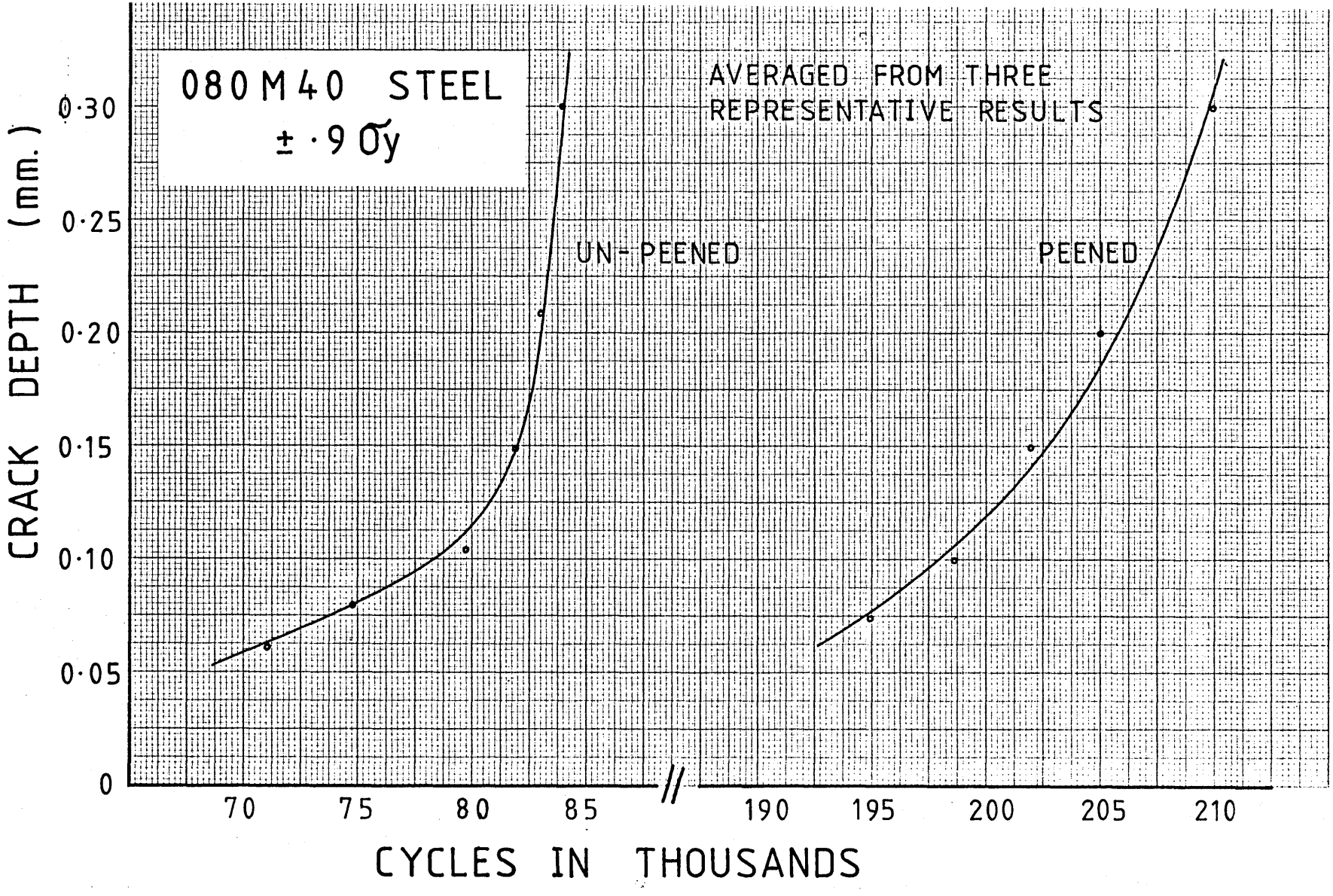

FIGURE 6.8 Crack depth versus cycles data for typical 080M40 steel specimens

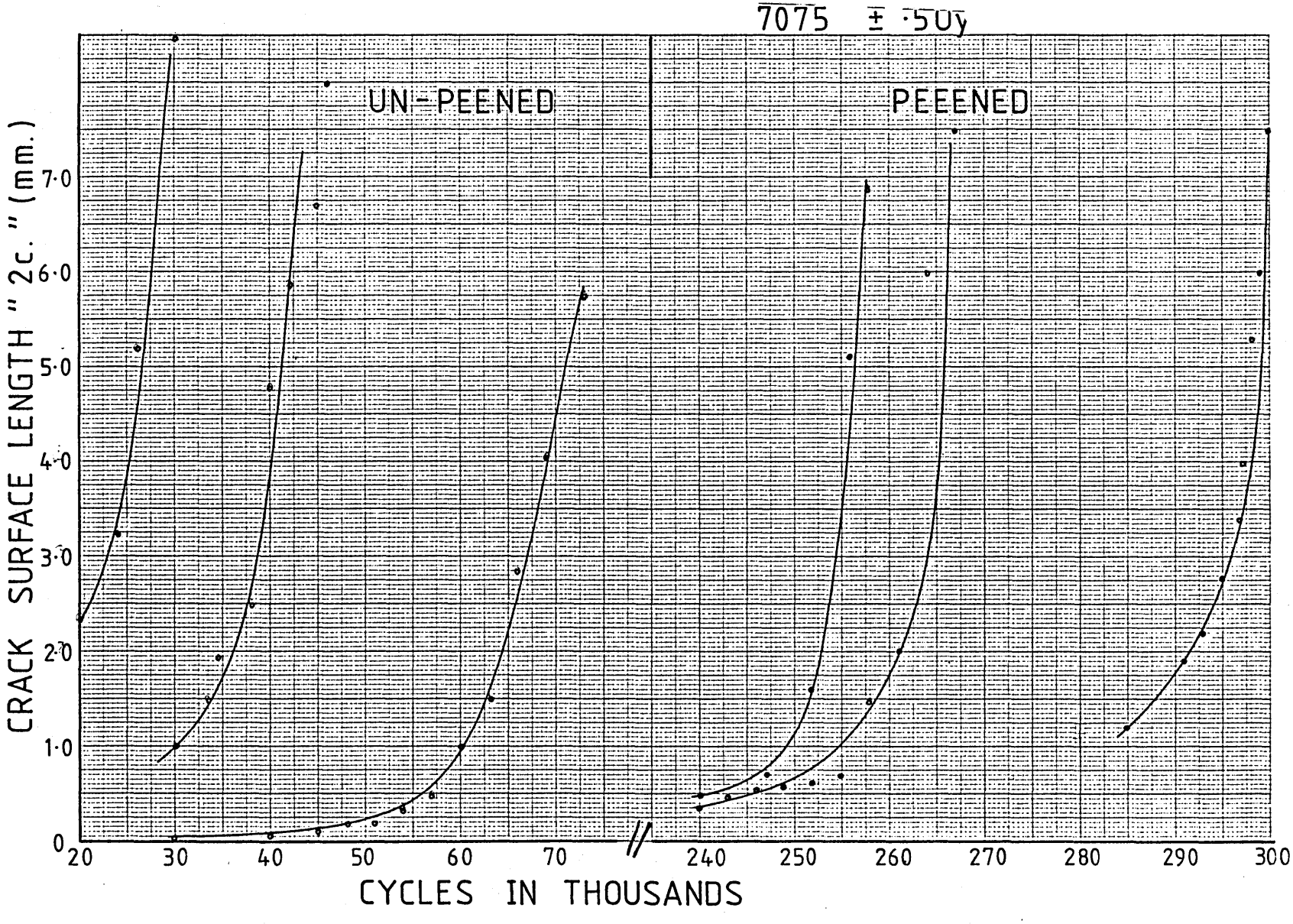

FIGURE 6.9 Crack surface length versus cycles data for typical 7075 specimens

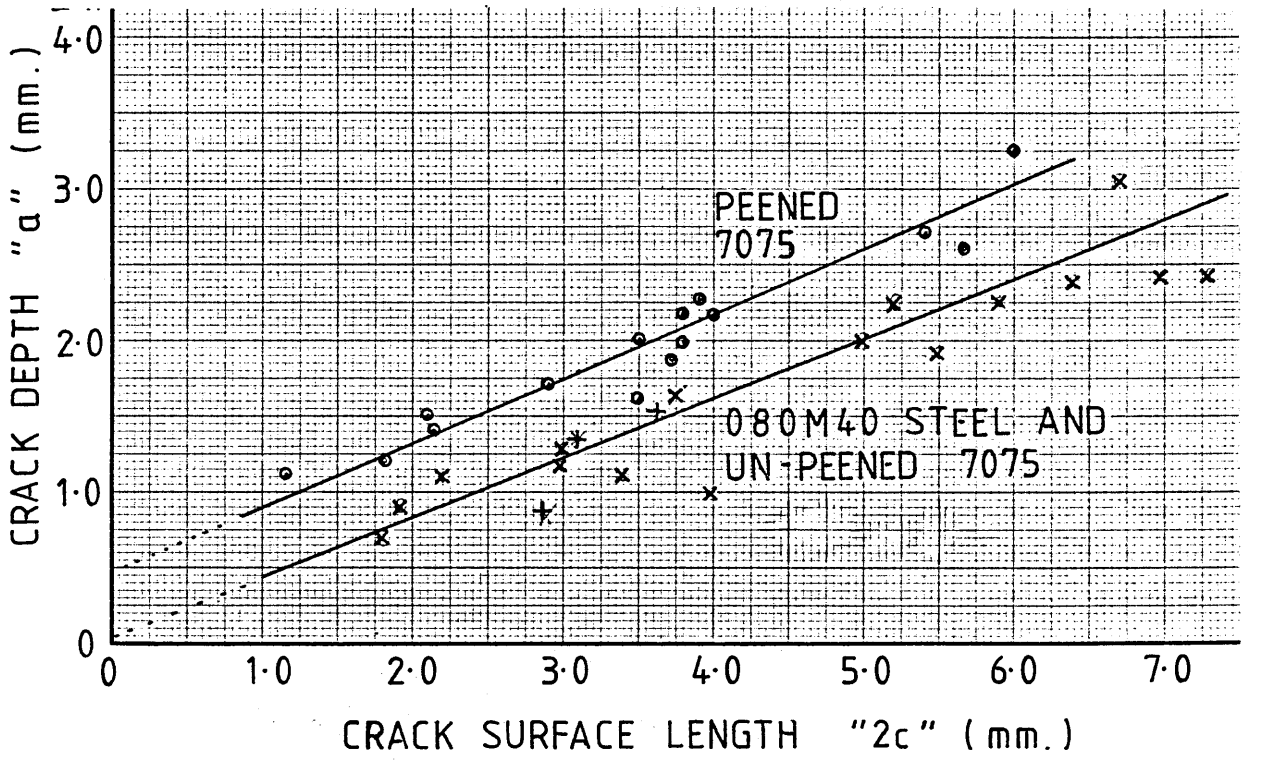

FIGURE 6.10 Relationship between crack surface length and crack depth for the rotating bend specimens

Variations in the peening treatment did not succeed in reversing this trend though no attempt was made to peen at Almen intensities greater than 1.0mm, A, (25A in thou.).

In order to try and elucidate this effect x-ray difractometry was used to attempt to measure the amount of retained austenite in the base material (after finish machining) and to try and detect any deformation induced transformation of the retained austenite to martensite due to the peening operation. This would provide a credible explanation for the early initiation of multiple cracks, but in the event the results were inconclusive. The only observation which could be made from the x-ray diffraction was that there had been a slight peak shift, presumably associated with the presence of the residual stress.

Similarly, discouraging results were experienced with the titanium alloy specimens. The S.N. curve for these is given in Fig. 6.16. Clearly the combined effects of the surface topographic and sub-structural changes due to peening have outweighed the influence of the residual compressive stress. An examination of the fracture surfaces did not suggest that sub-surface initiation was occurring.

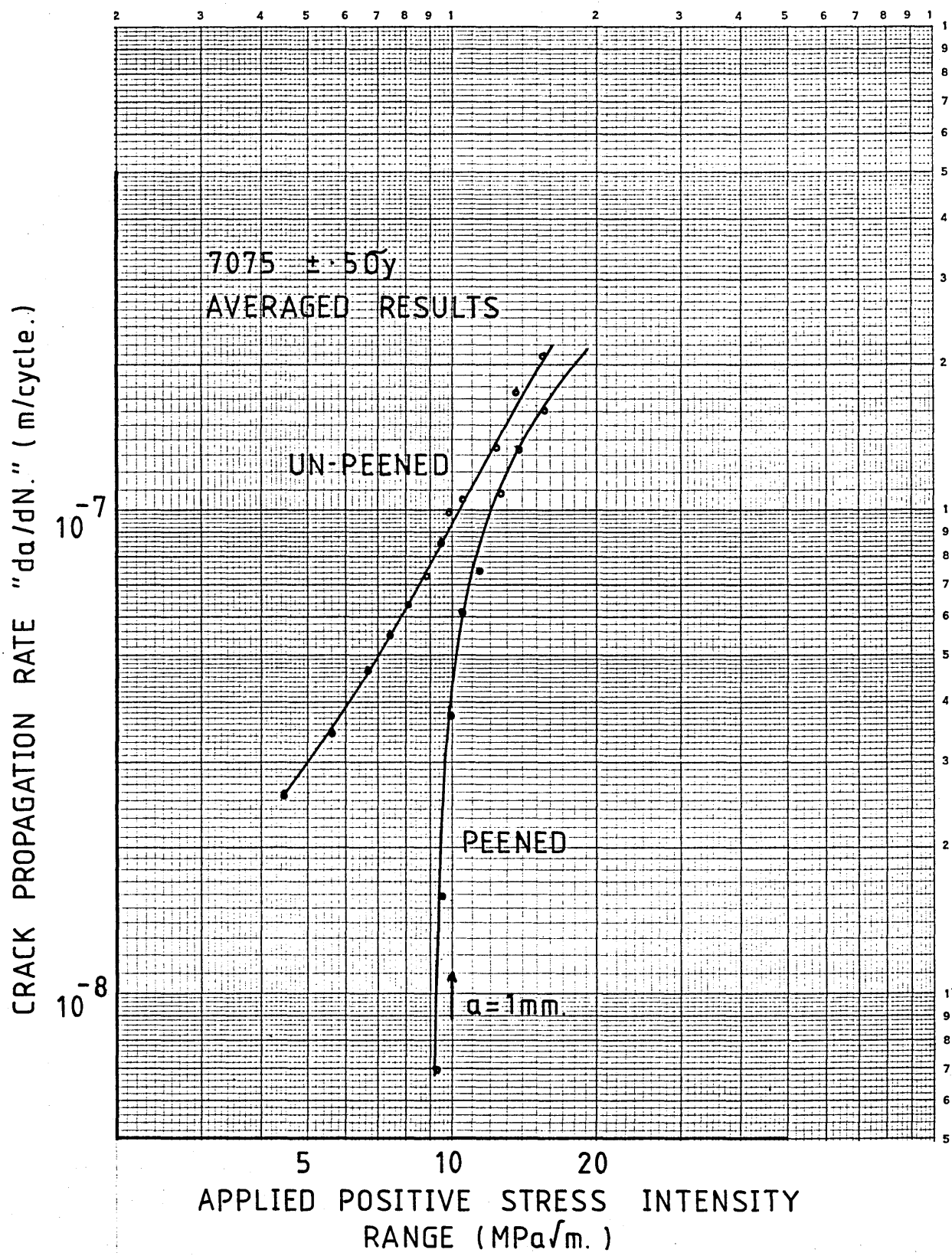

FIGURE 6.11 Crack growth rate as a function of applied stress intensity for the 7075 rotating bend specimens

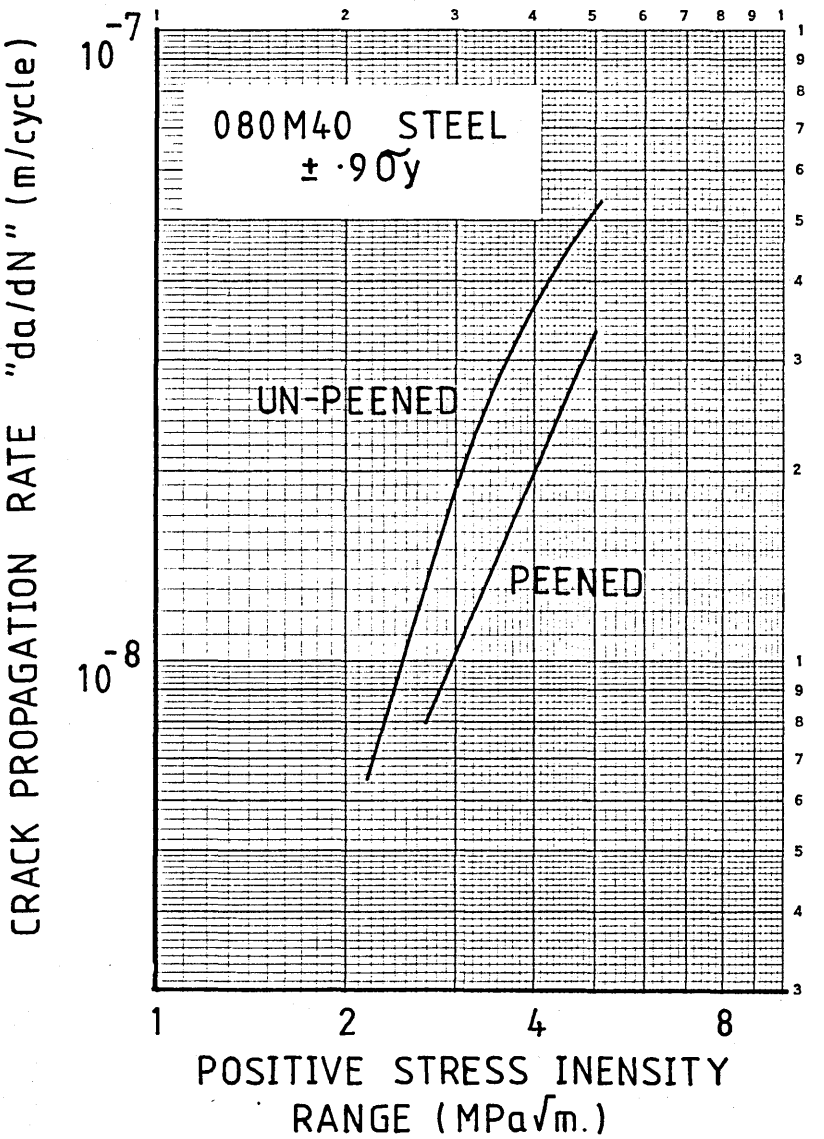

FIGURE 6.12 Crack growth rate as a function of applied stress intensity for the 080M40 rotating bend specimens

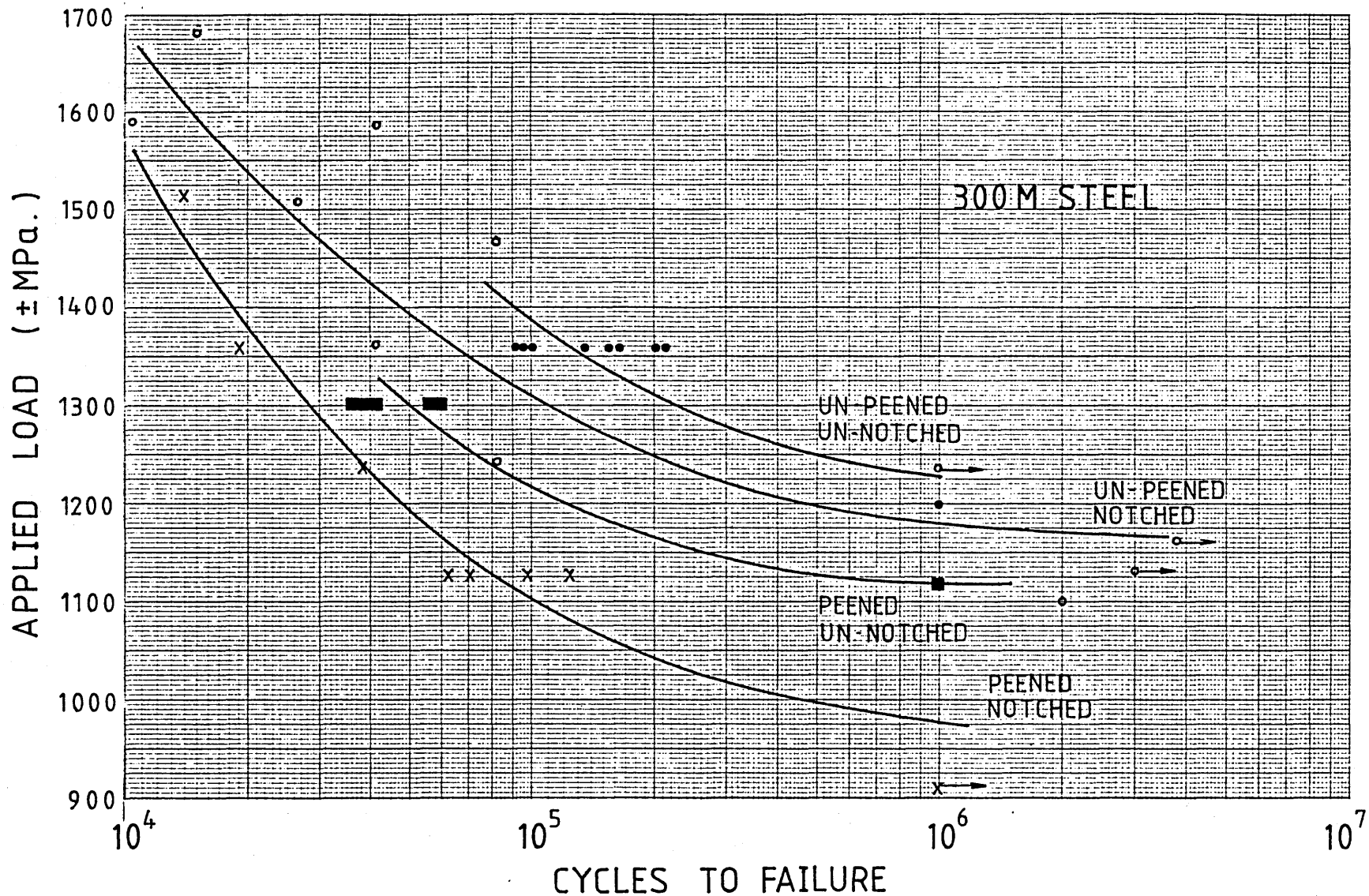

FIGURE 6.13 S.N. Curve for the 300 M material

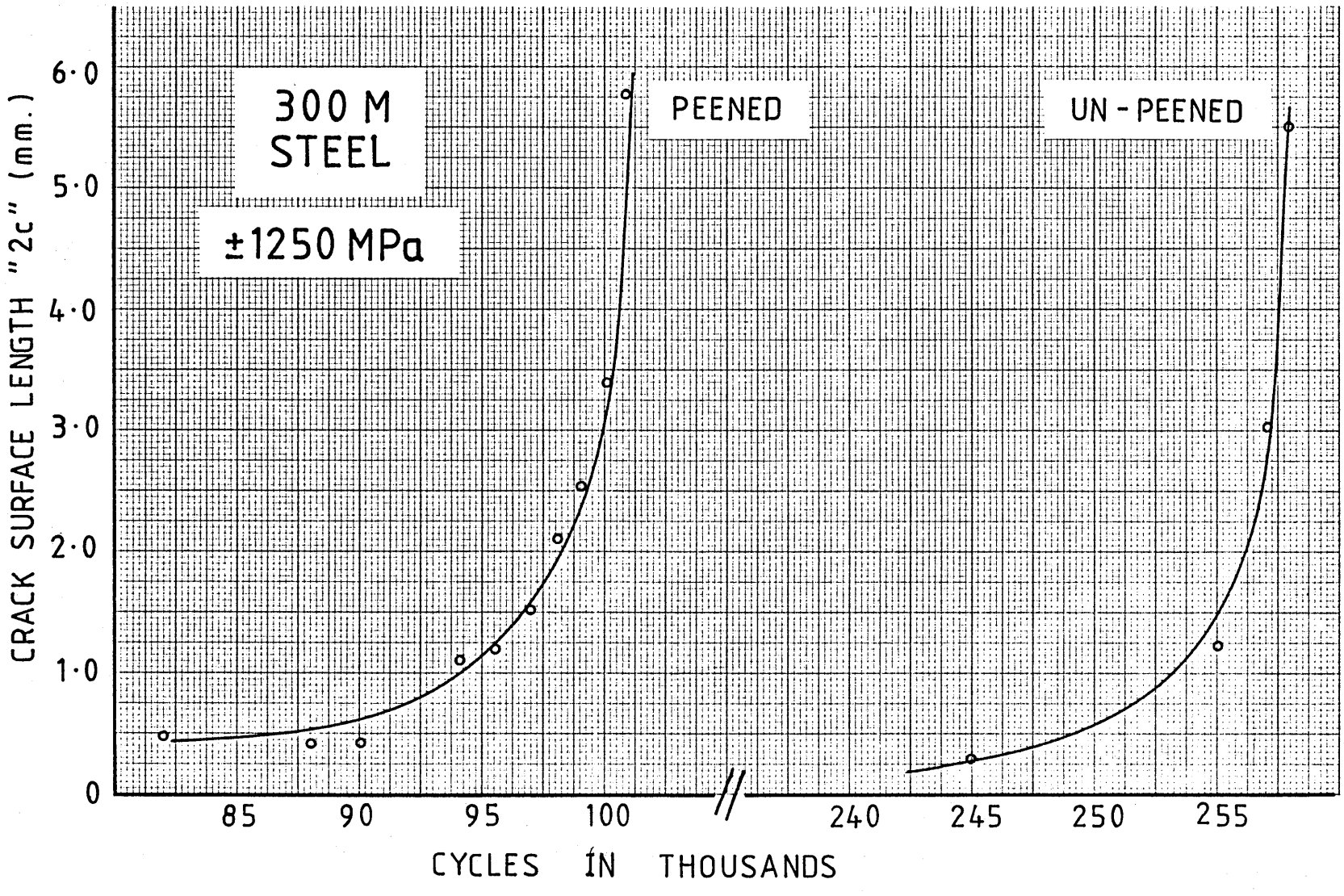

FIGURE 6.14 Crack surface length as a function of cycles for the 300 M material

PAGINATION
ERROR

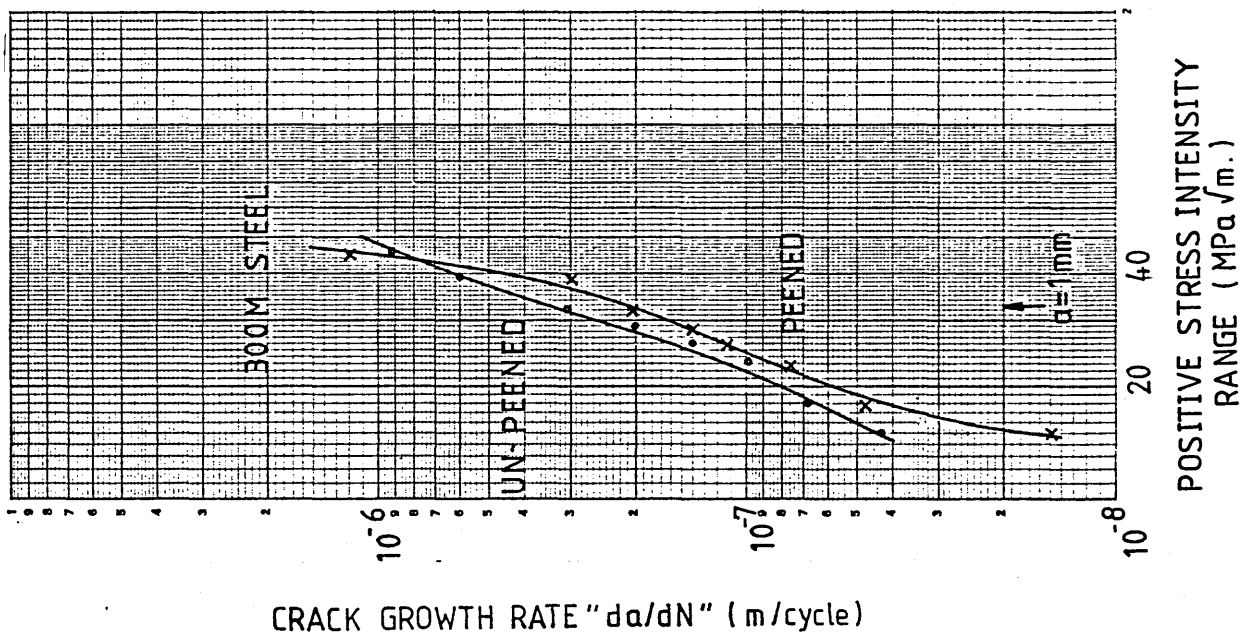

FIGURE 6.15 Crack growth rate as a function of applied stress intensity for the 300 M material

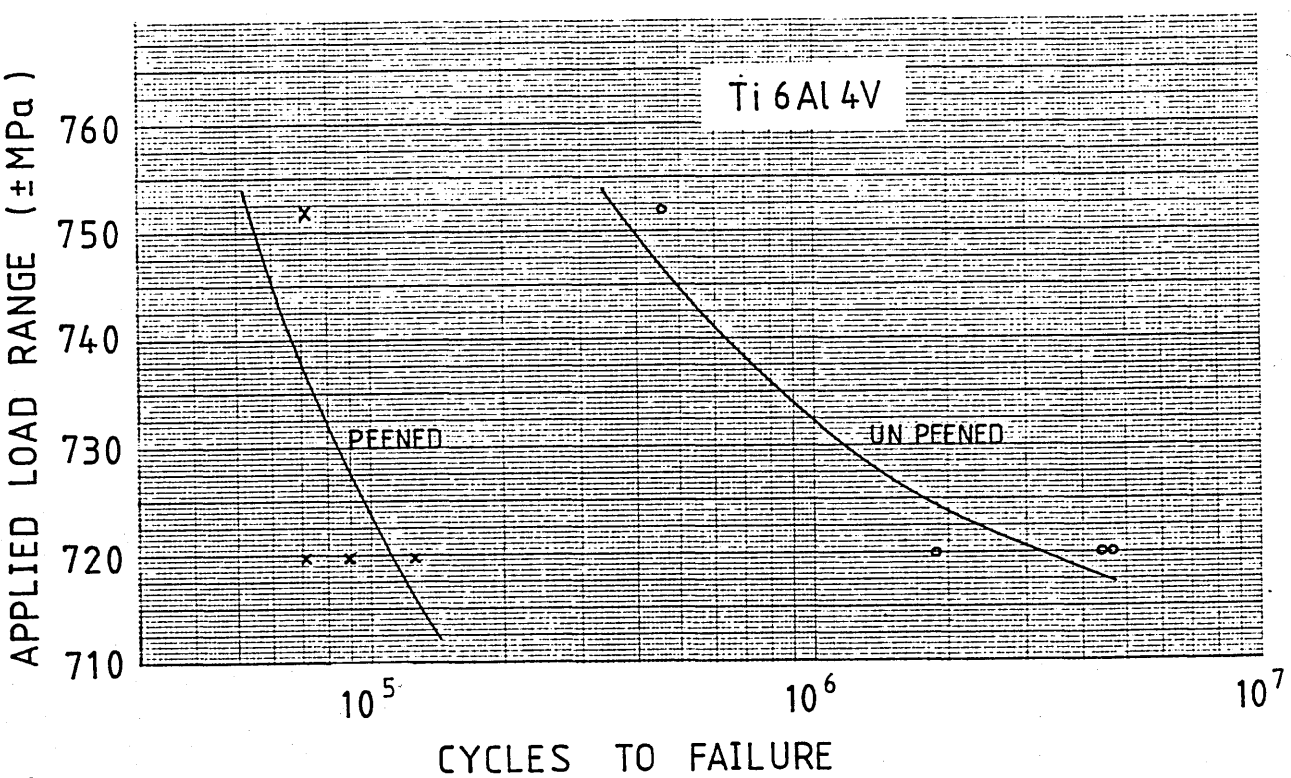

FIGURE 6.16 S.N. Curve for the Ti 6 Al 4 V material

Uniaxial testing aluminium

Having already established an S.N. curve for the 7075 alloy using rotating bend testing, only a small number of specimens were tested uniaxially to establish the basic strength of the uniaxial specimen in the peened and un-peened condition. This data is given in Fig. 6.17.

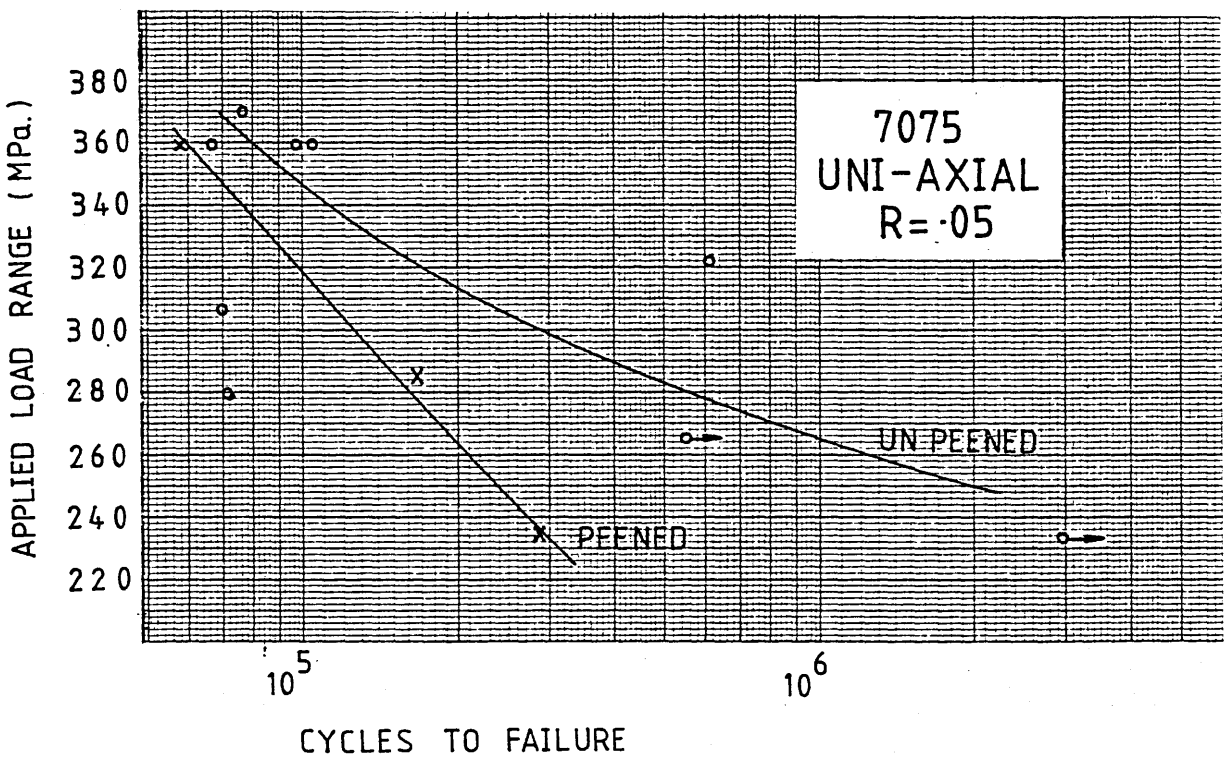

FIGURE 6.17 S.N. curve for the uniaxial 7075 specimens

Whilst a number of semi elliptical cracks did develop in specimens corner cracks were prevelant in both peened and un-peened specimens. Table 6.6 gives crack form and the number of cracks detected in each of the specimens tested.

Corner cracks in the peened specimens did give indications of having initially high depth to surface length ratios as depicted in Fig. 6.18 but this was rapidly evened out as the crack developed. Cracks of surface length less than 1mm proved difficult to locate by which time

crack form had become uniform. In all corner cracks monitored, both surface crack lengths were equal to within experimental error as can be seen from the sample crack size versus cycles data given in Fig. 6.19.

TABLE 6.6 Form of Cracks Observed in the 7075 Uniaxial Specimens

Condition	Number of Specimens	Number of Corner Cracks	Number of Face Cracks
Un-peened	3 1 1	1 0 1	0 1 1
Peened	4 1 1 0	1 2 1 0	0 0 1 1

In [6.6] stress intensity solutions for corner cracks infinite bodies are discussed in detail. For the purposes of this comparison the solution for a corner cracked plate of finite thickness and width as the slight error due to failing to consider stress gradient effects will affect both peened and un-peened data similarly. This solution is as follows:

$$K_I = \sigma \sqrt{\pi a/Q} \; Fc\left(\frac{a}{c}, \frac{a}{t}\phi\right) \tag{6.1}$$

where

$$Fc = \left[M_1 + M_2\left(\frac{a}{t}\right)^2 + M_3\left(\frac{a}{t}\right)^4\right] g_1 \; g_2 \; f(\phi) \tag{6.2}$$

$$f\phi = \text{Elliptic Integral} = \left[\left(\frac{a}{c}\right)^2 \cos^2\phi + \sin^2\phi\right]^{1/4} \tag{6.3}$$

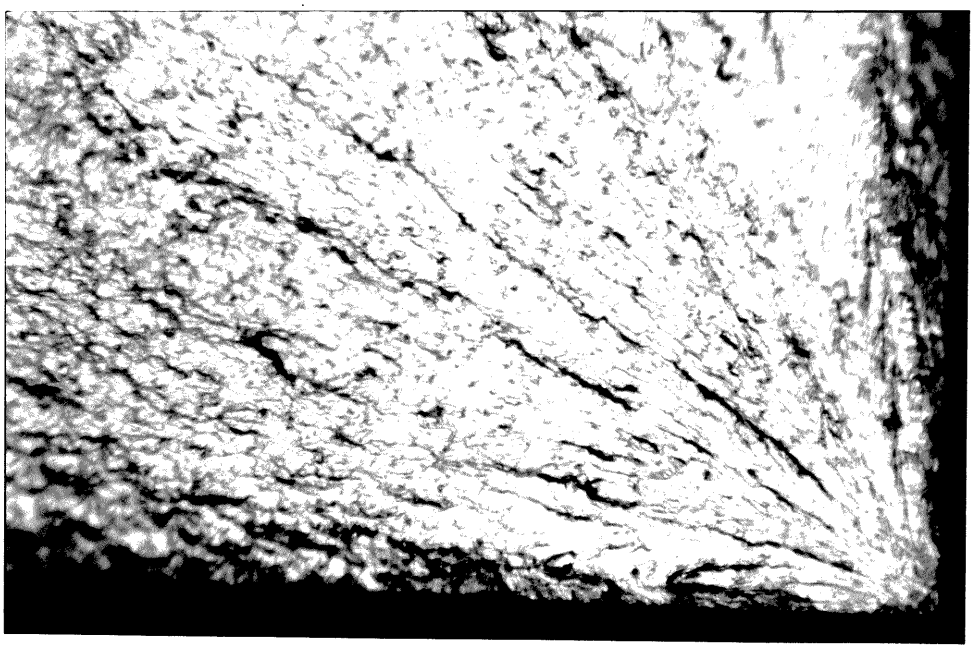

Un-peened 7075 alloy

1mm

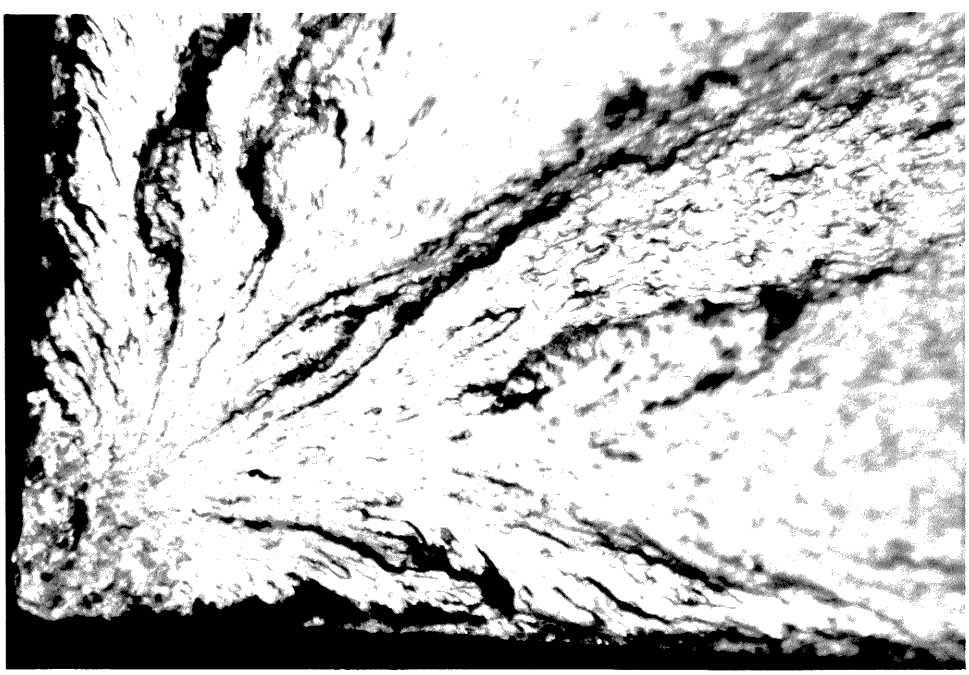

Peened 7075 alloy

1mm

FIGURE 6.18 Corner cracks in 7075 uniaxial 7075 specimens

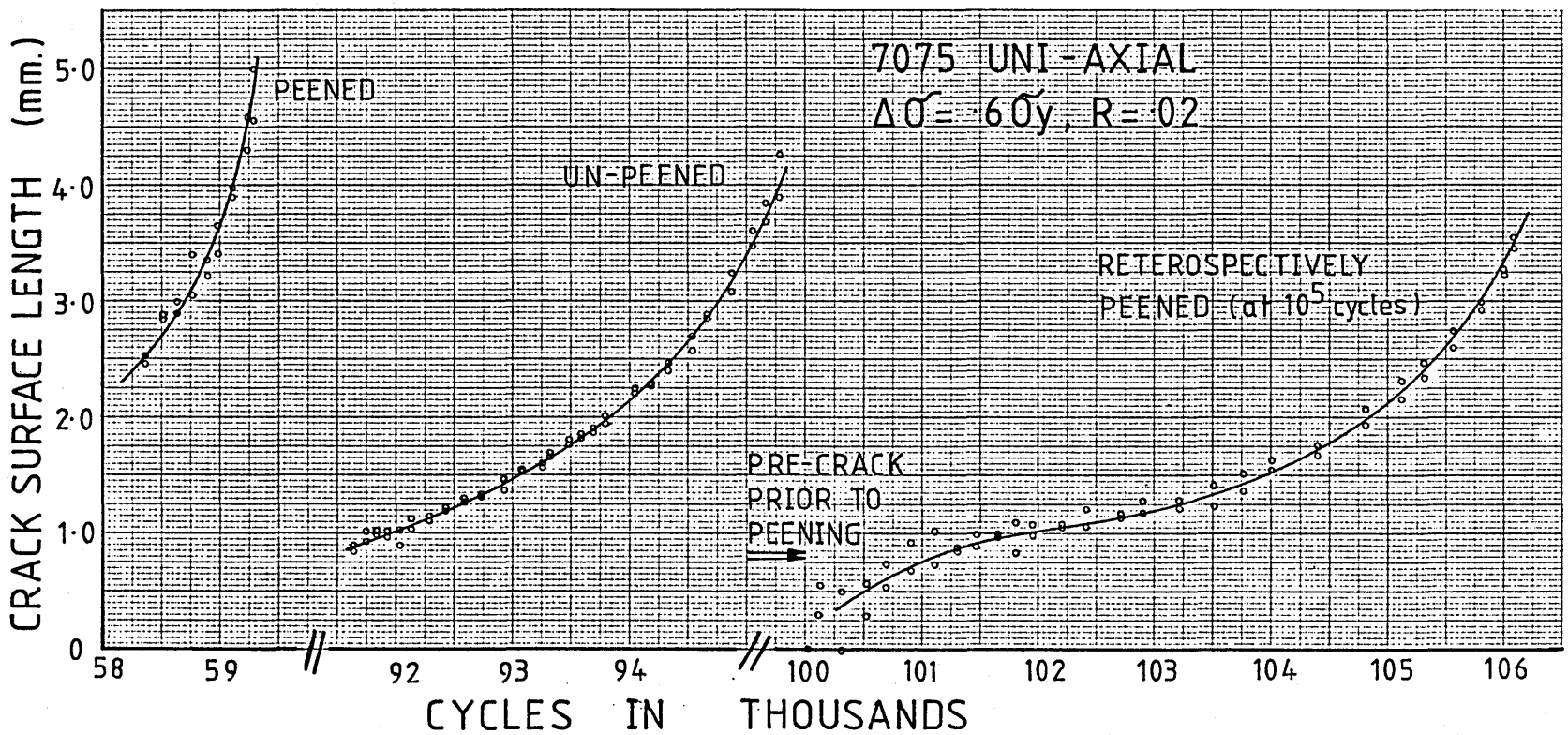

FIGURE 6.19 Crack size versus cycles data for the 7075 uniaxial specimens

$$M_1 = 1.08 - 0.03 \left(\frac{a}{c}\right) \tag{6.4}$$

$$M_2 = -0.44 + \frac{1.06}{0.3 + \left(\frac{a}{c}\right)} \tag{6.5}$$

$$M_3 = -0.5 + 0.25 \left(\frac{a}{c}\right) + 14.8 \left(1 - \frac{a}{c}\right)^{1.5} \tag{6.6}$$

$$g_1 = 1 + \left[0.08 + 0.4\left(\frac{a}{t}\right)^2\right](1 - \sin\phi)^3 \tag{6.7}$$

$$g_2 = 1 + \left[0.08 + 0.15\left(\frac{a}{t}\right)^2\right](1 - \cos\phi)^3 \tag{6.8}$$

Where ϕ is the angular position along the crack front measured from the face on which c is measured.

Clearly this solution may be simplified for cracks of a=c and the solution for guatri circular cracks at the intersection of the surface reduces to the following:

$$K_I = \sigma \frac{\sqrt{\pi a}}{Q}\left[1.05 + 0.375\left(\frac{a}{t}\right)^2 - 0.25\left(\frac{a}{t}\right)^4\right] x$$

$$\left[1 + \left(0.08 + 0.4\left(\frac{a}{t}\right)^2\right)\right] \tag{6.9}$$

Fig. 6.20 gives crack propagation rates in un-peened, peened and peened after pre-cracked specimens. It is important to note that the relative crack propagation rates of larger cracks in peened or un-peened components is of little significance to the total life whereas large proportions of the life are spent with smaller crack propagation rates.

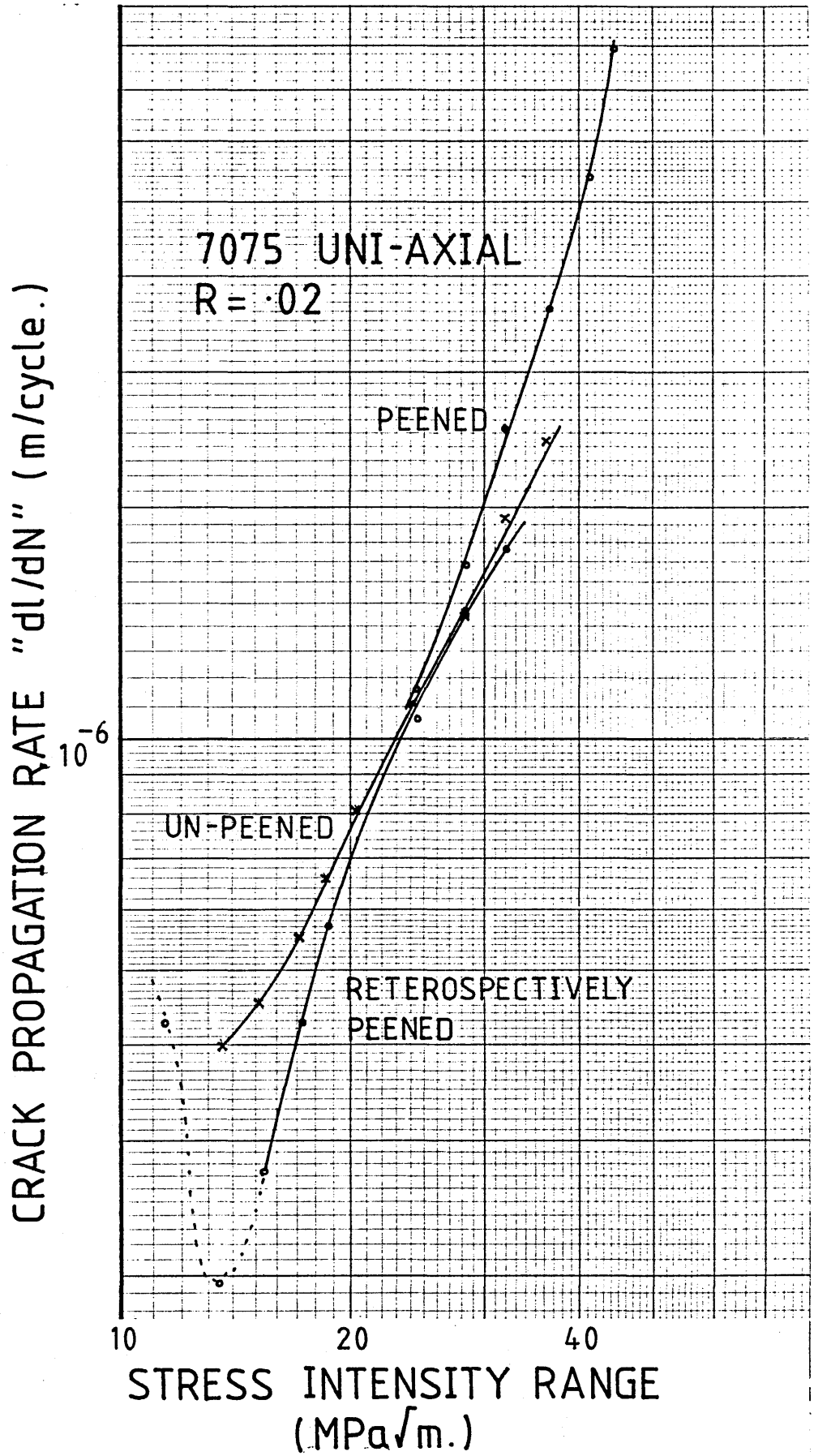

FIGURE 6.20 Crack growth rates as a function of applied stress intensity for the 7075 uniaxial specimens

It is of key significance that the crack growth rate in the specimen which had been fatigue pre-cracked prior to peening. A note was taken of the approximate crack opening load for a 1.5mm quatri circular crack in both the un-peened and the peened after cracking, and then subsequently fatigue tested. In the case of the un-peened specimen crack opening was observed at around 1kN, around 7% of the stress range. In the cracked and peened specimen however, the crack opening load was in excess of 7.5kN, 50% of the applied stress range.

6.4 CONCLUSIONS

The application of peening has been found to affect both the initiation and the propagation of fatigue cracks in four different materials. The points raised may be summarised as follows:

Initiation

- A possible increase in the initiation life as in the 080M40 material.

- An apparent increase in the initiion life due to sub-surface initiation as in the case of the 7075 material.

- An increase in the number of crack nuclei as in the 300m material.

- A decrease in the initiation life as in the case of both the 300M material and the Ti6 AC 4V.

Propagation

- A decrease in the crack propagation rate of short cracks.

- An increase in the closure stress of cracks subjected to peening.

- A change in the pattern of crack growth.

- A strong decrease in the propagation of cracks of even up to around 1mm in depth due to peening.

LIST OF FIGURES

Fig. 6.1 Microstructure of 300M, Etched 2½ Nital

Fig. 6.2 Microstructure of Ti 6Al 4V alloy

Fig. 6.3 Dimensions of aluminium alloy small rotating bend specimens

Fig. 6.4 Dimensions of ultra high strength steel rotating bend specimens

Fig. 6.5 Dimensions of the 7075 uniaxial fatigue specimen

Fig. 6.6 S-N Curve for the 7075 rotating bend specimens

Fig. 6.7 Fatigue life improvement due to peening as a function of applied stress gradient

Fig. 6.8 Crack depth versus cycles data for typical 080M40 steel specimens

Fig. 6.9 Crack surface length versus cycles data for typical 7075 specimens

Fig. 6.10 Relationship between crack surface length and crack depth for the rotating bend specimens

Fig. 6.11 Crack growth rate as a function of applied stress intensity for the 7075 rotating bend specimens

Fig. 6.12 Crack growth rate as a function of applied stress intensity for the 080M40 rotating bend specimens

Fig. 6.13 S-N curve for the 300M material

Fig. 6.14 Crack surface length as a function of cycles for the 300M material

Fig. 6.15 Crack growth rate as a function of applied stress intensity for the 300M material

Fig. 6.16 S-N curve for the Ti 6Al-4V material

Fig. 6.17 S-N curve for the uniaxial 7075 specimens

Fig. 6.18 Corner cracks in 7075 uniaxial specimens

Fig. 6.19 Crack size versus cycles data for the 7075 uniaxial specimens

Fig. 6.20 Crack growth rates as a function of applied stress intensity for the 7075 uniaxial specimens

LIST OF TABLES

6.1 Composition of 300M

6.2 Mechanical Properties of 300M

6.3 Details of the machining of titanium rotating bend specimens

6.4 Details of the machining of 300M rotating bend specimens

6.5 Details of the machining of 7075 uniaxial fatigue specimens

6.6 Form of cracks encountered in 7075 uniaxial fatigue specimens

REFERENCES

[6.1] Morrow, J., Cyclic plastic strain energy and fatigue of metals, Internal Friction, Damping and Cyclic Plasticity, ASTM STP 378, American Society for Testing and Materials, 1965, pp 45-87.

[6.2] Berus, H. and Weber, L, Influence of residual stresses on crack growth, Proc. Second International Conference on Impact Surface Treatment, Cranfield, Ed. S.A.Meguid, 1986, pp 31-44.

[6.3] Miller, K.J., The behaviour of short fatigue cracks. Ed. K J Miller, and E.R. de los Rios, London Mechanical Engineering Publication, 1986.

[6.4] Nelson, D.V., and Socie, D.F., Crack initiation and propagation approaches to fatigue and fracture resistant structures, ASTM STP 761, Ed. P.R. Abelkis and C.M. Hudson, American Society for Testing and Materials, 1982, pp 110-132.

[6.5] Hammond, D.W., The mechanics of peening and re-peening partially fatigued components, M.Phil. Dissertation, Cranfield Institute of Technology, 1986.

[6.6] Newman, J.C. Jr., and Raju, I.S., Stress-intensity factor equations for cracks in three-dimensional finite bodies. Fracture Mechanics: Fourteenth Symposium, Vol. 1: Theory and Analysis, ASTM STP 791, Ed. J.C. Lewis and G. Sines, American Society for Testing and Materials, 1983, pp 238-265.

CHAPTER SEVEN

CONCLUSIONS

The shot peening process demonstrably reduces the crack propagation rate of cracks even when the depth of the crack exceeds the thickness of the deformed layer due to the pinning of the edge of cracks at the peened surface.

The apparent initiation life of components may be increased by the peening process in the two following ways:

(i) Crack initiation may be manifest as the belated appearance of a detectable crack after some degree of residual stress has occurred.

(ii) Crack initiation may occur in the sub-surface of the material as the peened surface ceases to become the weakest part of the component.

Propagation of pre-existing cracks can be decelerated by the peening process as the crack corners tend to be pinned back where they intersect the peened surface. The application of peening also appears to greatly increase the minimum crack opening stress of pre-existing cracks.

Peening can appear to reduce the crack initiation life of components, where extreme changes in hardness or phase changes occur during the peening treatment. This is accompanied with a large increase in the number of initiaion sites.

The failure life of shot peened components is a result of three groups of changes produced by peening. These are as follows;

(i) A modification in the compressive sense of the residual stresses at and near the surface of the component.

(ii) The surface layer will be deformed and will show dramatic structural and sub-structural changes, possibly even involving phase changes. An increase in the surface hardness is the most obvious manifestation of these changes.

(iii) The topography of the surface will be modified by the deformation induced by the peening process. Depending on the nature and size of features already present on the surface, peening may refine or degrade the geometrical integrity of the surface.